



Vanessa Clemente Almeida

Licenciada em Química Aplicada

**Dry powder formulations containing
bioactive compounds from marine
*Actinobacteria***

Dissertação para obtenção do Grau de Mestre em
Biotecnologia

Orientador(es): Prof. Doutora Ana Aguiar-Ricardo, FCT-UNL
Doutora Susana P. Gaudêncio, FCT-UNL

Júri:

Presidente: Prof. Doutor Pedro Miguel Ribeiro Viana Baptista
Arguente: Doutora Ana Alexandra Figueiredo Matias
Vogais: Prof. Doutora Ana Isabel Nobre Martins Aguiar de Oliveira Ricardo
Doutora Susana Maria Pereira Gaudêncio



FACULDADE DE
CIÊNCIAS E TECNOLOGIA
UNIVERSIDADE NOVA DE LISBOA

Setembro 2015

Dry powder formulations containing bioactive compounds from marine

Actinobacteria

Copyright © Vanessa Clemente Almeida, FCT-UNL, FCT

A Faculdade de Ciências e Tecnologia e a Universidade Nova de Lisboa têm o direito, perpétuo e sem limites geográficos, de arquivar e publicar esta dissertação através de exemplares impressos reproduzidos em papel ou em forma digital, ou por qualquer outro meio conhecido ou que venha a ser inventado, e de a divulgar através de repositórios científicos e de admitir a sua cópia e distribuição com objetivos educacionais ou de investigação, não comerciais, desde que seja dado crédito ao autor e editor.

Acknowledgments

First of all I would offer my sincerest gratitude to my supervisor Prof. Doctor Ana Aguiar-Ricardo, for giving me the opportunity to work in the Polymer Synthesis and Processing laboratory and for all the guidance and support given throughout this year. Likewise, I want to thank to my supervisor Doctor Susana Gaudêncio, whom positive and enthusiastic supervision was very important to keep me on working without giving up.

Funding from Fundação para a Ciência e Tecnologia (FC&T-Lisbon) and FEDER through contracts PTDC/EQU-EQU/116097/2009, Pest-C/EQB/LA0006/2013, PTDC/QUI-QUI/119116/2010, UID/QUI/50006/2013 and UID/Multi/04378/2013), is acknowledged.

In relation to NMR spectroscopy, I would like to thank the NMR Service being the spectrometers NMR part of "The National NMR Facility", with support from the Fundação para a Ciência e a Tecnologia (RECI/BBB-BQB/0230/2012).

Dra Teresa Casimiro who always helped me by sharing ideas and by the interesting discussions with some relevant points contributing with a input in my work

Also, would like to thank Doctor Florbela Pereira for the guidance with such sympathy and enthusiasm, whose help and time I appreciate very much.

Dra Rosário Mato who provided the vancomycin resistant *Enterococcus faeciu* strain.

To my dearest friend, Márcia Tavares, who taught me so many useful things to my work, who supported me and who was always available to help with my SASD problems. Also, for the support, friendship and mostly patience to deal with me on a daily basis. I love you girl!

A special gratitude to Rita Pires, a person with a great heart and patience. She was inspiring, gave me a different motivation and energy by her presence. Thank you a lot dear Rituxa!

I would also like to thank Patrícia Morgado, Pedro Lisboa, Sara Correia and Vanessa Correia for all the incentive, advice and friendship, you are the best work buddies.

To all the 510/508 lab team: Sofia Silva, Dr. Vasco Bonifácio, Raquel Viveiros, Carmen Montoya, Gosia Zakrzewska, Fabiana Gonçalves and Marta Silva and to Tiago Dias from lab 333.

To Mrs. Maria José Carapinha, Mrs. Conceição and Mrs. Idalina for all the assistance.

To all my friends, in and outside the university campus, for the support and for the good moments that I had with all of you this last year.

At last, I have to thank my parents and my brother for all the help and support, without you none of this would be possible. You are my greatest inspiration and deserve the dedication of this entire work! Thank you for your love.

Abstract

Lower respiratory infections were the leading cause of sickness and mortality in 2013.¹ The treatment of such infections relies on antibiotic therapy. However, antibiotic resistance to human pathogens and the prevalence of new cancer types continues to increase, so it is imperative not only to discover new lead-like drugs agents, but also develop new drug delivery systems for pulmonary diseases.^{2,3} In order to achieve such goal, it was isolated and elucidated antibacterial compounds from a marine-sediment-derived *Actinobacteria*, collected along Madeira archipelago. These bioactive compounds were obtained from *Streptomyces aculeolatus*, PTM-029, belonging to the MAR4 group. The structures of these compounds were elucidated by 1D and 2D NMR, HR-MS and other spectroscopic data. The antibacterial activity against methicillin-resistant *Staphylococcus aureus* (MRSA) and vancomycin-resistant *Enterococcus faecium* EF82 (VRE) were determined for the most promising compound isolated from PTM-029, with a minimum inhibitory concentration (MIC) of 1,95 µg/mL for both bacterial pathogens. Subsequently, chitosan and cholesterol-based dry powder formulations were manufactured, containing encapsulated POxylated polymer, efficiently synthesized using a supercritical-assisted polymerization in carbon dioxide (CO₂), end-capped to a model drug ibuprofen (IBP) and a marine bioactive compound, PTM-029, F4, F39. The dry powder formulations (DPF) were then synthesized through the Supercritical Assisted Spray-Drying (SASD) technique. All the produced DPFs were characterized in detail in relation to their morphology, physical-chemical properties and aerodynamic performance. The resulting particles showed good aerodynamic diameters between the 1 and 7 µm, yields up to 45% and FPF percentages rounding the 71%, as well as the required morphology to make them suitable for pulmonary delivery.

Keywords: marine natural product, dry powder, supercritical assisted spray-drying.

Resumo

As infecções respiratórias constituíram uma das principais causas de doença e mortalidade em 2013.¹ O tratamento para este tipo de infecções realiza-se através do recurso a antibióticos. No entanto, devido ao aumento da resistência dos patogénicos humanos a antibióticos, bem como ao aparecimento de novos tipos de cancro, torna-se imperativo não só descobrir novos fármacos mas também desenvolver novos sistemas de administração de fármacos para doenças pulmonares.^{2,3} De modo a alcançar este objetivo, isolaram-se compostos antibacterianos a partir de sedimentos marinhos derivados de *Actinobacteria*, recolhidos ao largo do arquipélago da Madeira. Os compostos bioactivos foram obtidos a partir da estirpe *Streptomyces aculeolatus*, PTM-029, que pertence ao grupo MAR4. Elucidou-se a estrutura de um dos compostos por RMN a 1D e 2D, por HR-MS e outros dados espectroscópicos. A atividade antibacteriana contra *Staphylococcus aureus* resistente à meticilina (MRSA, de “Methicillin Resistant *Staphylococcus aureus*”) e *Enterococcus faecium* EF82 resistente à vancomicina (VRE, de “Vancomycin Resistant Enterococci”) foram determinados para o composto mais promissor isolado da PTM-029, com uma concentração inibitória mínima (MIC) de 1,95 µg/mL, para ambos os agentes patogénicos humanos. Consequentemente, foram produzidas formulações de pó seco à base de quitosano e colesterol, contendo um polímero POxilado encapsulado. Este polímero foi sintetizado de forma eficiente através de uma polimerização supercrítico-assistida em dióxido de carbono (CO₂), ligado a uma droga modelo, ibuprofeno (IBP) e a um composto bioactivo marinho PTM-029, F4, F39. As formulações de pó seco (FPS) foram sintetizadas através da técnica de secagem assistida por fluídos supercríticos (SASD). Todas as FPS produzidas foram caracterizadas em detalhe em relação à sua morfologia e às suas propriedades físico-químicas, bem como o seu desempenho aerodinâmico. As partículas obtidas apresentaram bons diâmetros aerodinâmicos entre 1 e 7 µm, rendimentos até os 45% e valores de FPF a rondar os 71%. Em geral, as micropartículas produzidas apresentam os requerimentos necessários para administração via pulmonar.

Palavras-Chave: Produtos naturais marinhos; Pós secos; Secagem assistida de spray por fluídos supercríticos.

Contents

Acknowledgments.....	I
Abstract	III
Resumo.....	V
Index of Figures	XI
Index of Tables.....	XV
List of Abbreviations.....	XVII
Overview	1
Part I - Isolation of bioactive compounds from marine <i>Actinobacteria</i>	3
1. Introduction	3
1.1 Natural products	3
1.2 Actinomycetess from marine sources	4
1.3 Actinomycetes terpenoids	5
1.4 Hybrid isoprenoids classes obtained from marine environmental bacteria sources	6
1.5 Phylogenetic and chemical diversity of a hybrid-isoprenoid-producing streptomycete lineage	7
1.6 Biosynthesis of hybrid isoprenoids from actinomycetes sources.....	11
1.7 Napyradiomycins.....	16
2. Experimental Section.....	19
2.1 Materials	20
2.2 General Experimental Procedures	20
2.3 Collection, Identification, Cultivation, and Extraction of Strain PTM-029.....	20
2.4 Isolation of Napyradiomycins	21
2.5 Antibiotic Assay.....	21
3. Results	22
3.1. PTM-029 crude extract, fractionation, and antibacterial activity assessment.....	22
3.2. Isolation of PTM-029 compounds by HPLC and its antibacterial activity.....	23
3.3. PTM-029 Structure elucidation	25
4. Discussion.....	26
5. Conclusion	31

6. References	32
Annex 1	38
Annex 2	46
Annex 3	54
Annex 4.....	59
Annex 5	73
Part II - Dry powder formulations containing encapsulated bioactive-agent by supercritical assisted spray-drying (SASD)	79
1. Introduction	79
1.1 Dry Powder Inhalers	80
1.2 Characterization of inhaled particles.....	82
1.3 Cholesterol and Chitosan excipients.....	84
1.4 PLGA	86
1.5 <i>Living polymer</i> end-capped with different compounds	87
1.6 Particle Production	89
1.7 Supercritical Fluid Technology	90
1.8 Supercritical assisted spray-drying (SASD)Supercritical Fluid Technology.....	91
2. Experimental Section.....	94
2.1 Materials	94
2.2 Polymer synthesis in scCO ₂	94
2.2.1 Synthesis of the living polymer.....	94
2.2.2 Synthesis of the living polymer end-capped with water	95
2.2.3 Synthesis of the living polymer with (S)-(+)-ibuprofen salt	95
2.2.4 Synthesis of the living polymer with PTM-029, F4, F39.....	96
2.3 Microparticles preparation	96
2.3.1 CLT Microparticles	96
2.3.2 CHT Microparticles.....	98
2.3.3 SASD Apparatus.....	98
2.4 Microparticles Characterization	100
2.4.1 Particle Size Distribution	100
2.4.2 Particle Morphology.....	100

2.4.3 Fourier Transform Infra Red (FT-IR).....	100
2.4.4 Water Content Determination	101
2.4.5 Aerodynamic Properties	101
2.4.5.1 Emitted Fraction.....	101
2.4.5.2 Anderson Cascade Impactor	102
2.4.6 Pharmacokinetic Studies	103
2.4.6.1 CLT and CHT microparticles.....	103
3. Results and Discussion	104
3.1 CLT Microparticles	104
3.1.1 Morphology	106
3.1.2 Aerodynamic Properties	112
3.1.3 Physical-Chemical Properties	114
3.1.4 Pharmacokinetic Studies	115
3.2 CHT Microparticles	117
3.2.1 Morphology	118
3.2.2 Aerodynamic Properties	122
3.2.3 Physical-Chemical Properties	123
3.2.4 Pharmacokinetic Studies	125
3.2.4 Biological Activity.....	126
4. Discussion	127
5. Conclusion	130
6. References.....	131
7. Annex 1.....	138

Index of Figures

Part I

Figure I. 1 - Radial tree depicting the phylogenetic relationships of 13 groups of actinomycetes within six different families. ⁷	5
Figure I. 2 - Structures of hybrid isoprenoids produced by actinomycetes. Isoprenoid portions of compounds are indicated in red ¹¹	7
Figure I. 3 - 16S rRNA gene phylogeny of the MAR4 clade. * and ** indicate that the clades represented by the <i>S. aculeolatus</i> and <i>S. synnematoformans</i> type strains, respectively. ⁸	9
Figure I. 4 - Hybrid isoprenoids structure classes detected from MAR4 strains. The terpene-derived portion of each molecule is highlighted in red. ⁸	10
Figure I. 5 - (A) Mevalonate pathway diagram showing the conversion of acetyl-CoA into isopentenyl pyrophosphate, the essential building block of all isoprenoids. The eukaryotic variant is shown in black. Archaeal variants are shown in red and blue. (B) Non-Mevalonate pathway. ¹⁰	13
Figure I. 6 - Examples of isoprenoids and their biosynthesis. ¹⁴	15
Figure I. 7 - Example of structures from napyradiomycins family A series (A), B series (B) and C series (C). ¹⁵	16
Figure I. 8 - UV profile of napyradiomycins family.	17
Figure I. 9 -Structures and proposed biosynthetic pathway of the chlorinated dihydroquinones 1–3. ¹⁶	18
Figure I. 10 - Diagram of experimental section: previously performed work is marked in blue and the one achieved in this project is presented in orange.	19
Figure I. 11 - (A) PTM-029 <i>Streptomyces aculeolatus</i> strain, (B) PTM-029 culture in 15 L medium and (C) PTM-029 crude extraction with EtOAc.	21
Figure I. 12 - Proposed structure of the pure compound PTM-029, F4, F39 based on NMR spectra.	26
Chromatogram 1 - (A) Chromatographic profile at $\lambda= 260\text{nm}$ and (B) DAD of fraction 2 (F2) from PTM-029 performed by HPLC. Fractions in highlight are pure compounds belonging to the napyradiomycins family.	54
Chromatogram 2 - (A) Chromatographic profile at $\lambda= 260\text{nm}$ and (B) DAD of fraction 3 (F3) from PTM-029 performed by HPLC. Fractions in highlight are pure compounds belonging to the napyradiomycins family.	54
Chromatogram 3 - (A) Chromatographic profile at $\lambda= 260\text{nm}$ and (B) DAD of fraction 4 (F4) from PTM-029 performed by HPLC. Fractions in highlight are pure compounds belonging to the napyradiomycins family.	55
Chromatogram 4 - (A) Chromatographic profile at $\lambda= 260\text{nm}$ and (B) DAD of fraction 5 (F5) from PTM-029 performed by HPLC. Fractions in highlight are pure compounds belonging to the napyradiomycins family.	55
Chromatogram 5 - (A) Chromatographic profile at $\lambda= 260\text{nm}$ and (B) DAD of fraction 6 (F6) from PTM-029 performed by HPLC. Fractions in highlight are pure compounds belonging to the napyradiomycin family.....	56
Chromatogram 6 - (A) Chromatographic profile at $\lambda= 260\text{nm}$ and (B) DAD of fraction 7 (F7) from PTM-029 performed by HPLC. Fractions in highlight are pure compounds belonging to the napyradiomycins family.	57
Chromatogram 7 - (A) Chromatographic profile at $\lambda= 260\text{nm}$ and (B) DAD of fraction 8+9 (F8+9, F1) from PTM-029 performed by HPLC. Fractions in highlight are pure compounds belonging to the napyradiomycins family.....	58

Chromatogram 8 - (A) Chromatographic profile at $\lambda = 260\text{nm}$ and (B) DAD of fraction 8+9 (F8+9, F2) from PTM-029 performed by HPLC.....	58
Annex 5. 1 - $^1\text{H-NMR}$ spectrum of PTM-029, F4, F39 in CDCl_3	73
Annex 5. 2 - $^{13}\text{C-NMR}$ spectrum of PTM-029, F4, F39 in CDCl_3	73
Annex 5. 3 - $^{13}\text{C-NMR DEPT 135}$ spectrum of PTM-029, F4, F39 in CDCl_3	74
Annex 5. 4 - COSY spectrum of PTM-029, F4, F39.	74
Annex 5. 5 - TOCSY spectrum of PTM-029, F4, F39.....	75
Annex 5. 6 - HSQC spectrum of PTM-029, F4, F39.	75
Annex 5. 7 - HMBC spectrum of PTM-029, F4, F39.	76
Annex 5. 8 - NOESY spectrum of PTM-029, F4, F39.....	76
Annex 5. 9 - ROESY spectrum of PTM-029, F4, F39.....	77
Annex 5. 10 - HR-Mass spectrum of PTM-029	77

Part II

Figure II. 1 - Example of different inhalers (a) is a nebulizer, (b) a pDMI and (c) a dry powder inhaler. ⁴¹	81
Figure II. 2 - (a) Representation of the different stages of the respiratory tract and the particles' deposition according to size. (b) Schematic representation of the Andersen Cascade Impactor, adapted from the European pharmacopoeia.	83
Figure II. 3 - Cholesterol structure.....	84
Figure II. 4 - Chitosan structure, where n is related to the DD % and m to $(100 - \text{DD} \%)$. Ideal chitosan would have $m=0$ and chitin would have $n=0$. Adapted from M. Dash et al. ⁵³ and J. Kumirska et al. ⁵²	85
Figure II. 5 - PLGA structure, with the lactic acid between the left-side brackets and the glycolic acid between the right-side brackets. x and y represent the number of times the unit it repeated.	87
Figure II. 6 - Mechanism of the living cationic ring-opening polymerization of 2-ethyl-2-oxazoline. ⁶⁷	88
Figure II. 7 - Phase diagram of CO_2 , adapted from W. Leitner et al. ⁸³	90
Figure II. 8 - Representation of the atomization mechanism, adapted from E. Reverchon et al. ⁷⁷ . 92	
Figure II. 9 - VLE of water- CO_2 -ethanol system, adapted from C. Duarte et al. ⁷⁹	92
Figure II. 10 - Schematic representation of the SASD apparatus: (CB) cryogenic bath; (LP) liquid pump; (HB) heating bath; (TC) temperature controller; (M) manometer; (S) saturator; (P) precipitator; (c) cyclone.....	99
Figure II. 11 - Schematic representation of the DUSA, adapted from Copley Scientific.	101
Figure II. 12 - Experimental set-up to perform ACI (adapted from European Pharmacopoeia).	103
Figure II. 13 - 0.25% (w/v) CLT-IBP ($\text{QCO}_2/\text{Qsol}=5$) microparticles. (A) SEM images of with a magnification of (a) 1,500x (b) 5,000x and (c) 10,000x and (B) Morphologi G3 images with magnification of (a) 20,000 and (b) 50,000 respectively.....	107
Figure II. 14 - 0.25% (w/v) CLT-IBP ($\text{QCO}_2/\text{Qsol}=8.3$) microparticles. (A) SEM images of with a magnification of (a) 1,500x (b) 5,000x and (c) 10,000x and (B) Morphologi G3 images with magnification of (a) 20,000 and (b) 50,000 respectively.....	108
Figure II. 15 - 0.5% (w/v) CLT-IBP ($\text{QCO}_2/\text{Qsol}=5$) microparticles. (A) SEM images of with a magnification of (a) 1,500x, (b) 5,000x and (c) 10,000x and (B) Morphologi G3 images with magnification of (a) 20,000 and (b) 50,000 respectively.....	108
Figure II. 16 - 0.5% (w/v) CLT-IBP ($\text{QCO}_2/\text{Qsol}=8.3$) microparticles. (A) SEM images of with a magnification of (a) 1,500x, (b) 5,000x and (c) 10,000x and (B) Morphologi G3 images with magnification of (a) 20,000 and (b) 50,000 respectively.....	109

Figure II. 17 - 0.5% (w/v) CLT-PLGA (40:60) microparticles. (A) SEM images of with a magnification of (a) 1,500x, (b) 5,000x and (c) 10,000x.....	109
Figure II. 18 - 0.5% (w/v) CLT-PLGA (50:50) microparticles. (A) SEM images of with a magnification of (a) 1,500x, (b) 5,000x and (c) 10,000x.....	109
Figure II. 19 - Figure 3.7 - 1% (w/v) CLT microparticles. (A) SEM images of with a magnification of (a) 1,500x, (b) 5,000x and (c) 10,000x and (B) Morphologi G3 images with magnification of (a) 20,000 and (b) 50,000 respectively.	110
Figure II. 20 - 1% (w/v) CLT-PEtOx-OH microparticles. (A) SEM images of with a magnification of (a) 1,500x, (b) 5,000x and (c) 10,000x and (B) Morphologi G3 images with magnification of (a) 20,000 and (b) 50,000 respectively.	110
Figure II. 21 - Figure 3.9 - 1% (w/v) CLT-PEtOx-IBP microparticles. (A) SEM images of with a magnification of (a) 1,500x, (b) 5,000x and (c) 10,000x and (B) Morphologi G3 images with magnification of (a) 20,000 and (b) 50,000 respectively.....	111
Figure II. 22 - Graphical representation of the powder distribution in the ACI stages for the CLT microparticles. (I.P. represents the induction port).	112
Figure II. 23 - FTIR. (a) CLT microparticles, (b) CLT-PEtOx-OH microparticles and (c) CLT-PEtOx-IBP microparticles.	114
Figure II. 24 - (A) In vitro drug release studies of PEtOx-IBP loaded in CLT microparticles at pH 7.4 and 35 °C and (B) release profile fitted through Korsmeyer-Peppas mathematical model for the first 60% of release.	116
Figure II. 25 - Korsmeyer-Peppas Model for mechanism of PEtOx-IBP release from the CLT microparticles at pH 7.4 and 35° C.....	117
Figure II. 26 - 1% (w/v) CHT microparticles. (A) SEM images of with a magnification of (a) 1,500x, (b) 5,000x and (c) 10,000x and (B) Morphologi G3 images with magnification of (a) 20,000 and (b) 50,000 respectively.	120
Figure II. 27 - 1% (w/v) CHT-PEtOx-OH microparticles. (A) SEM images of with a magnification of (a) 1,500x, (b) 5,000x and (c) 10,000x and (B) Morphologi G3 images with magnification of (a) 20,000 and (b) 50,000 respectively.	120
Figure II. 28 - 1% (w/v) CHT-PEtOx-IBP microparticles. (A) SEM images of with a magnification of (a) 1,500x, (b) 5,000x and (c) 10,000x and (B) Morphologi G3 images with magnification of (a) 20,000 and (b) 50,000 respectively.....	121
Figure II. 29 - 1% (w/v) CHT-PEtOx-PTM-029, F4, F39 microparticles. (A) Morphologi G3 images with magnification of (a) 20,000 and (b) 50,000 respectively.	121
Figure II. 30 - Graphical representation of the powder distribution in the ACI apparatus for the CHT microparticles.....	122
Figure II. 31 - FTIR. (a) CHT microparticles, (b) CHT-PEtOx-OH microparticles and (c) CHT-PEtOx-IBP microparticles.	124
Figure II. 32 - (A) In vitro drug release studies of PEtOx-IBP loaded in CLT microparticles at pH 7.4 and 35 °C and (B) release profile fitted through Korsmeyer Peppas mathematical model for the first 60% of release.	125
Figure II. 33 - Korsmeyer-Peppas Model for mechanism of PEtOx-IBP release from the CLT microparticles at pH 8 and 35° C.	126
Annex 1. Figure 1 - ¹ H-NMR spectrum of PEtOx-OH in DMSO- <i>d</i> ₆	137
Annex 1. Figure 2 - ¹³ C-NMR spectrum of PEtOx-OH in DMSO- <i>d</i> ₆	137
Annex 1. Figure 3 - ¹ H-NMR spectrum of PEtOx-IBP in DMSO- <i>d</i> ₆	138
Annex 1. Figure 4 - ¹³ C-NMR spectrum of PEtOx-IBP in DMSO- <i>d</i> ₆	138
Annex 1. Figure 5 - ¹ H-NMR spectrum of PEtOx-PTM-029, F4, F39 in DMSO- <i>d</i> ₆	139
Annex 1. Figure 6 - ¹³ C-NMR spectrum of PEtOx-PTM-029, F4, F39 in DMSO- <i>d</i> ₆	139

Index of Tables

Part I

Table I. 1 - Antibacterial activities and mass of the PTM-029 fractions obtained from the crude extract.	22
Table I. 2 - The eight fractions from PTM-029 with their total of pure compounds.	23
Table I. 3 - Antibacterial activity and respectively mass of pure compounds of F4 from PTM-029.	24
Table I. 4 - NMR spectroscopic data for a napyradiomycin derivative PTM-029, F4, F39 ^a	27

Part II

Table II. 1 - Comparison between the different inhalers relatively to different characteristics.	80
Table II. 2 - Composition of casting solutions with various concentrations of 0.25%, 0.5% and 1% (w/v) of total solids used for the preparation of CLT microparticles.	97
Table II. 3 - Composition of casting solutions with 1% (w/v) of total solids used for the preparation of CHT microparticles	98
Table II. 4 - Operating parameters of the CLT assays and the respective yields.	105
Table II. 5 - Properties of CLT microparticles.	106
Table II. 6 - Representation of the aerodynamic properties determined by ACI and DUSA for the CLT microparticles.	113
Table II. 7 - Water content values for 1% (w/v) CLT, 1% (w/v) CLT-PEtOx-OH and 1% (w/v) CLT-PEtOx-IBP microparticles.	115
Table II. 8 - Kinetic values obtained from the Korsmeyer equation for the 1% (w/v) CLT-PEtOx-IBP microparticles.	116
Table II. 9 - Operating parameters of the CHT assays and the respective yields.	118
Table II. 10 - Properties of CHT microparticles.	118
Table II. 11 - Representation of the aerodynamic properties determined by ACI and DUSA for the CHT microparticles.	123
Table II. 12 - Water content values for the CHT, CHT-PEtOx-OH and CHT-PEtOx-IBP microparticles.	124
Table II. 13 - Kinetic values obtained from the Korsmeyer equation for the 1% (w/v) CLT-PEtOx-IBP microparticles.	126

List of Abbreviations

ACI: Andersen cascade impactor
API: Active pharmaceutical ingredient
ACN: Acetonitrile
BSA: Bovine serum albumin
CHT: Chitosan
CLT: Cholesterol
EtOx: 2-ethyl-oxazoline
¹³C-NMR: Carbon-13 nuclear magnetic resonance
CROP: cationic ring-opening polymerization
COPD: Chronic obstructive pulmonary disease
COSY: Correlation Spectroscopy
Da: Aerodynamic diameter
DAD: Diode array detector
DMAPP: Dimethylallyl diphosphate
DMSO: Dimethyl Sulfoxide
D_{n,50}: Particle mean numeric diameter
DPI: Dry powder inhaler
DUSA: Dosage unit sampling apparatus
D_{v,50}: Particle mean volumetric diameter
EF: Emitted fraction
FDA: Food and Drug Administration
FPF: Fine particle fraction
FPP: Farnesyl diphosphate
FTIR: Fourier transform infrared
GGPP: Geranylgeranyl diphosphate
GPP: Diphosphate
GSD: Geometric standard deviation
HI: Hybrid isoprenoids
HMBC: Heteronuclear Multiple-Bond Correlation
HPLC: High-performance liquid chromatography
¹H-RMN: Proton nuclear magnetic resonance
HSQC: Heteronuclear Single Quantum Coherence

IBP: Ibuprofen
IPP: Isopentenyl diphosphate
LC-MS: Liquid Chromatography–Mass Spectrometry
MEP: Methylerythritol phosphate pathway
MMAD: Mass median aerodynamic diameter
MIC: Minimum Inhibitory Concentration
MRSA: Methicilin-resistant *Staphylococcus aureus*
NGI: Next Generation Impactor
pDMI: Pressurized metered dose inhalers
PEG: Polyethylene glycol
PEtOx-IBP: 2-ethyl-oxazoline end-capp with Ibuprofen salt
PEtOx-PTM-029, F4, F39: 2-ethyl-oxazoline end-capp with marine bioactive compound
PEtOx-OH: 2-ethyl-oxazoline end-capp with water
PLGA: Poly (lactic-co-glycolic acid)
PTases: Prenyltransferases enzymes
PTM- # - the strain code and /or extract obtained from ocean sediments of Archipelago Madeira
PS: Particle size
PSD: Particle size distribution
RESS: Rapid expansion of a supercritical solution
SAS: Supercritical antisolvent
SASD: Supercritical assisted spray-drying
scCO₂: Supercritical carbon dioxide
SEM: Scanning electron microscope
THN: Pentaketide 1,3,6,8-tetrahydroxynaphthalene
T_g: Glass transition temperature
TOCSY: Total Correlation Spectroscopy
V-CIPOs: Vanadium-dependent haloperoxidases
VLE: High-pressure vapor liquid equilibria
VRE: Vancomycin-resistant *Enterococcus faecium*

Overview

This thesis theme emerges from the need to fight lower respiratory infections which affects the lower airways (trachea, bronchi, bronchioles and lungs) caused by pathogenic bacteria, virus or fungi.⁴ In 2013 infections such as pneumonia, pulmonary tuberculosis, bronchitis, among others were the leading cause of sickness and mortality, both in children and adults, causing 2.7 million deaths worldwide, 4.8% of the overall deaths.¹ Therefore consists in a health, societal and economic problem. The treatment of such infections relies on antibiotic therapy. However, antibiotic resistance to human pathogens continues to increase, as a consequence of the misuse of antibiotics and pathogen evolution.^{2,5} It is, more than ever, imperative not only to discover new lead-like drug agents, but also to develop new drug delivery systems for pulmonary diseases.^{3,5}

Part I - Isolation of bioactive compounds from marine *Actinobacteria*

1. Introduction

1.1 Natural products

Natural products are chemical compounds produced by living organisms that are found in nature, from prokaryotic bacteria and eukaryotic microorganisms to fungi, plants and animals.⁶ These compounds are produced by the pathways of primary or secondary metabolism from living organisms. The primary metabolites (amino acids, nucleotides, and vitamins) are common in all biological systems. The secondary metabolites are, however, low molecular weight (MW<3000), chemically diverse compounds, usually exhibiting a wide range of biological activities.⁶

Since the discovery of the antibiotic properties of penicillin by Alexander Fleming in 1928, through the “golden age” of antibiotics and into to our days, the result of this frenzied research lead to the discover of ten thousands of natural products derived from microbial sources. Even though, drug discovery strategies changed in the 1990s, techniques such as combinatorial chemistry, high-throughput screening, and computer-assisted design of small-molecule ligands created alternatives to traditional drug discovery paradigms. Yet like many trends, the interest towards these fields showed some cyclic features with successes and failures associated with the evolution around the clinical needs and new enabling technology. The renewed interest in drug discovery comes at a time when it is widely perceived that the pipeline for new antibiotics discovery is running dangerously low. It is also a response to the realization that bacterial diversity and major environmental habitats have not been efficiently explored.^{6,7}

Given the vastness of the world’s oceans (70% of the Earth’s surface) harboring most of the planet’s biodiversity, the oceans are a highly complex microbiological environment with typical microbial abundances of 10^6 and 10^9 per ml in seawater and ocean-bottom sediments, respectively. As DNA sequencing based methods are applied to the field of marine microbial ecology, it is known how complex, exquisitely unique and highly adapted these organisms are.

Natural products remain both a fundamental source of new chemical diversity and an integral constituent of today’s pharmaceutical compendium.⁷

1.2 Actinomycetes from marine sources

Bacteria are an exceptional source of chemical diversity. Among them, species of the Order *Actinomycetales* (commonly called actinomycetes), a group of Gram-positive bacteria, are the single most productive source of microbial derived natural products, accounting for *ca.* 75% of all antibiotics discovered from the genus *Streptomyces*, as well as a broad range of anticancer agents.^{6,7,8} Therefore, marine bacteria are an important resource for drug discovery.

Although actinomycetes are best known as soil bacteria, a growing interest in its distribution and ecological role in the marine environment has been observed. Thus, in the last decades several research efforts have been done to tackle the marine actinomycetes biodiversity, which allowed to discover a significant number of new marine-derived actinomycetes belonging to the genus *Micromonospora*, *Streptomyces*, *Nocardia*, *Rhodococcus*, *Dietzia*, *Prauserella*, *Serinicoccus*, *Marinophilus*, *Solwaraspora*, *Lamerjespora*, *Aeromicrobium*, *Williamsia*, *Marinactinospora*, *Sciscionella*, *Salinospora* and *Marinospora*.⁹

The actinomycetes can be divided into MAR groups, *Salinispora* genus has an obligate requirement of seawater, or more specifically sodium, for growth. Actinomycetes genera are spread into 13 MAR groups, in which there are 6 distinct families (Figure I. 1). Among this new diversity there are specimens of MAR4 streptomycete lineage⁷ which is the object of the present study.

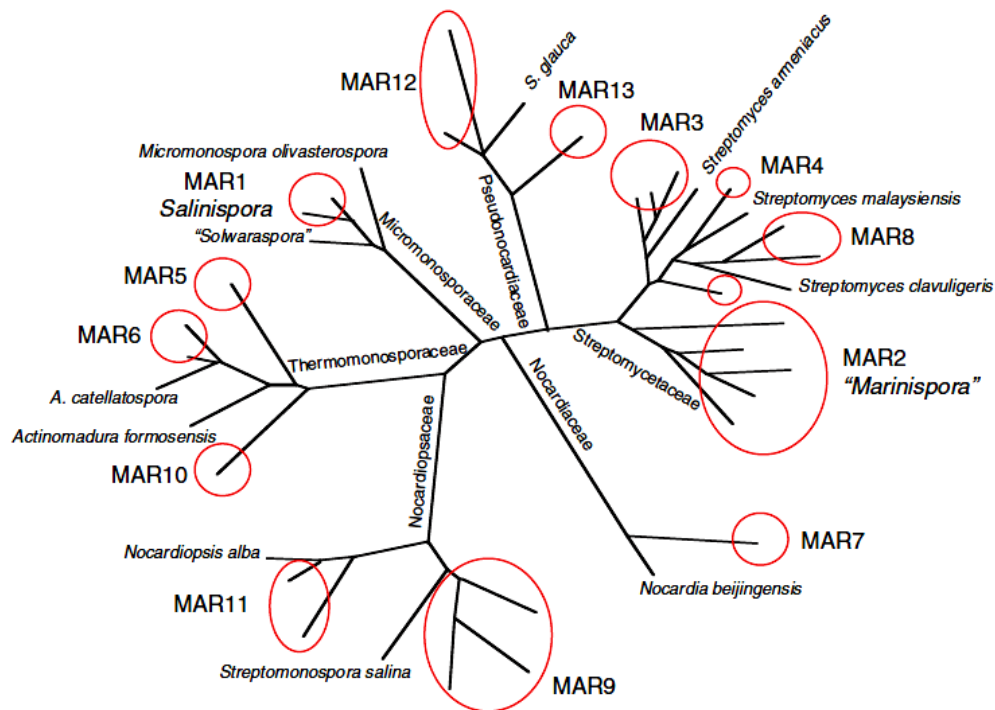


Figure I. 1 -Radial tree depicting the phylogenetic relationships of 13 groups of actinomycetes within six different families.

1.3 Actinomycetes terpenoids

Terpenoids play important roles in all living organisms; they function as steroid hormones in mammals, carotenoids in plants, and ubiquinone or menaquinone in bacteria. They are the most ubiquitous class of metabolites observed in nature that provide diverse functions in both primary and secondary metabolism. Also, they are assembled from five-carbon isoprene subunits into a wide assortment of structures that generally range from monoterpenes (two isoprene units) to triterpenes (six isoprene units), and in certain cases can also be larger [monoterpenes (C₁₀), sesquiterpenes (C₁₅), and diterpenes (C₂₀)].^{10,11,12}

Although actinomycetes bacteria are one of the primary sources of microbial derived secondary metabolites, they rarely produce compounds with this biosynthetic class.¹⁰ Terpenoid moieties can be attached to molecules produced via non-terpenoid biosynthetic routes forming products known as hybrid isoprenoids (HIs). As secondary metabolites, they are common in plants, insects, fungi, and some marine invertebrates such as soft corals.¹³ They are known to play diverse ecological roles in signaling and chemical defense and are responsible for many of the common

odors and flavors associated with plants and fruits. HIs include significant structural diversity and biological activity and thus are important targets for drug discovery.¹¹

1.4 Hybrid isoprenoids classes obtained from marine environmental bacteria sources

HIs are metabolites in which terpenoid moieties of varying levels of complexity are attached to diverse molecules such as polyketides, ribosomal and non-ribosomal peptides, phenazines and pyrroles. The attachment of an isoprenoid to another molecule is referred to as 'prenylation' and can increase biological activity, perhaps due to the increased affinity of the isoprene unit for biological membranes. Isoprenoid units are attached to non-terpenoid small molecules via prenyltransferase enzymes (PTases). The point of attachment can be a carbon, oxygen, or nitrogen atom or another isoprene unit, in which case head to tail assembly is the norm but reverse prenylation is also observed. These processes result in the generation of extraordinary chemical diversity and although HIs are generally considered in this context of secondary metabolism, not all fall into this category. Although reports of HI secondary metabolites from actinomycetes are relatively rare, the first been discovered from a marine-derived actinomycetes was marinone (Figure I. 2, **(9)**) in 1992, being a significant compound in terms of both structural novelty and biological activity. Figure I. 2 shows a list of the several most important HI secondary metabolites that have been isolated from actinomycetes, showing how diverse they can be.¹¹

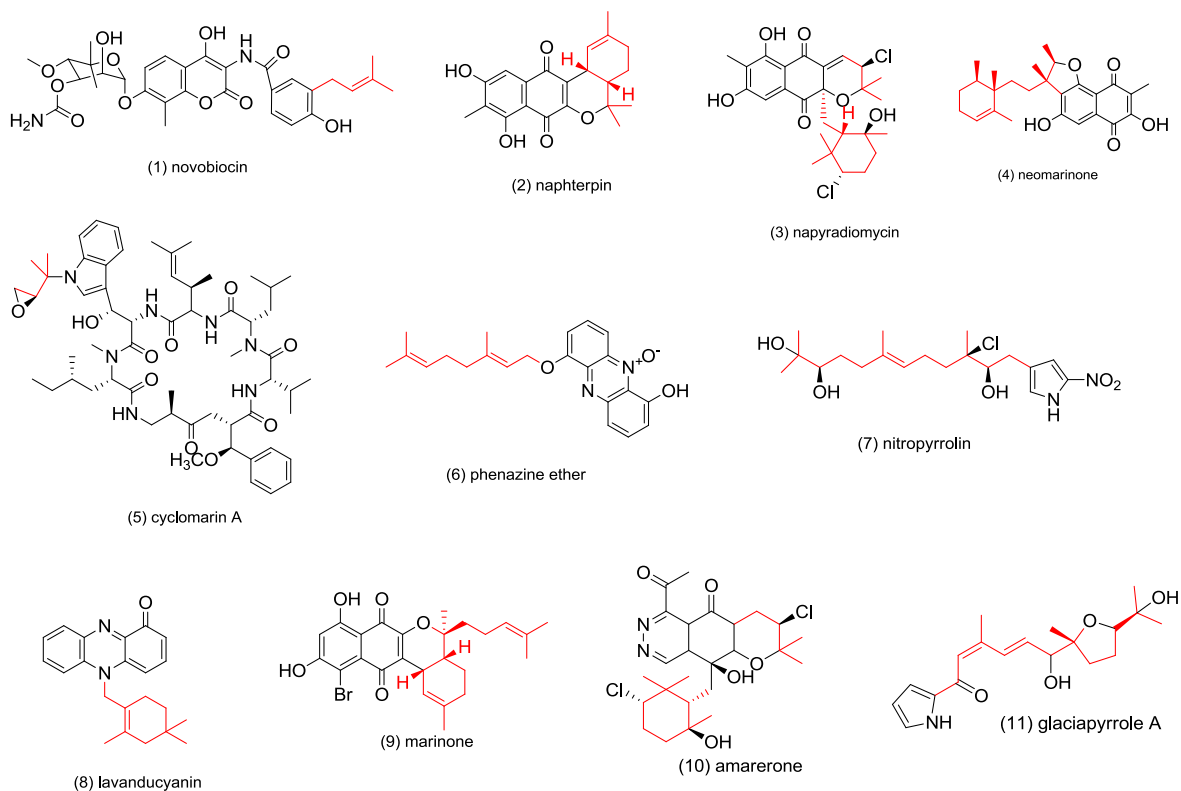


Figure I. 2 - Structures of hybrid isoprenoids produced by actinomycetes. Isoprenoid portions of compounds are indicated in red¹¹

1.5 Phylogenetic and chemical diversity of a hybrid-isoprenoid-producing streptomycete lineage

The genus *Streptomyces* is extraordinarily diverse, with nearly 600 formally described species. These filamentous, Gram-positive bacteria dedicate a large portion of their genomes to produce structurally diverse secondary metabolites, many of which have become useful pharmaceutical agents. *Streptomyces* spp. are generally saprophytic and known soil inhabitants, where they play important ecological roles in the breakdown of recalcitrant organic materials and the suppression of plant pathogens. They are also widely distributed in marine sediments, form symbiotic relationships with plants and insects, and are observed in association with marine sponges. Some streptomycete lineages have been observed broadly both in soils and in marine sediments, suggesting a high degree of environmental flexibility. The ecological functions of most streptomycete secondary metabolites have not been defined, and thus, potential links between secondary metabolite production and environmental adaptation remain largely unknown.^{6, 8}

A phylogenetic analysis of HI producers reveals how they are sporadically distributed throughout the *Streptomyces* phylogenetic tree. From all the thirteen MAR groups, a robust clade enriched in strains is able to produce this class of compounds. From phylogenetic studies this clade is identified as a marine lineage within the genus *Streptomyces*, and it was given the designation MAR4.^{8, 11}

The MAR4 clade currently includes 57 strains, 47 of which were isolated from marine sediments. To date, are recognized within this clade, the type strains of *S. aculeolatus* and *S. synnematoformans*, which were isolated from a terrestrial soil sample and a sand dune sample, respectively, being the only formally described species within the clade (Figure I. 3). The 57 members of the MAR4 clade share as little as 96.2% 16S rRNA gene sequence identity and thus contain as much phylogenetic diversity as many bacterial genera.⁸

The MAR4 lineage has been reported to be mainly of marine source origin and recognized as a prolific source of hybrid isoprenoids secondary metabolites. While terpenoids are relatively common plant secondary metabolites, they are considered a rare part of actinomycetes secondary metabolism.^{8, 11}

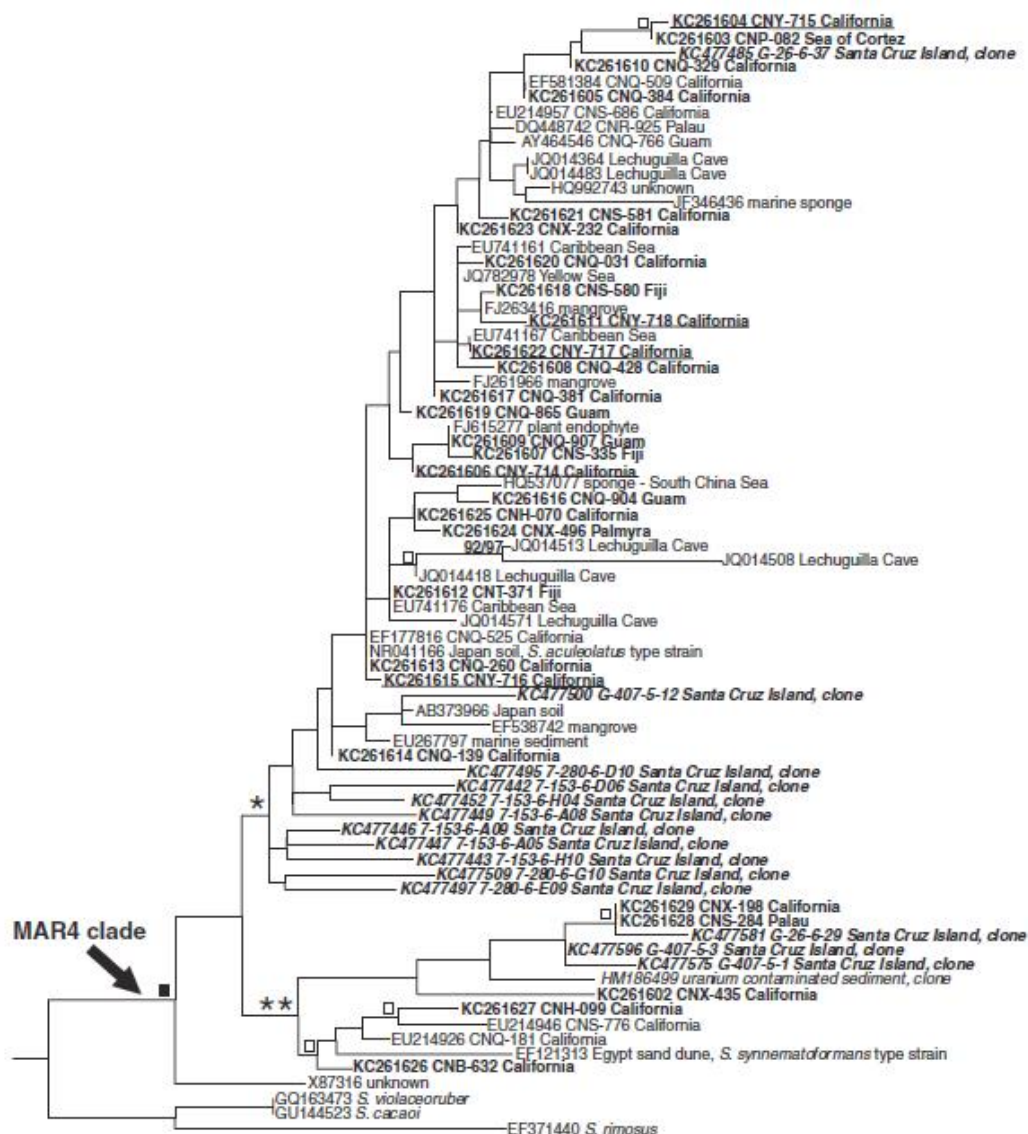


Figure I. 3 - 16S rRNA gene phylogeny of the MAR4 clade. * and ** indicate that the clades represented by the *S. aculeolatus* and *S. synnematoformans* type strains, respectively.⁸

The actinomycete-derived HI secondary metabolites discovered from MAR4 clade include napyradiomycins, marinones, nitropyrrolins, and lavanducyanis (Figure I. 4). These compounds are not only structurally diverse but can also display potent biological activities (antitumor, antibiotic, antioxidant, and other biological activities), supporting their value as a relevant target and resource for drug discovery.^{7, 8}

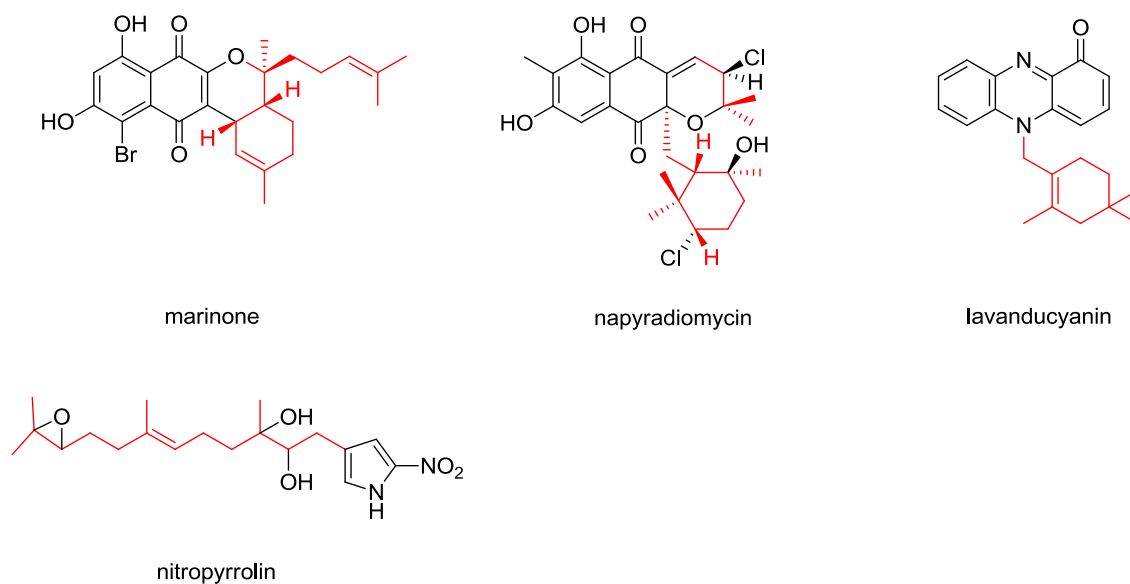


Figure I. 4 - Hybrid isoprenoids structure classes detected from MAR4 strains. The terpene-derived portion of each molecule is highlighted in red. ⁸

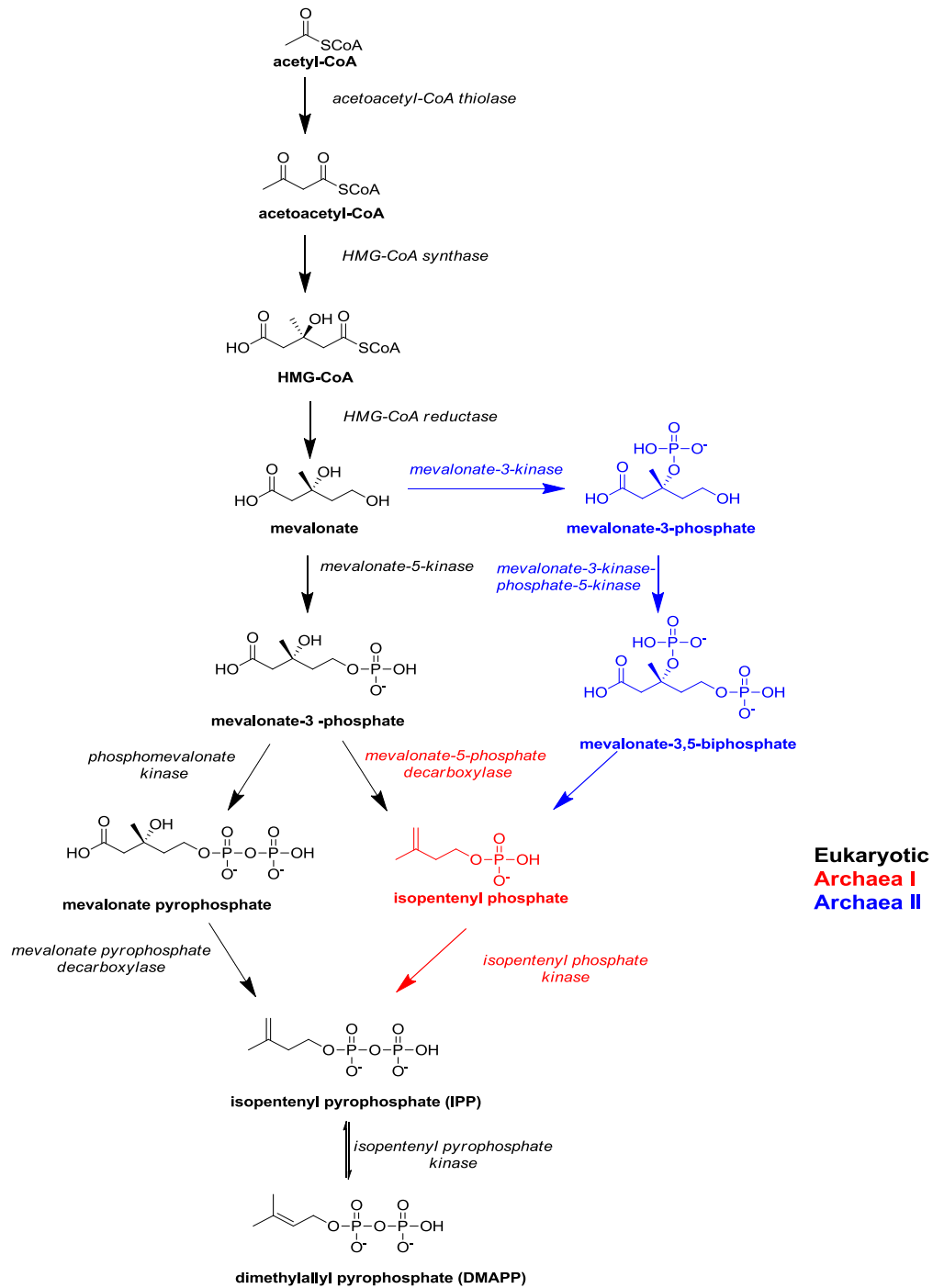
Interestingly, the compounds produced by the MAR4 strains show some evidence of phylogenetic clustering, with all of the napyradiomycin producers falling into the clade represented by *S. aculeolatus*. Most notable among these strains is CNQ-509, which is able to produce HI compounds incorporating, besides napyradiomycin class, phenazine and pyrrole scaffolds. The production of such diverse HIs by one strain is remarkable considering the relative rarity of terpenoid chemistry in actinomycetes secondary metabolism. Six additional MAR4 strains produce HIs that incorporate at least two different scaffolds revealing that the production of diverse HIs is a common feature of this group. Additional phylogenetic clustering is observed in the *S. synnematoformans* lineage of the MAR4 clade, *S. synnematoformans* where all of the marinone producers reside with the exception of strain CNQ-381. The correlation between 16S phylotype and secondary metabolite production provides evidence of vertical inheritance within more recently evolved lineages. The observation that all MAR4 strains, with the exception of *S. synnematoformans*, have demonstrable capacities to produce HI secondary metabolites indicates that the selective cultivation of new MAR4 diversity represents a logical and potentially productive strategy for the isolation of new HI secondary metabolites. No other similarly related cluster of strains within the phylogenetic tree shows a comparable prolificacy for HI production. ¹¹

1.6 Biosynthesis of hybrid isoprenoids from actinomycetes sources

Terpenoids are synthesized by consecutive condensations of an isoprene unit, isopentenyl diphosphate (IPP), to its isomer, dimethylallyl diphosphate (DMAPP).¹⁰

Isoprenoids are the largest single family of natural products, with more than 23,000 known examples, and include industrially useful compounds such as flavors, antibiotics, and plant hormones. All of these metabolites can be classified into several groups. This classification is based on the number of C5 units derived from isopentenyl diphosphate (IPP), which is biosynthesized via the mevalonate pathway in eukaryotes, archae, and the cytoplasm of plants, while the methylerythritol phosphate pathway (MEP) is used in prokaryotes and the chloroplasts of plants (Figure I. 5). The groups include monoterpenes (C10), sesquiterpenes (C15), and diterpenes (C20). All these compounds are biosynthesized from the corresponding polyprenyl diphosphate. Geranyl diphosphate gives rise to monoterpenes, farnesyl diphosphate to sesquiterpenes, and geranylgeranyl diphosphate to diterpenes.¹²

(A)



(B)

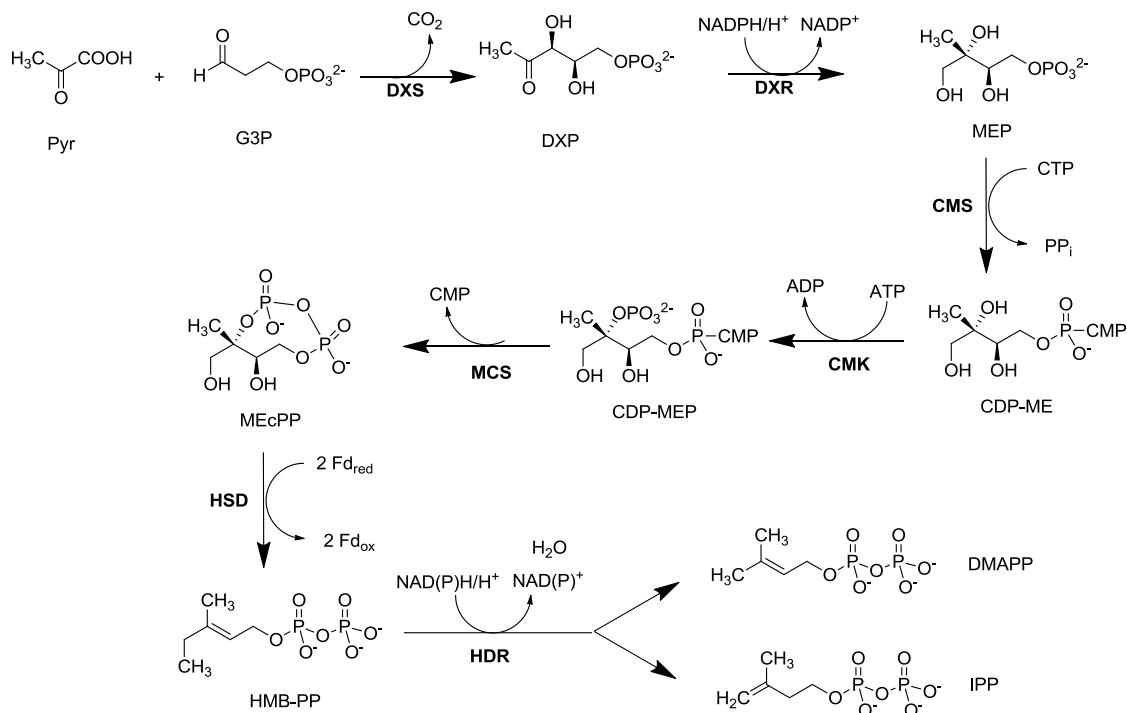


Figure I. 5 - (A) Mevalonate pathway diagram showing the conversion of acetyl-CoA into isopentenyl pyrophosphate, the essential building block of all isoprenoids. The eukaryotic variant is shown in black. Archaeal variants are shown in red and blue. (B) Non-Mevalonate pathway.¹⁰

In eukaryotes such as plants and fungi, which produce the vast majority of isoprenoids, the polyprenyl diphosphate is generally cyclized by an organism-specific isoprenoid cyclase to form a basic skeleton. This is followed by successive reactions, such as hydroxylation, methylation, and glycosylation that give rise to many thousands of compounds. In contrast to eukaryotes, prokaryotes are known to produce a limited number of isoprenoids. Moreover, it was recently revealed that among prokaryotes, actinomycetes produce many types of isoprenoids in relatively large numbers, and the structures of these compounds are unique and different from those of eukaryotic origin. In particular, isoprenoid moieties of the compounds produced by actinomycetes are generally attached to other moieties, such as an aromatic ring, an amino acid, and a phenazine moiety.^{12, 14}

All isoprenoid backbones (Figure I. 6) are constructed using dimethylallyl diphosphate (DMAPP, 2) as the chain initiation unit and isopentenyl diphosphate (IPP, 1) as the chain elongation unit. The chain length and stereochemistry of the resulting prenyl diphosphate are specified by the corresponding prenyltransferases. For example, the formation of geranyl diphosphate (GPP, 3), farnesyl diphosphate (FPP, 4) and geranylgeranyl diphosphate (GGPP, 5) are

controlled by the size of the hydrophobic channels in the GPP synthase, FPP synthase and GGPP synthase active sites, respectively. Further chain elongation from FPP by isoprene (C5) units leads to the production of polyprenol with the isoprene units in either a *cis*- or a *trans*-stereochemistry (Figure I. 6). These prenyl diphosphates are the starting material for the construction of all isoprenoids with diverse structures. There are two major types of isoprenoid skeleton construction mechanisms and the first type is the prenyltransferase-catalyzed reaction (*e.g.*, squalenes (8) in Figure I. 6). Alternatively, the acceptors of the prenyltransfer reactions can be other families of natural products (*e.g.*, flavonoids, polyketides) and this results in the formation of hybrid-types of isoprenoids (*e.g.*, napyradiomycin A (9) and naphterpin (10), in Figure I. 6). The second type of isoprenoid skeleton is constructed through cyclase catalyzed cyclization reactions (*e.g.*, the red portion in taxol (11), in Figure I 6.). After the isoprenoid skeletons are constructed, they are further tailored by many subsequent modifications to form the final products with their complex structures.¹⁴

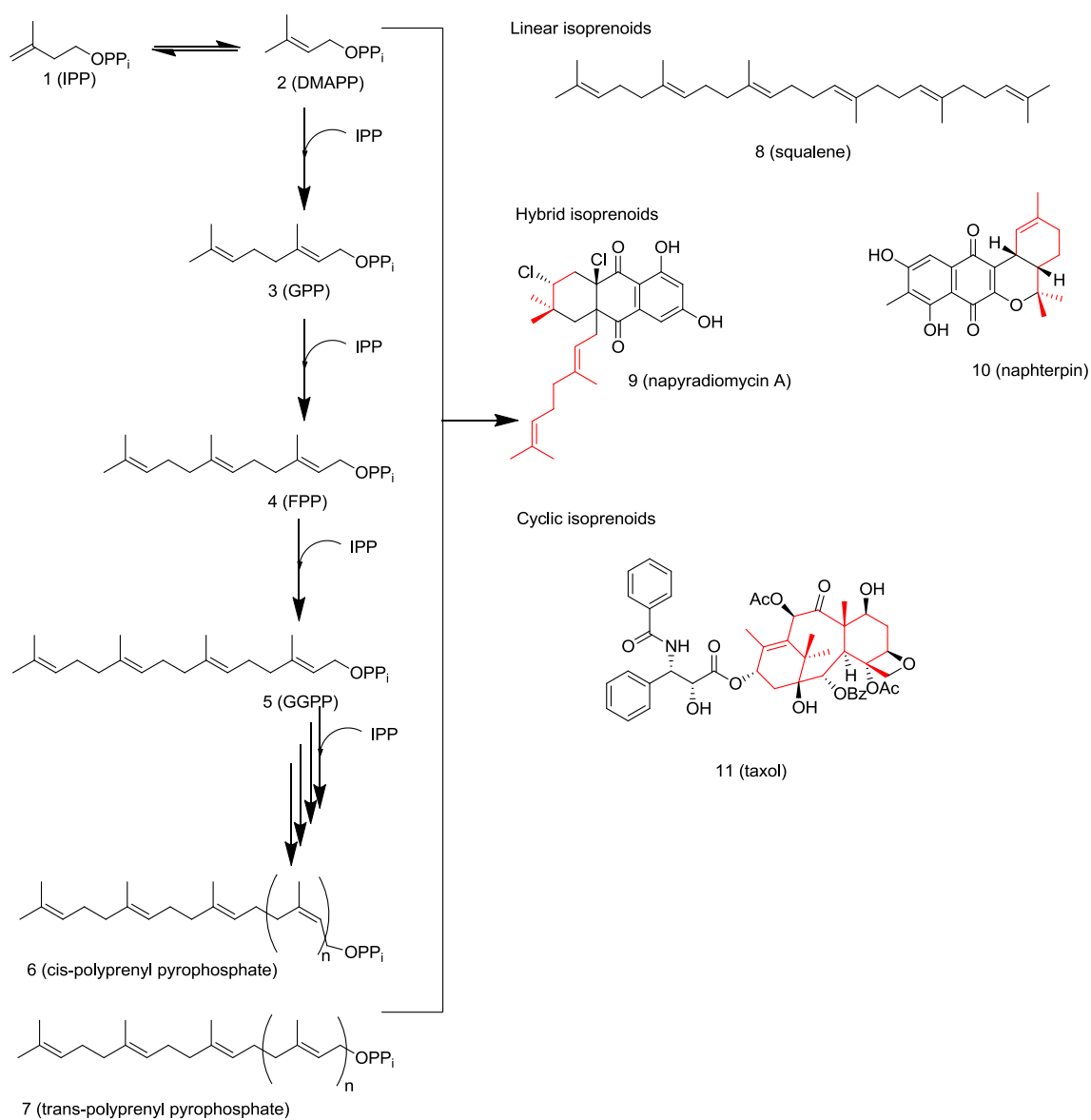


Figure I. 6 - Examples of isoprenoids and their biosynthesis. ¹⁴

1.7 Napyradiomycins

Within MAR4 clade, a group of novel antibacterial agents, napyradiomycins, was first isolated from the soil-derived bacterium *Chainia rubra* G802-AF, from Japan in 1986. As time passed, a series of congeners were isolated from different actinomycetes, such as *Streptomyces antimycoticus*, *S. aculeolatus*, and other *Streptomyces* species, and also from a marine source derived strain. The napyradiomycins are meroterpenoids composed of polyketide and terpenoid components which are formed by a process that involves halogen-induced cyclization. In annex 1 are listed all the napyradiomycins discovered since 1986 until now, in the MAR4 clade.²

Structurally, napyradiomycins consist of a semi-naphthoquinone core, a prenyl unit attached at C-4a that is cyclized to form a tetrahydropyran ring in most cases, and a monoterpene substituent attached at C-10a. Structure variations of napyradiomycins arise mainly from the 10-carbon monoterpene subunit, which is linear (napyradiomycin A series), or cyclized to a 6-membered ring (napyradiomycin B series), or cyclized to a 14-membered ring (napyradiomycin C series) (Figure I. 7). The different halogenation patterns also contribute largely to structure variations of napyradiomycins.¹⁵

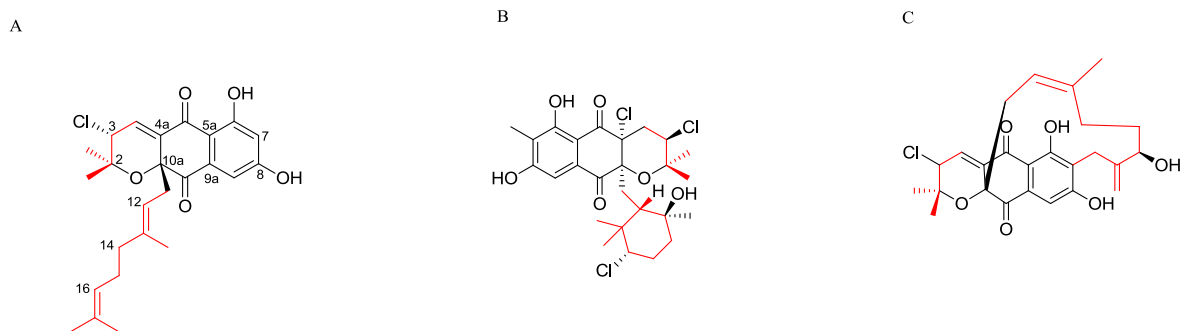


Figure I. 7 - Example of structures from napyradiomycins family A series (A), B series (B) and C series (C).¹⁵

Napyradiomycins family has a characteristic UV profile at maximum of absorbance of 260 nm which allows their easy identification (Figure I. 8).

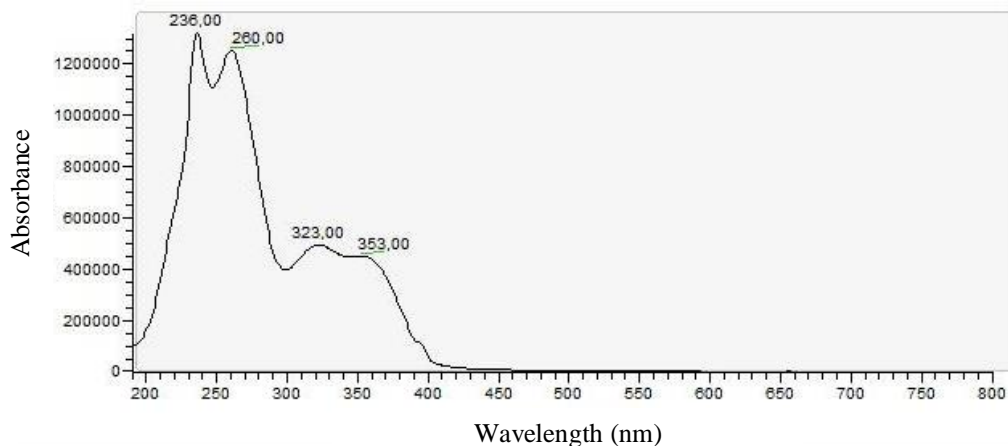


Figure I. 8 -UV profile of napyradiomycins family.

Biosynthetically, napyradiomycins originate from a HI / polyketide pathway which is rare in nature. Bacterial meroterpenoid antibiotics belonging to the napyradiomycin family of chlorinated dihydroquinones suggests that the biosynthetic cyclization of their terpenoid subunits is initiated via a chloronium ion. The vanadium-dependent haloperoxidases that catalyze such reactions are distributed in fungi and marine algae.¹⁶

Winter *et al.* in 2007 studied the napyradiomycin biosynthetic cluster (nap) and, not only demonstrated that the enzymes were able to initiate cyclization of a terpene by a bromonium ion, but also proved that the halogenation reaction occurred with stereochemical control.¹⁶

Napyradiomycins family of chlorodihydroquinones are biosynthesized from the symmetrical pentaketide 1,3,6,8-tetrahydroxynaphthalene (THN) and isoprenoid units. In most cases, the isoprenoid building blocks are derived from the mevalonic acid biosynthetic pathway. A biosynthetic scheme for the production of this compound was proposed on the basis of the molecular logic of the nap cluster (Figure I. 9). The dihydroquinone core is catalyzed by the type III polyketide synthase homologous THN synthase NapB1, which condenses five malonyl-CoA molecules to THN. The monooxygenase NapB2 putatively oxidizes THN to flaviolin, which is then methylated by the methyltransferase NapB5. Attachment of the first isoprene unit, using dimethylallyl pyrophosphate as the substrate, occurs through a nucleophilic attack involving one of the two prenyltransferases (NapT8/T9). Hydrogenation or chlorination at C-2 by the FADH2-

dependent halogenase NapH2 may facilitate the second prenylation reaction at C-3 with geranyl pyrophosphate by the second nap prenyltransferase to yield the diprenylated intermediate SF2415B1. Cyclization of the hemiterpene subunit via a chloronium ion is putatively catalyzed by one of the three nap V-CIPOs (NapH1, H3, H4) giving rise to the 7-methyl derivative of napyradiomycin A1. The monoterpene subunit of 7-methylnapyradiomycin A1 putatively undergoes a related V-CIPO-facilitated cyclization to form 1 and 3, in which a molecule of water is incorporated into the cyclohexanol moiety. Further dechlorination of 1 likely gives rise to 2 (Figure I. 9).¹⁶

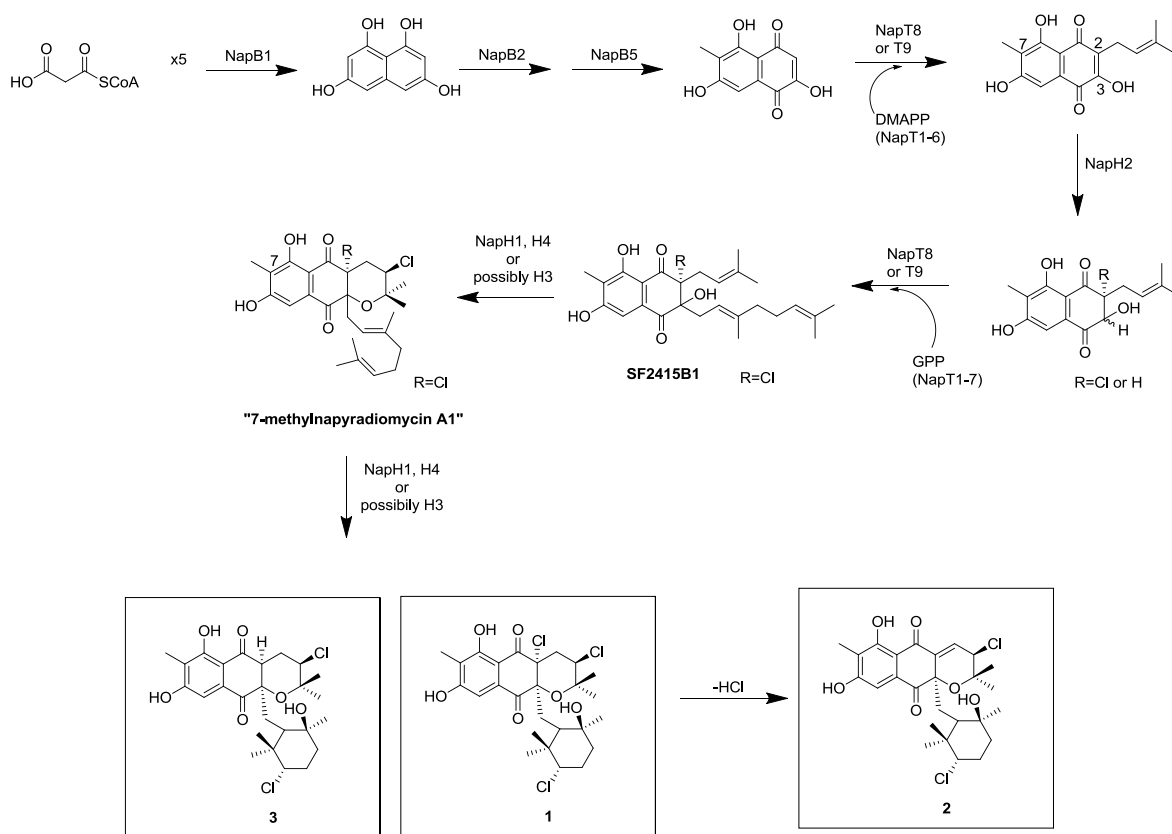


Figure I. 9 - Structures and proposed biosynthetic pathway of the chlorinated dihydroquinones 1-3.¹⁶

Napyradiomycins exhibit a diverse range of biological activities, including antimicrobial activity against methicillin-resistant *Staphylococcus aureus* (MRSA) or vancomycin-resistant *Enterococcus* (VRE), cytotoxicity against HCT-116 human colon adenocarcinoma cells (Annex 2), gastric (H^+ - K^+) ATPases inhibiting activities, as estrogen receptor antagonists, as well as apoptosis-inducing activities.¹⁵

2. Experimental Section

This work was conducted under the project: "Tesouros Oceânicos- Sedimentos oceânicos do arquipélago da Madeira: nova fonte de compostos inovativos e bioativos" ref. PTDC / QUI-QUI / 119116/2010. The global procedure steps are outlined in the following diagram:

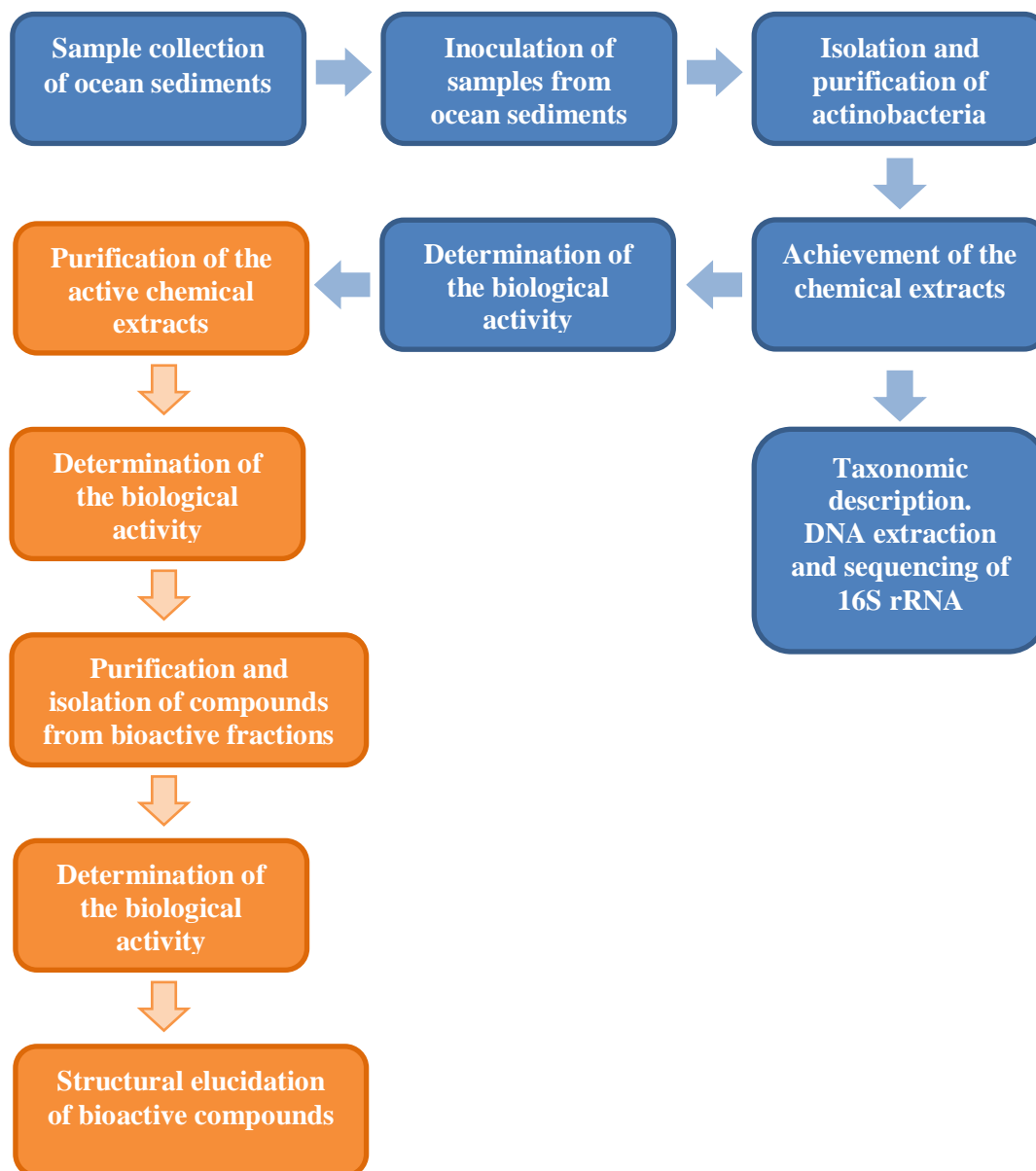


Figure I. 10 - Diagram of experimental section: previously performed work is marked in blue and the one achieved in this project is presented in orange.

2.1 Materials

All chemicals and solvents were used without further purification. Ethyl acetate (99.8% purity), isooctane (99.5% purity), methanol (99.9% purity), water and acetonitrile (99.9% purity, HPLC grade) were purchased from ProLabo. Silica gel 60 was purchased from Merck, sea and sand washed from Panreac, chloroform-D ($\geq 99.8\%$ purity) and dimethyl Sulfoxide (99.9% purity) from Cambridge Isotope Lab. and trifluoroacetic acid ($\geq 99.9\%$ purity) from Sigma-Aldrich.

2.2 General Experimental Procedures

1D and 2D NMR spectroscopic data were performed with a Bruker Advance 400MHz with samples in CDCl_3 . Low-resolution LC/MS data were measured using a Finnigan Surveyor by Thermo ScientificTM equipped with a reversed-phase C_{18} column (Phenomenex Luna, 4.6 x 100 mm, 5 μm) at a flow rate of 0.9 mL/min. High-resolution mass spectra were obtained using an GC-TOF method. HPLC purifications were performed using a Dionex Ultimate 3000 system controller and pumps with a model 300 spectrophotometer, using Phenomenex Luna semipreparative C_{18} (250 x 10 mm, 5 μm) column at flow rates of 1.5 mL/ min with various ratios of ACN/ H_2O gradient.

2.3 Collection, Identification, Cultivation, and Extraction of Strain PTM-029

Actinomycetes strain PTM-029 was isolated on A1 agar medium (10 g of starch, 4 g of yeast extract, 2g of peptone, 18 g of agar, and 0.75 L of seawater and 0.25 L distilled water) from a sediment sample collected at a depth at 728 m along Madeira Archipelago, in June 2012. The 16S rRNA gene sequence for this strain has been identified in CREM (Centro de Recursos Microbiológicos). It shares 97.0% sequence identity with the type strain for *Streptomyces aculeolatus*, found to be part of the MAR4 group. The strain was cultured in a liquid medium composed of the previously described nutrients, at 25 °C for 7 days with shaking at 200 rpm. The strain was extracted with ethyl acetate, and the solvent removed under vacuum to generate the crude extract.

2.4 Isolation of Napyradiomycins

The extract was fractionated by silica flash chromatography using various ratios of isooctane/EtOAc (100:0, 80:20, 60:40, 40:60, 20:80 and 0:100) and methanol/EtOAc (10:90, 50:50 and 100:0) to produce 9 fractions of increasing polarity. These fractions were then analyzed by LC-MS. Pure compounds were obtained by HPLC (Table I. 2).



Figure I. 11 - (A) PTM-029 *Streptomyces aculeolatus* strain, (B) PTM-029 culture in 15 L medium and (C) PTM-029 crude extraction with EtOAc.

2.5 Antibiotic Assay

The antibiotic assays were performed by the laboratory technician Tiago Dias.

Methicillin-resistant *Staphylococcus aureus* (MRSA)¹⁷ and vancomycin-resistant *Enterococcus faecium* EF82 (VRE) strains were grown overnight at 37 °C in BHI media (17.5g brain heart infusion, 10g enzymatic digest of gelatin, 2g dextrose, 5g sodium chloride and 5g disodium phosphate). The culture was diluted to 0.04-0.06 OD, further diluted 1:10, and then added to the top row of a 96-well microtiter plate. Test materials were added to the top row, serially diluted (1:2) downward, and incubated for 18-24 h at 37 °C. DMSO was used to monitor the viability of the culture without the crude extract, vancomycin solution was used to monitor the cell growth inhibition of MRSA strain and if does not inhibit the culture of VRE EF82 strain. Optical density (OD) was measured at 600 nm using a Ultrospec™ 3100 pro UV/Visible reader.

3. Results

3.1. PTM-029 crude extract, fractionation, and antibacterial activity assessment

After PTM-029 fractionation, biological tests were performed to determine the minimum inhibitory concentration (MIC) as described in chapter 2.5, against pathogenic bacteria MRSA and VRE EF82. Table I.1 describes the biological activity obtained for the PTM-029 fractions.

Table I. 1 - Antibacterial activities and mass of the PTM-029 fractions obtained from the crude extract.

PTM-029 fraction	Mass of the fraction (g)	MIC ($\mu\text{g/mL}$)	
		MRSA	VRE EF82
F1	0.0492	-	-
F2	0.1717	62.50	62.50
F3	0.1689	15.60	31.30
F4	0.1016	7.81	3.91
F5	0.0532	15.60	3.91
F6	0.0664	31.30	3.91
F7	0.1809	0	31.30
F8	0.1126	0	250
F9	0.0177	0	62.50

3.2. Isolation of PTM-029 compounds by HPLC and its antibacterial activity

The fractions from PTM-029 that showed biological activity, proceeded to separation of the existing compounds by HPLC, as described in chapter 2.2 and 2.4. The HPLC chromatograms of PTM-029 fractions can be seen in Annex 3, as well as the pure compounds that are highlighted in each one.

The pure compounds were also subjected to biological tests against pathogenic bacteria MRSA and VRE EF82, as described in section 2.5 and the values of the biological activity can be seen in Annex 4. In Table I. 2 are presented the total pure compounds obtained from each fraction of PTM-029 and in Table I. 3 the antibacterial activity of fraction 4, and the most promising compound PTM-029,F4,F39 proceeded for structure elucidation.

Table I. 2 - The eight fractions from PTM-029 with their total of pure compounds.

Fraction	Total pure compounds	Number of bioactive compounds	Napyradiomycin UV profile
F2	34	8	5
F3	63	24	8
F4	49	21	18
F5	46	23	6
F6	60	35	4
F7	46	20	9
F8+9	25	17	1

Table I. 3 - Antibacterial activity and respectively mass of pure compounds of F4 from PTM-029.

Sample	Samples mass (mg)	MIC ($\mu\text{g/mL}$)	
		MRSA	VRE EF82
PTM-29 F4, F27	2	62.50	125
PTM-29 F4, F28	2.80	31.30	0
PTM-29 F4, F29	2.60	62.50	62.50
PTM-29 F4, F30	2.50	62.50	62.50
PTM-29 F4, F31	2	31.30	15.60
PTM-29 F4, F32	3.10	250	0
PTM-29 F4, F33	2.60	31.25	250
PTM-29 F4, F34	2.40	62.5	125
PTM-29 F4, F35	1.20	31.30	15.60
PTM-29 F4, F36	3.10	62.50	250
PTM-29 F4, F37	1.40	62.50	15.60
PTM-29 F4, F38	1.80	3.91	0.24
PTM-29 F4, F39	13.20	1.95	1.95
PTM-29 F4, F40	3.40	3.91	0.98
PTM-29 F4, F42	5.30	3.91	0.98
PTM-29 F4, F44	6.10	3.91	0.98
PTM-29 F4, F45	3.40	3.91	1.95
PTM-29 F4, F46	1.60	15.60	7.81
PTM-29 F4, F47	2.10	15.60	7.81

3.3 PTM-029,F4,F39 Structure elucidation

It was performed the structural elucidation in a selected pure compound PTM-029 F4, F39 by NMR spectroscopy (^1H , ^{13}C , DEPT 135, COSY ^1H - ^1H , TOCSY ^1H - ^1H , HSQC ^1H - ^{13}C , HMBC ^1H - ^{13}C and ROESY ^1H - ^1H), the spectra are in Annex 5.

PTM-029, F4, F39: Yellow oil (13.2 mg); **UVmax:** 260 nm; **^1H NMR (400 MHz, CDCl_3):** δ 12.28 (s, 3H), 7.93 (s, 3H), 6.55 (s, 3H), 4.57 (dd, $J = 11.9, 3.7$ Hz, 3H), 3.43 (dd, $J = 12.1, 3.5$ Hz, 3H), 2.73 – 2.35 (m, 10H), 2.22 (s, 9H), 2.20 – 1.66 (m, 16H), 1.66 – 1.55 (m, 11H), 1.38 (dd, $J = 30.7, 12.0$ Hz, 27H), 1.29 – 0.75 (m, 16H), 0.98 – 0.84 (m, 3H), 1.08 – 0.75 (m, 11H), 0.73 (d, $J = 18.6$ Hz, 10H), 0.47 (s, 1H), 0.42 (s, 9H). **^{13}C NMR (101 MHz, CDCl_3):** δ 192.62, 190.98, 164.37, 163.34, 131.81, 120.39, 108.68, 107.04, 85.58, 81.52, 80.33, 72.28, 71.02, 57.88, 52.21, 42.06, 40.79, 40.51, 38.22, 29.79, 29.23, 28.50, 24.38, 22.96, 15.68, 8.43.

4. Discussion

PTM-029, F4 was the fraction with the best antibacterial activity, since it shows the lowest MIC against the two pathogenic bacteria, MRSA (7.8 $\mu\text{g/mL}$) and VRE EF82 (3.9 $\mu\text{g/mL}$). PTM-029, F8 was the fraction with the lower antibacterial activity with a MIC of 250 $\mu\text{g/mL}$ against VRE EF82.

The focus of this work turned to isolate pure bioactive compounds belonging to the napyradiomycins family by HPLC. PTM-029, F4 was also the one with the higher amount of pure compounds possible belonging to the napyradiomycins family. From all the 49 isolated compounds, obtained from PTM-029, F4, the compound with the higher antibacterial activity against MRSA was PTM-029, F4, F39 with a MIC of 1.9 $\mu\text{g/mL}$ and against VRE EF82 was fractions PTM-029, F4, F40; PTM-029, F4, F42 and PTM-029, F4, F44 with the same MIC of 0.98 $\mu\text{g/mL}$.

PTM-029, F4, F39 was the most promising compound not only due to the presence of napyradiomycins UV profile (Annex 3, Chromatogram 3), but also because it was the compound obtained in higher amount (13.2 mg) and the most active, i.e. with the lower MIC against MRSA (1.95 $\mu\text{g/mL}$) and VRE EF82 (1.95 $\mu\text{g/mL}$). Exhibiting or meeting, the requirements to procedure the structure elucidation.

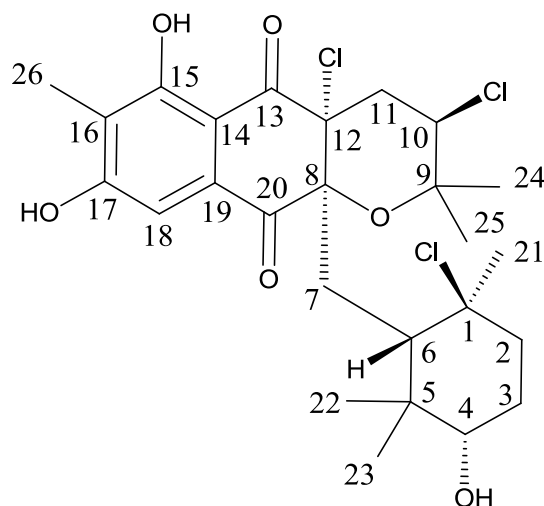


Figure I. 12 - Proposed structure of the pure compound PTM-029, F4, F39 based on NMR spectra.

Table I. 4 - NMR spectroscopic data for a napyradiomycin derivative PTM-029, F4, F39 ^a

Carbon no.	δ_c , type	δ_H , mult. (J in Hz)	COSY	TOCSY	HMBC	ROESY
1	72.28, C	-				
2	40.79, CH ₂	1.78, m 1.94, m	H3	H3,H4,H6	C1	
3	29.79, CH ₂	1.44, m 1.94, m	H2, H4	H2, H4	C1, C5	
4	71.03, CH	3.43 dd (12.2, 3.5)	H3	H2, H3, H22	C2, C22, C23	H21, H22
4		6.55, s (OH)			C5	H6, H24, H25
5	40.51, C	-				
6	52.21, CH	1.44, m	H7	H7, H22	C1, C7, C22, C23	H4, OH4, H22
7	38.22, CH ₂	1.59, m 2.51, m	H6	H6, H22, H23	C1, C6, C8, C20	
8	85.58, C	-				
9	81.52, C	-				
10	57.89, CH	4.57 dd (11.9, 3.5)	H11	H11, H24, H25	C9	H24

Carbon no.	δ_c , type	δ_H , mult. (J in Hz)	COSY	TOCSY	HMBC	ROESY
11	42.06, CH ₂	2.51, m 2.64, dd (14.2, 3.8)	H10	H10, H11	C12, C10	
12	80.33, C	-				
13	192.63, C	-				
14	107.05, C	-				
15	163.34, C	12.28,s (OH)			C14, C15, C16	
16	120.40, C	-				
17	164.37, C					
18	108.69, CH	7.93, s		H26	C10, C14, C16,	
19	131.81, C	-				
20	190.98, C	-				
21	24.38, CH ₃	1.33, s		H3, H4	C1, C5, C6	OH4, H4
22	28.51, CH ₃	0.42, s		H4, H6, H7, H23	C4, C6, C5, C23	H4, H6, H23
23	15.68, CH ₃	0.76, s		H6, H7, H22	C4, C6, C5, C22	H21, H22

Carbon no.	δ_c , type	δ_H , mult. (J in Hz)	COSY	TOCSY	HMBC	ROESY
25	22.95, CH ₃	1.37, s		H24	C9,C10, C24	
26	8.44 CH ₃	2.22, s		H18	C15, C16, C17, C18	

^a Spectra were recorded in CDCl₃ at 400 MHz (¹H) and 101 MHz (¹³C). Assignments were made on the basis of DEPT, HSQC and HMBC sequence experiments.

The structure of this pure bioactive compound, PTM-029, F4, F39 was established by interpretation of spectroscopic data, especially 2D NMR spectroscopic data. The complex molecular ion cluster in the ESI mass spectrum of PTM-029, F4, F39 clearly showed the presence of three chlorine atoms in the molecule. HR-Mass analysis suggested the molecular formula C₂₆H₃₃Cl₃O₆ ([M - H]⁻ m/z (obsd) 545.127), indicating 9° of unsaturation. PTM-029, F4, F39 showed strong UV absorptions at 210, 260, 320 and 360 nm, consistent with characteristic UV profile of a napyradiomycin derivative (Figure I. 8). Analysis of ¹H and ¹³C NMR and 2D spectral data (Table I. 4) and comparison with the same data from compound A-80915C (Annex 1, compound (25)) allowed the structure of PTM-029, F4, F39 to be assigned.¹⁸ The ¹H NMR spectrum of PTM-029, F4, F39 illustrated a single aromatic proton (C-18, δ ¹H 7.93 s), one aromatic methyl group (C-26, δ ¹H 2.22 s), five quaternary methyl groups (C-21-C-25), one methine proton adjacent to chlorine (C-10 δ ¹H 4.57 dd, J = 11.9 Hz) and another one methine proton adjacent to a hydroxyl group (C-4 δ ¹H 3.43 dd, J = 12.1 Hz). Analysis of HMBC and HSQC NMR data confirmed these assignments and allowed other proton assignments to be made. Two low field aromatic carbons, C-15 and C-17 (δ ¹³C 163.34 and 164.37, respectively), suggested the presence of two phenolic hydroxyl groups. Besides, ¹H NMR spectrum showed the lability of OH-15 proton (δ ¹H 12.28 s) since it formed a hydrogen bridge with quinone's ketone C- 13, changing the chemical shift to lower field compared with the other OH-4 (δ ¹H 6.55, s). These observations suggested that PTM-029, F4, F39 possessed the same terpenoid substituents and a regiochemistry identical to that of compound (25), Annex 1. Analysis of ¹H NMR data for the monoterpene unit (C-1 to C-7 and C-

21, -22, -32) in PTM029, F4, F39 showed that it formed a typical chair cyclohexane ring. Analysis of NMR data showed this ring is not identical to the one observed in the structure of A80915C^{18,19} (Annex 1, compound (25)) suggesting that in this ring the chlorine and the hydroxyl group can switch positions confirmed by the appearance of a new signal 6.55 ppm by ¹H NMR spectrum, corresponding to the hydroxyl group attached to C-4 and its correlation with C-5 in HMBC spectrum. The relative stereochemistry was assigned by interpretation of 2D NMR ROESY data. ROESY correlations between the C-22 methyl protons and the methine protons at C-4 and C-6 showed these protons were on the same face of the cyclohexane ring. Correlations between the C-21 and C-23 methyl group protons showed that the orientation of the C-21 and C-23 methyl groups were α (axial) and on the bottom face of the ring.

Relatively to the antibacterial activity between A80915C¹⁹ (Annex 2, compound (25)) and PTM-29, F4, F39, both compounds show the same MIC against MRSA (1.9 μ g/mL), although against VRE EF82, PTM-029, F4, F39 shows a better MIC (1.95 μ g/mL) two times lower than compound A80915C (3.95 μ g/mL).

5. Conclusion

In this work 323 compounds were isolated and purified from the *Streptomyces aculeolatus*, PTM-029 obtained from ocean sediments and 148 were bioactive compounds being 51 from the napyradiomycins family. Napyradiomycin-derived secondary metabolites were the most predominantly produced by this strain. A novel napyradiomycin derivative, PTM-029, F4, 39, exhibiting antimicrobial activity against pathogenic bacteria MRSA (1.95 µg/mL) and VRE EF82 (1.95 µg/mL) was structurally elucidated. This compound is structurally related with the previously reported compound A80915C^{18, 19} (Annex 1, compound (25)). In future work, it would be interesting to study the biosynthetic differences between compound A80915C and PTM-029, F4, F39, performing full genome sequencing.

This study suggests that napyradiomycin family is worthy of further exploration as novel drug candidates, proceeding PTM-029, F4, F39 to subsequent studies as dry powder formulations, as described in Part II.

6. References

1. Draft, C. *et al.* *Global , regional and national levels of age-specific mortality and 240 causes of death , 1990-2013 : A systematic analysis for the Global Burden of Disease Study 2013. The Lancet* **385**, (Elsevier Ltd, 2015).
2. Cheng, Y.-B., Jensen, P. R. & Fenical, W. Cytotoxic and Antimicrobial Napyradiomycins from Two Marine-Derived Streptomyces Strains. *European J. Org. Chem.* **2013**, 3751–3757 (2013).
3. Ungaro, F. & Vanbever, R. Improving the efficacy of inhaled drugs for severe lung diseases: Emerging pulmonary delivery strategies. *Adv. Drug Deliv. Rev.* **75**, 1–2 (2014).
4. Dasaraju PV, L. C. in *Medical Microbiology* (ed. S, B.) 93 (1996).
5. Haste, N., Farnaes, L., Perera, V. & Fenical, W. Bactericidal kinetics of marine-derived napyradiomycins against contemporary methicillin-resistant *Staphylococcus aureus*. *Mar. Drugs* **9**, 680–689 (2011).
6. Bérdy, J. Bioactive microbial metabolites. *J. Antibiot. (Tokyo)*. **58**, 1–26 (2005).
7. Fenical, W. & Jensen, P. R. Developing a new resource for drug discovery: marine actinomycete bacteria. *Nat. Chem. Biol.* **2**, 666–673 (2006).
8. Gallagher, K. a, Rauscher, K., Pavan Ioca, L. & Jensen, P. R. Phylogenetic and chemical diversity of a hybrid-isoprenoid-producing streptomycete lineage. *Appl. Environ. Microbiol.* **79**, 6894–902 (2013).
9. Subramani, R. & Aalbersberg, W. Marine actinomycetes: An ongoing source of novel bioactive metabolites. *Microbiol. Res.* **167**, 571–580 (2012).
10. Kuzuyama, T. & Seto, H. Diversity of the biosynthesis of the isoprene units. *Nat. Prod. Rep.* **20**, 171–183 (2003).
11. Gallagher, K. a, Fenical, W. & Jensen, P. R. Hybrid isoprenoid secondary metabolite production in terrestrial and marine actinomycetes. *Curr. Opin. Biotechnol.* **21**, 794–800 (2010).
12. Kawasaki, T. & Hayashi, Y. Biosynthesis of a natural polyketide-isoprenoid hybrid compound, furaquinocin A: identification and heterologous expression of the gene cluster. *J. Bacteriol.* **188**, 1236–1244 (2006).
13. Pawlik, J. R. Marine chemical ecology. *Mar. Ecol. Prog. Ser.* **207**, 225–226 (2000).
14. Xiao, Y., Machacek, M., Lee, K., Kuzuyama, T. & Liu, P. Prenyltransferase substrate binding pocket flexibility and its application in isoprenoid profiling. *Mol. Biosyst.* **5**, 913 (2009).

15. Wu, Zhengchao; Li, Sumei, et al. Antibacterial and Cytotoxic New Napyradiomycins from the *Mar. Drugs* **11**, 2113–2125 (2013).
16. Winter, Jaclyn M., Moffitt, Michelle C., et al. Molecular Basis for Chloronium-mediated Meroterpene Cyclization CLONING, SEQUENCING, AND HETEROLOGOUS EXPRESSION OF THE NAPYRADIOMYCIN BIOSYNTHETIC GENE CLUSTER. *J. Biol. Chem.* **282**, 16362–16368 (2007).
17. Gill SR, et al. Insights on evolution of virulence and resistance from the complete genome analysis of an early methicillin-resistant *Staphylococcus aureus* strain and a biofilm-producing methicillin-resistant *Staphylococcus epidermidis* strain. *J. Bacteriol.* **187**, 2426–2438 (2005).
18. Soria-Mercado, I. Antibiotic terpenoid chloro-dihydroquinones from a new marine actinomycete. *J. Nat. Prod.* **68**, 904–910 (2005).
19. Soria-Mercado, I. E., Jensen, P. R., Fenical, W., Kassel, S. & Golen, J. 3,4a-Dichloro-10a-(3-chloro-6-hydroxy-2,2,6-trimethylcyclohexylmethyl)-6,8-dihydroxy-2,2,7-trimethyl-3,4,4a,10a-tetrahydro-2 H -benzo[g]chromene-5,10-dione. *Acta Crystallogr. Sect. E Struct. Reports Online* **60**, o1627–o1629 (2004).
20. Shiomi, K. *et al.* STRUCTURES OF NEW ANTIBIOTICS NAPYRADIOMYCINS. *J. Antibiot. (Tokyo)*. **XXXIX**, 494–501 (1986).
21. Shiomi, K., Nakamura, H. & Inuma, H. NEW ANTIBIOTIC NAPYRADIOMYCINS A2 AND B4 AND STEREOCHEMISTRY OF NAPYRADIOMYCINS. *J. Antibiot. (Tokyo)*. **XL**, (1987).
22. Shiomi, K. I. H. Biosynthesis of Napyradiomycins. *J. Antibiot. (Tokyo)*. **XL**, 1740–1745 (1987).
23. Mynderse, J. S. Antibiotic A80915 and process for its production. (1990). at <<http://scholar.google.com/scholar?hl=en&btnG=Search&q=intitle:No+Title#0>>
24. Hori, Yasuhiro, Abe, Yukiko, et al. NAPYRADIOMYCINS A AND B1: NON-STEROIDAL ESTROGEN-RECEPTOR ANTAGONISTS PRODUCED BY A *Streptomyces*. *J. Antibiot. (Tokyo)*. **46**, 1890–1893 (1993).
25. Motohashi, K., Sue, M. & Furihata, K. Terpenoids produced by actinomycetes: Napyradiomycins from *Streptomyces antimycoticus* NT17. *J. Nat. Prod.* **71**, 595–601 (2008).
26. Farnaes, L. & Coufal, N. Napyradiomycin Derivatives, Produced by a Marine-Derived Actinomycete, Illustrate Cytotoxicity by Induction of Apoptosis. *J. Nat. Prod.* **77**, 15–21 (2013).
27. Farnaes, L., La Clair, J. J. & Fenical, W. Napyradiomycins CNQ525.510B and A80915C target the Hsp90 paralogue Grp94. *Org. Biomol. Chem.* **12**, 418 (2014).

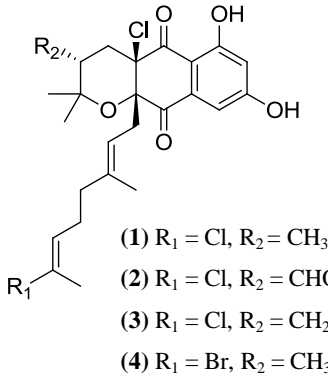
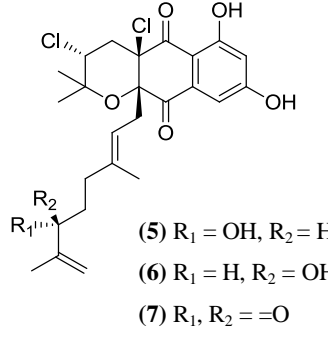
28. Takemura, S., Hirayama, A. & Tokunaga, J. A concise total synthesis of (\pm)-A80915G, a member of the napyradiomycin family of antibiotics. *Tetrahedron Lett.* **40**, 7501–7505 (1999).
29. Shirai, M. *et al.* Terpenoids produced by actinomycetes: isolation, structural elucidation and biosynthesis of new diterpenes, gifhornenolones A and B from *Verrucosipora gifhornensis* YM28-088. *J. Antibiot. (Tokyo)*. **63**, 245–250 (2010).
30. Griffith, L. G. Polymeric biomaterials. *Acta Mater.* **48**, 263–277 (2000).
31. Buttini, F., Colombo, P., Rossi, A., Sonvico, F. & Colombo, G. Particles and powders: Tools of innovation for non-invasive drug administration. *J. Control. Release* **161**, 693–702 (2012).
32. Takami, T. & Murakami, Y. Development of PEG-PLA/PLGA microparticles for pulmonary drug delivery prepared by a novel emulsification technique assisted with amphiphilic block copolymers. *Colloids Surfaces B Biointerfaces* **87**, 433–438 (2011).
33. Sung, J. C., Pulliam, B. L. & Edwards, D. a. Nanoparticles for drug delivery to the lungs. *Trends Biotechnol.* **25**, 563–570 (2007).
34. Pilcer, G. & Amighi, K. Formulation strategy and use of excipients in pulmonary drug delivery. *Int. J. Pharm.* **392**, 1–19 (2010).
35. Beck-Broichsitter, M. *et al.* Characterization of novel spray-dried polymeric particles for controlled pulmonary drug delivery. *J. Control. Release* **158**, 329–335 (2012).
36. Chow, a. H. L., Tong, H. H. Y., Chattopadhyay, P. & Shekunov, B. Y. Particle engineering for pulmonary drug delivery. *Pharm. Res.* **24**, 411–437 (2007).
37. Geiser, M. *et al.* Cellular uptake and localization of inhaled gold nanoparticles in lungs of mice with chronic obstructive pulmonary disease. *Part. Fibre Toxicol.* **10**, 19 (2013).
38. Newman, S. P. & Busse, W. W. Evolution of dry powder inhaler design, formulation, and performance. *Respir. Med.* **96**, 293–304 (2002).
39. Shoyele, S. a. & Slowey, A. Prospects of formulating proteins/peptides as aerosols for pulmonary drug delivery. *Int. J. Pharm.* **314**, 1–8 (2006).
40. Healy, A. M., Amaro, M. I., Paluch, K. J. & Tajber, L. Dry powders for oral inhalation free of lactose carrier particles. *Adv. Drug Deliv. Rev.* **75C**, 32–52 (2014).
41. Malcolmson, R. J. & Embleton, J. K. Dry powder formulations for pulmonary delivery. *Pharm. Sci. Technol. Today* **1**, 394–398 (1998).
42. Zhou, Q. T., Tang, P., Leung, S. S. Y., Chan, J. G. Y. & Chan, H.-K. Emerging inhalation aerosol devices and strategies: Where are we headed? *Adv. Drug Deliv. Rev.* **75C**, 3–17 (2014).

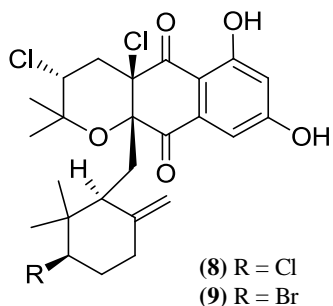
43. Choi, H. S. *et al.* Rapid translocation of nanoparticles from the lung airspaces to the body. *Nat. Biotechnol.* **28**, 1300–1303 (2010).
44. Wanakule, P., Liu, G. W., Fleury, A. T. & Roy, K. Nano-inside-micro: Disease-responsive microgels with encapsulated nanoparticles for intracellular drug delivery to the deep lung. *J. Control. Release* **162**, 429–437 (2012).
45. Li, Y. Z. *et al.* Inhalable microparticles as carriers for pulmonary delivery of thymopentin-loaded solid lipid nanoparticles. *Pharm. Res.* **27**, 1977–1986 (2010).
46. Yang, Y. *et al.* Development of highly porous large PLGA microparticles for pulmonary drug delivery. *Biomaterials* **30**, 1947–1953 (2009).
47. Bosquillon, C., Lombry, C., Pr eat, V. & Vanbever, R. Influence of formulation excipients and physical characteristics of inhalation dry powders on their aerosolization performance. *J. Control. Release* **70**, 329–339 (2001).
48. Arifin, D. Y., Lee, L. Y. & Wang, C.-H. Mathematical modeling and simulation of drug release from microspheres: Implications to drug delivery systems. *Adv. Drug Deliv. Rev.* **58**, 1274–1325 (2006).
49. Ritger, P. L. & Peppas, N. a. A simple equation for description of solute release I. Fickian and non-fickian release from non-swellable devices in the form of slabs, spheres, cylinders or discs. *J. Control. Release* **5**, 23–36 (1987).
50. Cipolla, D., Shekunov, B., Blanchard, J. & Hickey, A. Lipid-based carriers for pulmonary products: Preclinical development and case studies in humans. *Adv. Drug Deliv. Rev.* **75**, 53–80 (2014).
51. Loira-Pastoriza, C., Todoroff, J. & Vanbever, R. Delivery strategies for sustained drug release in the lungs. *Adv. Drug Deliv. Rev.* **75C**, 81–91 (2014).
52. Van Der Schueren, L. *et al.* Polycaprolactone and polycaprolactone/chitosan nanofibres functionalised with the pH-sensitive dye Nitrazine Yellow. *Carbohydr. Polym.* **91**, 284–293 (2013).
53. Alvarenga, E. S. De. Characterization and Properties of Chitosan. *Biotechnol. Biopolym.* 91–108 (2011). at <<http://www.intechopen.com/books/biotechnology-of-biopolymers/characterization-and-properties-of-chitosan>>
54. Dash, M., Chiellini, F., Ottenbrite, R. M. & Chiellini, E. Chitosan - A versatile semi-synthetic polymer in biomedical applications. *Prog. Polym. Sci.* **36**, 981–1014 (2011).
55. Temtem, M., Barroso, T., Casimiro, T., Mano, J. F. & Aguiar-Ricardo, A. Dual stimuli responsive poly(N-isopropylacrylamide) coated chitosan scaffolds for controlled release prepared from a non residue technology. *J. Supercrit. Fluids* **66**, 398–404 (2012).
56. Jae, H. P. *et al.* Self-assembled nanoparticles based on glycol chitosan bearing hydrophobic moieties as carriers for doxorubicin: In vivo biodistribution and anti-tumor activity. *Biomaterials* **27**, 119–126 (2006).

57. Trapani, A. *et al.* Characterization and evaluation of chitosan nanoparticles for dopamine brain delivery. *Int. J. Pharm.* **419**, 296–307 (2011).
58. Kumirska, J. *et al.* Application of spectroscopic methods for structural analysis of chitin and chitosan. *Mar. Drugs* **8**, 1567–1636 (2010).
59. Kean, T. & Thanou, M. Biodegradation, biodistribution and toxicity of chitosan. *Adv. Drug Deliv. Rev.* **62**, 3–11 (2010).
60. Cruz, L. J. *et al.* Targeted PLGA nano- but not microparticles specifically deliver antigen to human dendritic cells via DC-SIGN in vitro. *J. Control. Release* **144**, 118–126 (2010).
61. Ding, A. G. & Schwendeman, S. P. Determination of Water-Soluble Acid Distribution in Poly(lactide-co-glycolide). *J. Pharm. Sci.* **93**, 322–331 (2004).
62. Casettari, L. *et al.* Surface characterisation of bioadhesive PLGA/chitosan microparticles produced by supercritical fluid technology. *Pharm. Res.* **28**, 1668–1682 (2011).
63. Steve, Makadia Hirenkumar and Siegel Steve, P., Drug, C. & Carrier, D. Poly Lactic-co-Glycolic Acid (PLGA) as Biodegradable Controlled Drug Delivery Carrier. *Polymers (Basel)*. **3**, 1–19 (2012).
64. Woodle, M. C., Engbers, C. M. & Zalipsky, S. New amphipatic polymer-lipid conjugates forming long-circulating reticuloendothelial system-evading liposomes. *Bioconjug. Chem.* **5**, 493–496 (1994).
65. Mero, A. *et al.* Synthesis and characterization of poly(2-ethyl 2-oxazoline)-conjugates with proteins and drugs: Suitable alternatives to PEG-conjugates? *J. Control. Release* **125**, 87–95 (2008).
66. Huang, H. W. Action of Antimicrobial Peptides : Two-State Model Current Topics Action of Antimicrobial Peptides : Two-State Model. *Biochemistry* **39**, 25–30 (2000).
67. A. Aguiar-Ricardo, V.D.B. Bonifacio, T. Casimiro, V. G. C. Supercritical carbon dioxide design strategies: from drug carriers to soft killers. *Phil. Trans. R. Soc. A* (2015). doi:10.1084/jem.20072208
68. De Macedo, C. V., da Silva, M. S., Casimiro, T., Cabrita, E. J. & Aguiar-Ricardo, A. Boron trifluoride catalyzed polymerisation of 2-substituted-2-oxazolines in supercritical carbon dioxide. *Green Chem.* **9**, 948 (2007).
69. Mansour, H. M., Rhee, Y. S. & Wu, X. Nanomedicine in pulmonary delivery. *Int. J. Nanomedicine* **4**, 299–319 (2009).
70. Martín, Á., Pham, H. M., Kilzer, A., Kareth, S. & Weidner, E. Micronization of polyethylene glycol by PGSS (Particles from Gas Saturated Solutions)-drying of aqueous solutions. *Chem. Eng. Process. Process Intensif.* **49**, 1259–1266 (2010).

71. Zhang, J., Wu, L., Chan, H. K. & Watanabe, W. Formation, characterization, and fate of inhaled drug nanoparticles. *Adv. Drug Deliv. Rev.* **63**, 441–455 (2011).
72. Marco, G. I. L., Vicente, J. & Gaspar, F. Scale-up methodology for pharmaceutical spray drying. *Chim. Oggi* **28**, 18–22 (2010).
73. Nie, H., Lee, L. Y., Tong, H. & Wang, C. H. PLGA/chitosan composites from a combination of spray drying and supercritical fluid foaming techniques: New carriers for DNA delivery. *J. Control. Release* **129**, 207–214 (2008).
74. Tong, H. H. Y. & Chow, a H. L. Control of Physical Forms of Drug Particles for Pulmonary Delivery by Spray Drying and Supercritical Fluid Processing. **24**, 27–40 (2006).
75. Chattopadhyay, P. & Gupta, R. B. Supercritical CO₂ Based Production of Magnetically Responsive Micro- and Nanoparticles for Drug Targeting. 6049–6058 (2002).
76. Reverchon, E. & Caputo, G. Role of phase behavior and atomization in the supercritical antisolvent precipitation. *Ind. & Eng. Chem.* **42**, 6406–6414 (2003).
77. Reverchon, E., Adami, R. & Caputo, G. Supercritical assisted atomization: Performance comparison between laboratory and pilot scale. *J. Supercrit. Fluids* **37**, 298–306 (2006).
78. Porta, G. Della & Reverchon, E. Engineering Powder Properties By Supercritical Fluid for Optimum Drug Delivery. *Bioprocess Int.* 54–60 (2005).
79. Reighard, T. S., Lee, S. T. & Olesik, S. V. Determination of methanol/CO₂ and acetonitrile/CO₂ vapor-liquid phase equilibria using a variable-volume view cell. *Fluid Phase Equilib.* **123**, 215–230 (1996).
80. Duarte, C., Aguiar-Ricardo, A., Ribeiro, N., Casimiro, T. & Da Ponte, M. N. Correlation of Vapor–Liquid Equilibrium for Carbon Dioxide + Ethanol + Water at Temperatures from 35 to 70°C. *Sep. Sci. Technol.* **35**, 2187–2201 (2000).
81. Adami, R., Liparoti, S. & Reverchon, E. A new supercritical assisted atomization configuration, for the micronization of thermolabile compounds. *Chem. Eng. J.* **173**, 55–61 (2011).
82. Wang, Q., Guan, Y. X., Yao, S. J. & Zhu, Z. Q. The liquid volume expansion effect as a simple thermodynamic criterion in cholesterol micronization by supercritical assisted atomization. *Chem. Eng. Sci.* **75**, 38–48 (2012).
83. Agrawal, N. Polymeric Prodrugs: Recent Achievements and General Strategies. *J. Antivir. Antiretrovir.* **01**, (2015).
84. W, L. & PG, J. *Handb. Green Chem. Weinhelm: Wiley-VCH* **1–30**, (2010).

Annex 1

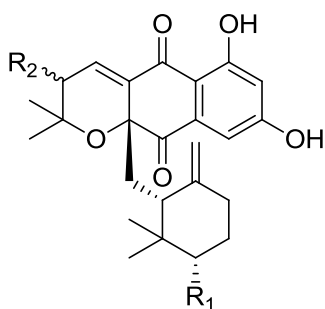
Name and Structure	Year	Molecular Formula	MW (g/mol)	Ref.
 <p>(1) R₁ = Cl, R₂ = CH₃ (2) R₁ = Cl, R₂ = CHO (3) R₁ = Cl, R₂ = CH₂OH (4) R₁ = Br, R₂ = CH₃</p>	(1) – 1986	C ₂₅ H ₃₀ Cl ₂ O ₅	481.409	10, 15, 20, 21, 22, 23, 24, 25
	(2) – 2008	C ₂₅ H ₂₈ Cl ₂ O ₆	495.392	15, 25
	(3) – 2008	C ₂₅ H ₃₀ Cl ₂ O ₆	497.408	15, 25
	(4) – 2013	C ₂₅ H ₃₁ ClBrO ₅	525.1047 [M + H] ⁺ (HRESIMS)	15
<p>(1) Napyradiomycin A1 (2) 18-oxonapyradiomycin A1 (3) 18-hydroxynapyradiomycin A1 (4) 3-dechloro-3-bromonapyradiomycin A1</p>				
 <p>(5) R₁ = OH, R₂ = H (6) R₁ = H, R₂ = OH (7) R₁, R₂ = =O</p>	(5) – 1987	C ₂₅ H ₃₀ Cl ₂ O ₆	497.408	21, 22, 25
	(6) – 2008	C ₂₅ H ₂₈ Cl ₂ O ₆	495.392	25
	(7) – 2008	C ₂₅ H ₂₈ Cl ₂ O ₆	495.392	25
<p>(5) Napyradiomycin A2a (6) Napyradiomycin A2b (7) 16-oxonapyradiomycin A2</p>				



(8) – 1986 C₂₅H₂₉Cl₃O₅ 515.854 20, 22,
23, 24

(9) – 2013 C₂₅H₂₉BrCl₂O₅ 560.305 2, 15, 26

(8) Napyradiomycin B1
(9) Napyradiomycin B3



(10), (11) –
1986 C₂₅H₂₈Cl₂O₅ 479.393 2, 15,
20, 26,
27

(10) R₂ = (R) - Cl, R₁ = (S) - Cl

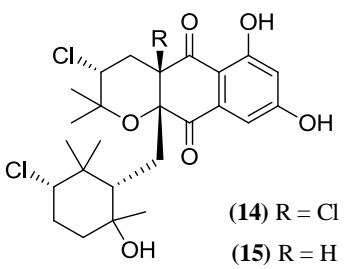
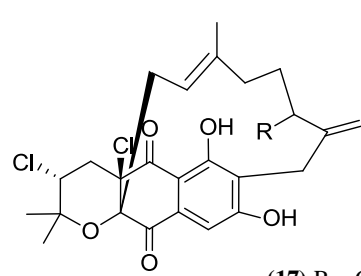
(11) R₂ = (S) - Cl, R₁ = (R) - Cl

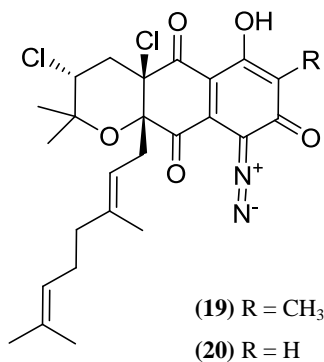
(12) R₂ = (R) - Cl, R₁ = (S) - Br

(13) R₂ = (S) - Cl, R₁ = (R) - Br

(12), (13) –
2013 C₂₅H₂₈BrClO₅ 479.393 2, 26, 15

(10), (11) Napyradiomycin B2
(12), (13) Napyradiomycin

 <p>(14) R = Cl (15) R = H</p>	(14) - 1987	C ₂₅ H ₃₁ Cl ₃ O ₆	533.869	2, 20, 26, 28
	(15) - 2013	C ₂₅ H ₃₂ Cl ₂ O ₆	498.1566 [M + Na] ⁺ (HRMS)	2
<hr/>				
(16) Napyradiomycin C1	(16) - 1986	C ₂₅ H ₂₈ Cl ₂ O ₅	489.393	20, 21, 22
<hr/>				
 <p>(17) R = Cl (18) R = OH</p>	(17) - 1986	C ₂₅ H ₂₇ Cl ₃ O ₅	513.838	2, 20, 22, 25
	(18) - 2008	C ₂₅ H ₂₈ Cl ₂ O ₆	495.392	25
(17) Napyradiomycin C2 (18) 16-dechloro-16-hydroxynapyradiomycin C2				

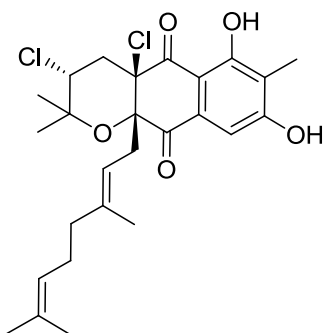


(19) SF2415 A3

(20) 7-demethyl SF2415 A3

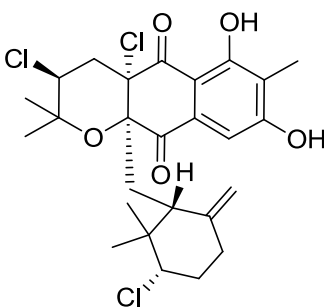
(19) - 1987 C₂₆H₃₀Cl₂N₂O₅ 521.433 22, 25

(20) - 2008 C₂₅H₂₈³⁵Cl₂N₂O₅ 507.1490
[M + H]⁺ 25
(HR-MS)



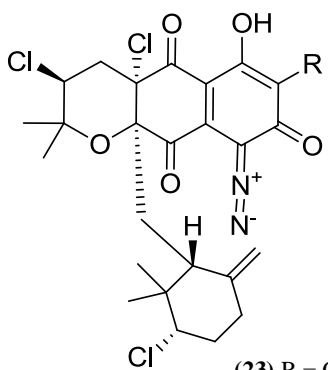
(21) SF2415 B3

(21) - 1987 C₂₆H₃₂Cl₂O₅ 495.435 22, 25,
26



(22) - A80915 A

(22) - 1990 C₂₆H₃₁Cl₃O₅ 529.88 18, 23,
5, 26, 27



(23) - 1990

C₂₆H₂₉Cl₃N₂O₅

555,88
[M + H]⁺
(FABMS)

5, 23,
25

(23) R = CH₃

(24) R = H

(24) - 2008

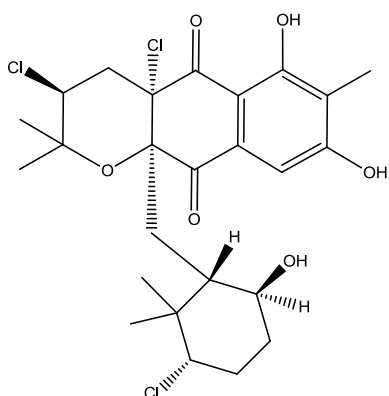
C₂₅H₂₇³⁵Cl₃N₂O₆

541.1039
[M + H]⁺
(HR-MS)

25

(23) A80915 B

(24) 7-demethyl A80915 B



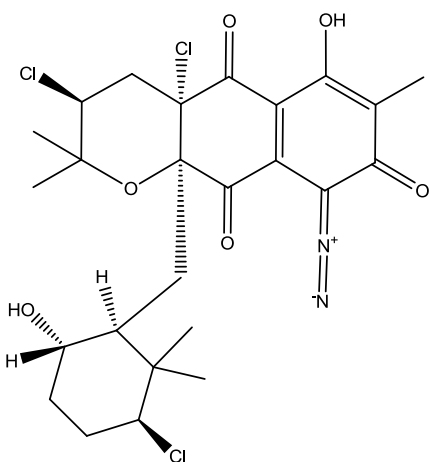
(25) - 1990

C₂₆H₃₃Cl₃O₆

547.896
[M + H
isotopic
cluster]
(FABMS)

5, 11,
16, 18,
23, 26,
27, 19,
29

(25) A80915C



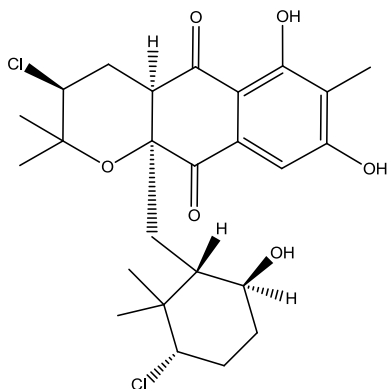
(26) - 1990

C₂₆H₃₁Cl₃N₂O₆

573.893

23, 26

(26) A80915 D



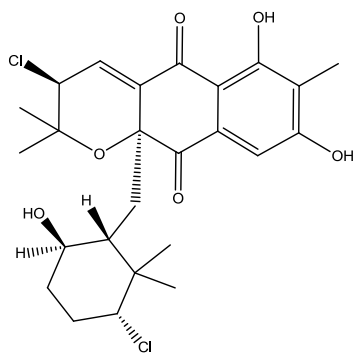
(27) - 2005

$C_{26}H_{34}^{35}Cl_2O_6$

513.1805
[M + H]⁺
(HRESI-
TOFMS)

18

(27) Chlorinated Dihydroquinone 1



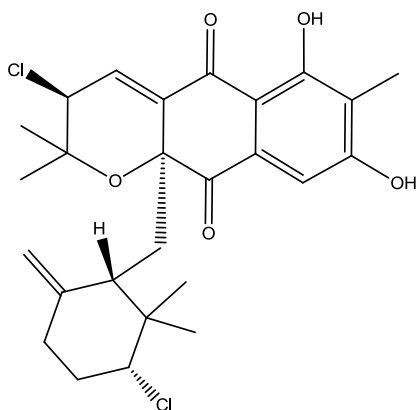
(28) - 2005

$C_{26}H_{32}^{35}Cl_2O_6$

533.1470
[M + Na]⁺
(HRESI-
TOFMS)

18

(28) Chlorinated Dihydroquinone 2



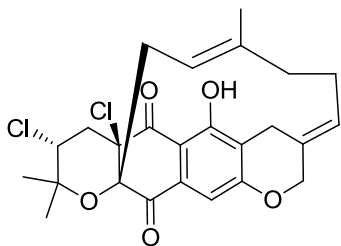
(29) - 2005

$C_{26}H_{30}^{35}Cl_2O_5$

491.1395
[M - H]⁺
(HRESI-
TOFMS)

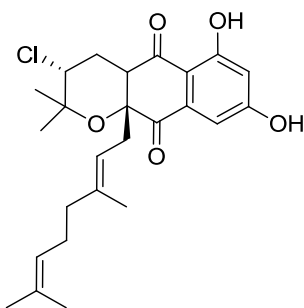
18

(29) Chlorinated Dihydroquinone 3



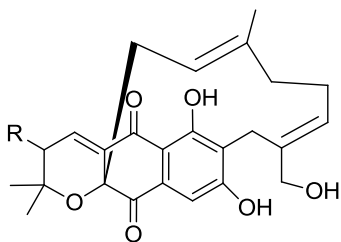
(30) - 2008 $C_{25}H_{26}Cl_2O_5$ 477.377 2, 15, 25

(30) Napyradiomycin SR



(31) - 2013 $C_{25}H_{29}ClO_5$ 467.1595
[M + Na]⁺
(HRESIMS) 15

(31) 4-dehydro-4a-dechloronapyradiomycin A1



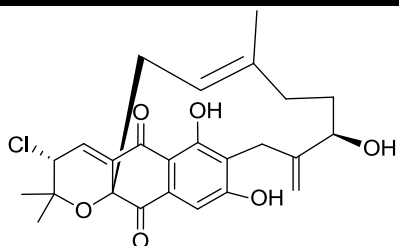
(32) - 2013 $C_{25}H_{27}ClO_6$ 459.1596
[M + H]⁺
(HRMS) 2

(32) R = α -Cl

(33) R = β -OH

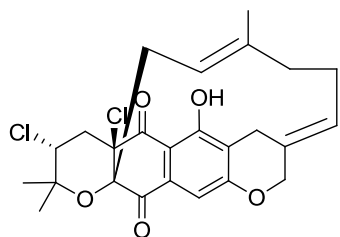
(32) Napyradiomycin 1
(33) Napyradiomycin 2

(33) - 2013 $C_{25}H_{28}O_7$ 463.1723
[M + Na]⁺
(HRMS) 2



(34) - 2013 $C_{25}H_{27}ClO_6$ 481.1386
[M + Na]⁺
(HRMS) 2

(34) Napyradiomycin 3



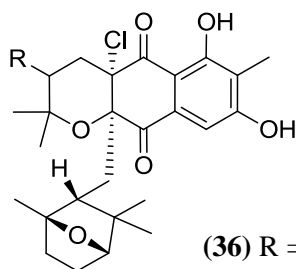
(35) - 2013

$C_{25}H_{26}Cl_2O_5$

499.1105
[M + Na]⁺
(HRMS)

2

(35) Napyrodiomycin 4



(36) - 2014

$C_{26}H_{32}^{35}Cl_2O_6$

511.1652
[M + H]⁺
(HR-TOF)

27

(36) R = Cl

(37) R = Br

(36) CNQ525.510B

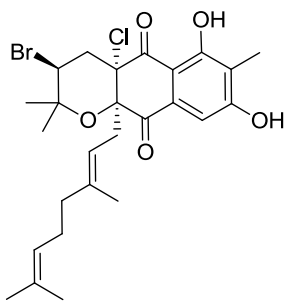
(37) CNQ525.554

(37) - 2014

$C_{26}H_{32}^{79}Br_{35}ClO_6$

555.1150
[M + H]⁺
(HRFTMS)

26



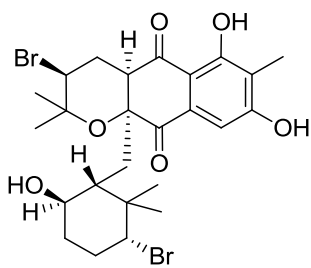
(38) - 2014

$C_{26}H_{32}^{79}Br_{35}ClO_5$

537.1042
[M - H]⁻
(HR-TOF)

26

(38) CNQ525.538



(39) - 2014

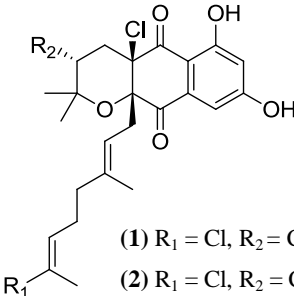
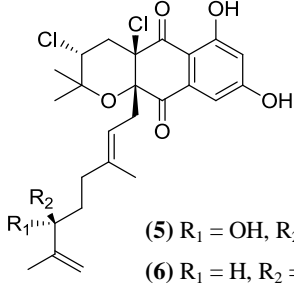
$C_{26}H_{34}^{79}Br_2O_6$

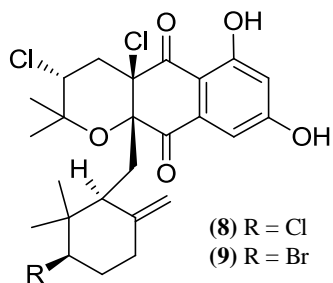
599.0649
[M - H]⁻
(HR-MALDI
TOF MS)

26

(39) CNQ525.600

Annex 2

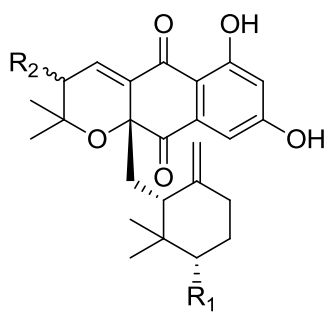
Name and Structure	MIC ($\mu\text{g/mL}$)				IC ₅₀ ($\mu\text{g/mL}$)	Ref.
	MRSA	VRE		HCT		
		<i>E. faecium</i>	<i>E. faecalis</i>			
 <p>(1) R₁ = Cl, R₂ = CH₃ (2) R₁ = Cl, R₂ = CHO (3) R₁ = Cl, R₂ = CH₂OH (4) R₁ = Br, R₂ = CH₃</p>	(1)	1	N.D.	N.D.	N.D.	10, 15, 20, 21, 22, 23, 24, 25
	(2)	>16	>16	>16	N.D.	15, 25
	(3)	>16	>16	>16	N.D.	15, 25
<p>(1) Napyradiomycin A1 (2) 18-oxonapyradiomycin A1 (3) 18-hydroxynapyradiomycin A1 (4) 3-dechloro-3-bromonapyradiomycin A1</p>	(4)	0.5	N.D.	N.D.	N.D.	15
 <p>(5) R₁ = OH, R₂ = H (6) R₁ = H, R₂ = OH (7) R₁, R₂ = =O</p>	(5)	>16	>16	>16	N.D.	21, 22, 25
	(6)	>16	>16	>16	N.D.	25
<p>(5) Napyradiomycin A2a (6) Napyradiomycin A2b (7) 16-oxonapyradiomycin A2</p>	(7)	>16	>16	>16	N.D.	25



(8)	1	N.D.	N.D.	2 (μM)	20, 22, 23, 24
-----	---	------	------	--------	----------------

(9)	32	N.D.	N.D.	1.41	2, 15, 26
-----	----	------	------	------	-----------

(8) Napyradiomycin B1
(9) Napyradiomycin B3



(10, 11)	N.D.	N.D.	N.D.	N.D.	2, 15, 20, 26, 27
-------------	------	------	------	------	-------------------

(10) R₂ = (R) - Cl, R₁ = (S) - Cl

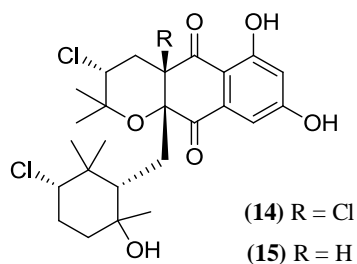
(11) R₂ = (S) - Cl, R₁ = (R) - Cl

(12) R₂ = (R) - Cl, R₁ = (S) - Br

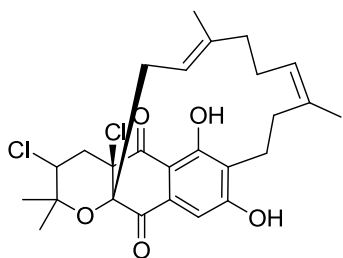
(13) R₂ = (S) - Cl, R₁ = (R) - Br

(12, 13)	>64	N.D.	N.D.	4.81	2, 26, 15
-------------	-----	------	------	------	-----------

(10), (11) Napyradiomycin B2
(12), (13) Napyradiomycin

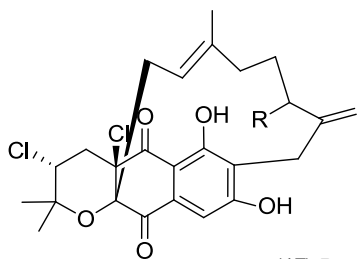


(14) Napyradiomycin B4	(14)	2	N.D.	N.D.	0.19	2, 20, 26, 28
(15) Napyradiomycin B4	(15)	>64	N.D.	N.D.	9.24	2



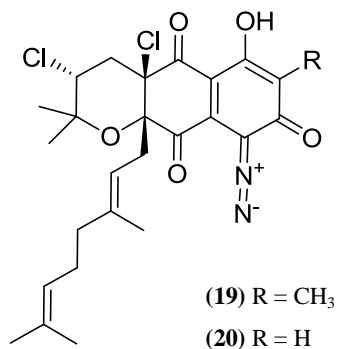
(16) Napyradiomycin C1

(16) Napyradiomycin C1	(16)	N.D.	N.D.	N.D.	N.D.	20, 21, 22
------------------------	------	------	------	------	------	------------



(17) Napyradiomycin C2
(18) 16-dechloro-16-hydroxynapyradiomycin C2

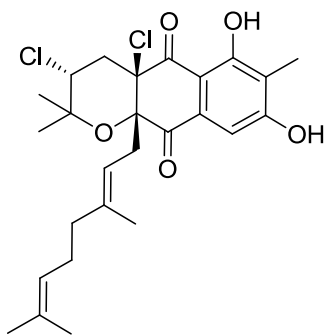
(17) Napyradiomycin C2	(17)	>16	>16	>16	N.D.	2, 20, 22, 25
(18) 16-dechloro-16-hydroxynapyradiomycin C2	(18)	>16	>16	>16	N.D.	25



(19)	N.D.	N.D.	N.D.	N.D.	22, 25
(20)	2 (nM/mL)	15.8 (nM/mL)	31.6 (nM/mL)	N.D.	25

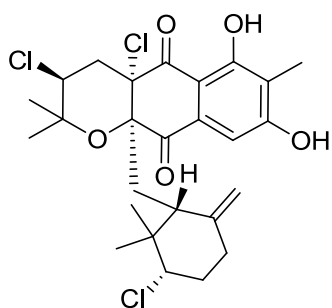
(19) SF2415 A3

(20) 7-demethyl SF2415 A3



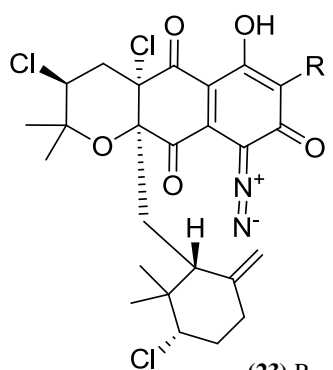
(21)	N.D.	N.D.	N.D.	N.D.	22, 25, 26
------	------	------	------	------	---------------

(21) SF2415 B3



(22)	1.90	3.90	N.D.	3 (μM)	18, 23, 5, 26, 27
------	------	------	------	-----------	-------------------------

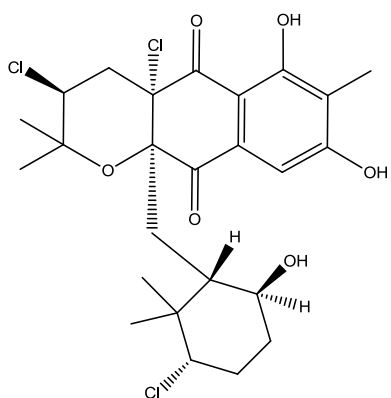
(22) A80915 A



(23)	1.5	N.D.	N.D.	<1 (μM)	5, 23, 25
(24)	3.7 (nM/mL)	14.8 (nM/mL)	14.8 (nM/mL)	N.D.	25

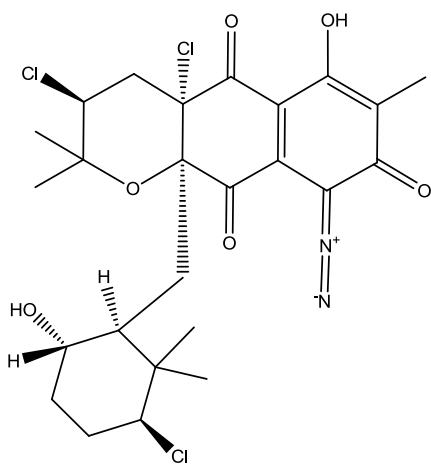
(23) A80915 B

(24) 7-demethyl A80915 B



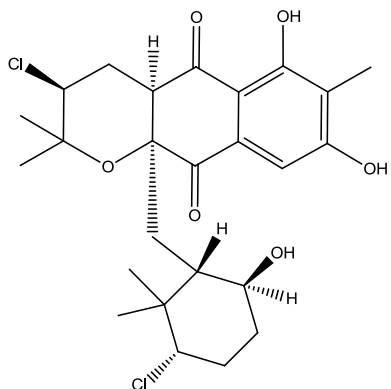
(25)	1.9	3.9	N.D.	15 (μM)	5, 11, 16, 18, 23, 26, 27, 19, 29
------	-----	-----	------	-------------------------	---

(25) A80915C



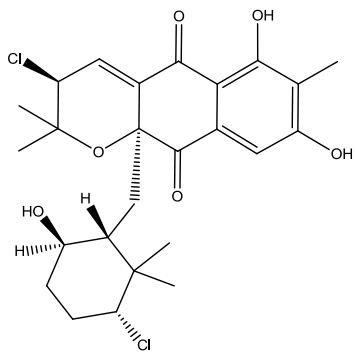
(26)	N.D.	N.D.	N.D.	<1 (μM)	23, 26
------	------	------	------	-------------------------	--------

(26) A80915 D



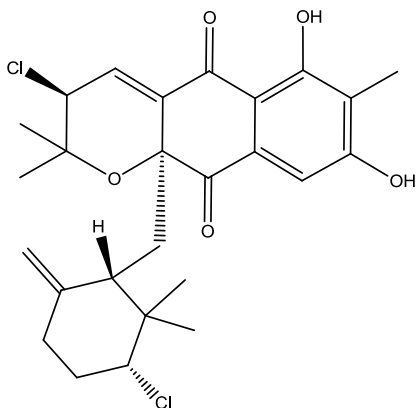
(27) 1.95 N.D. 3.90 2.40 18

(27) Chlorinated Dihydroquinone 1



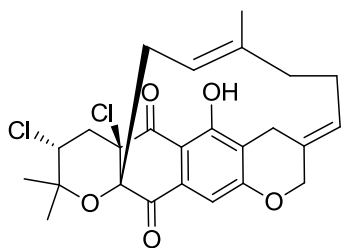
(28) 15.6 N.D. 15.6 0.97 18

(28) Chlorinated Dihydroquinone 2



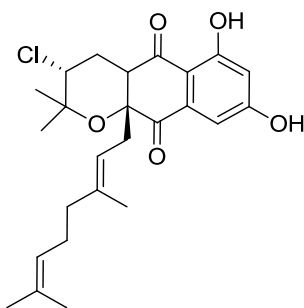
(29) 1.95 N.D. 1.95 N.D. 18

(29) Chlorinated Dihydroquinone 3



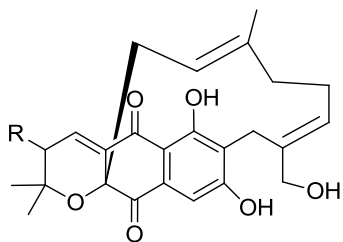
(30) >16 >16 >16 N.D. 2, 15, 25

(30) Napyradiomycin SR



(31) 4 N.D. N.D. N.D. 15

(31) 4-dehydro-4a-dechloronapyradiomycin A1



(32) 16 N.D. N.D. 4.19 2

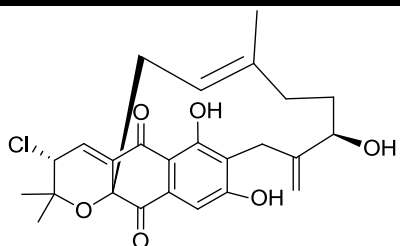
(32) R = α -Cl

(33) R = β -OH

(33) 64 N.D. N.D. >20 2

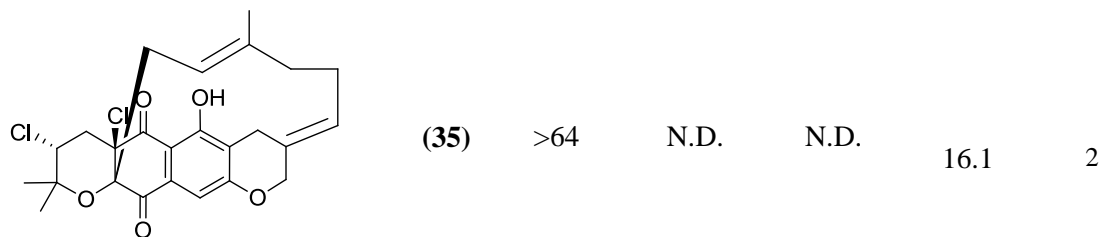
(32) Napyradiomycin 1

(33) Napyradiomycin 2

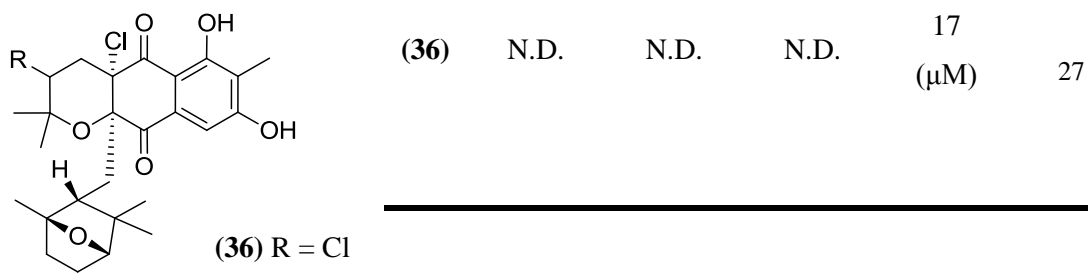


(34) >64 N.D. N.D. >20 2

(34) Napyradiomycin 3



(35) Napyrodiomycin 4

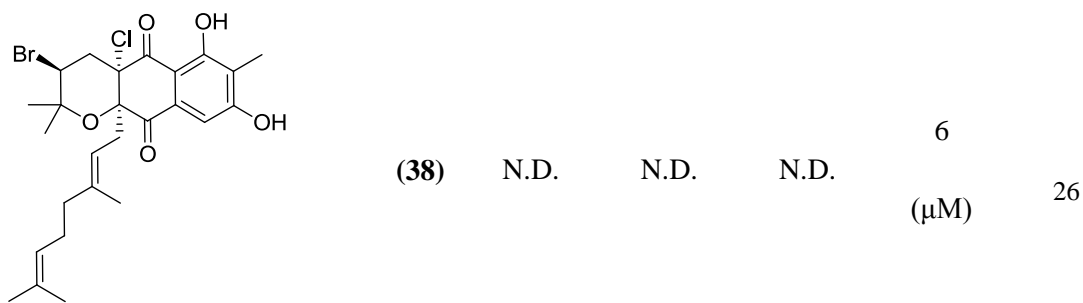
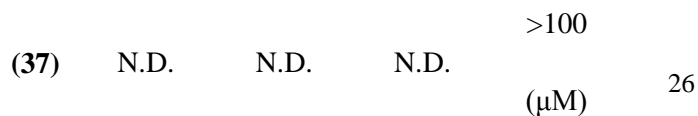


(36) R = Cl

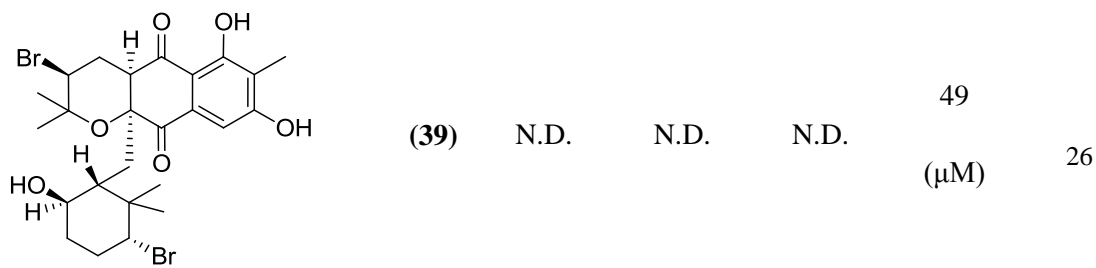
(37) R = Br

(36) CNQ525.510B

(37) CNQ525.554



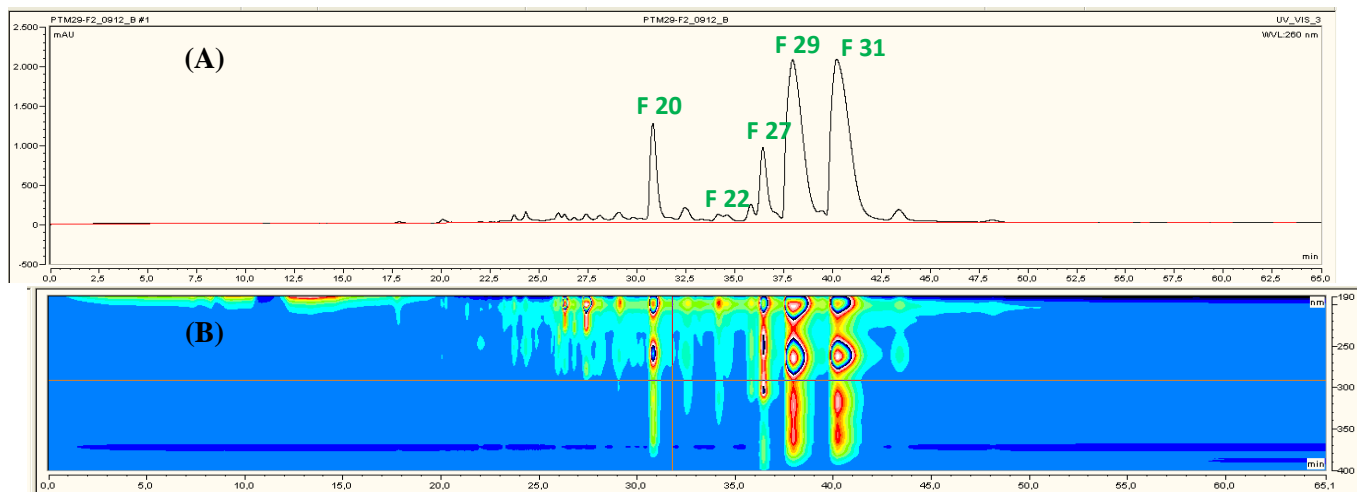
(38) CNQ525.538



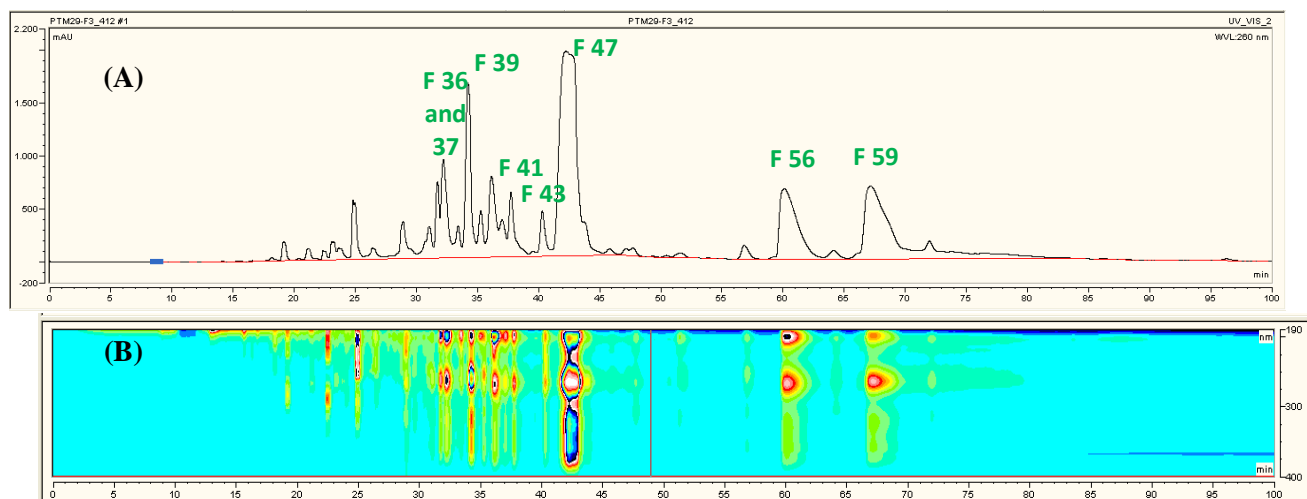
(39) CNQ525.600

Annex 3

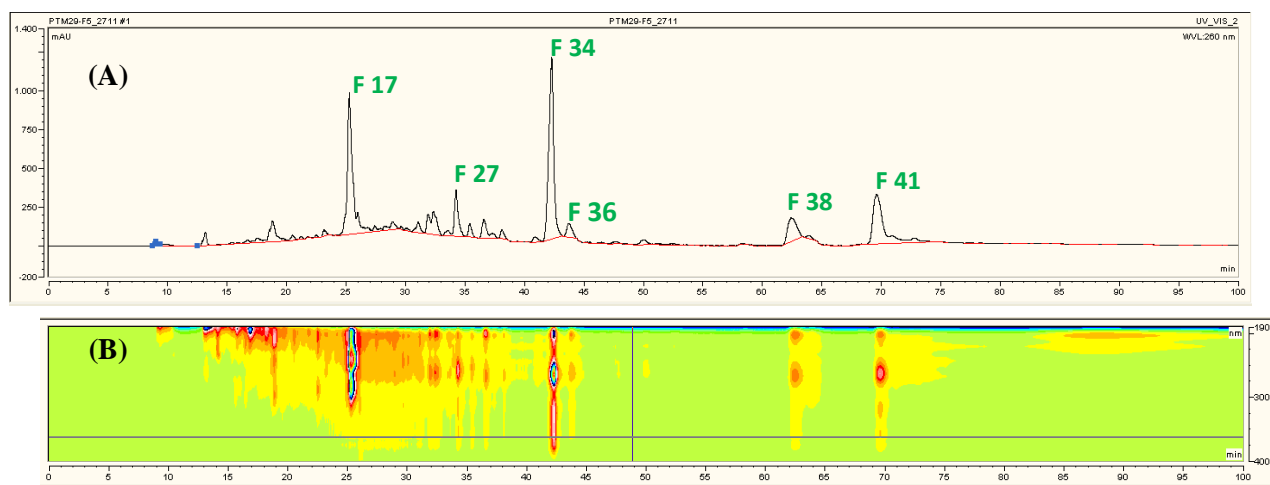
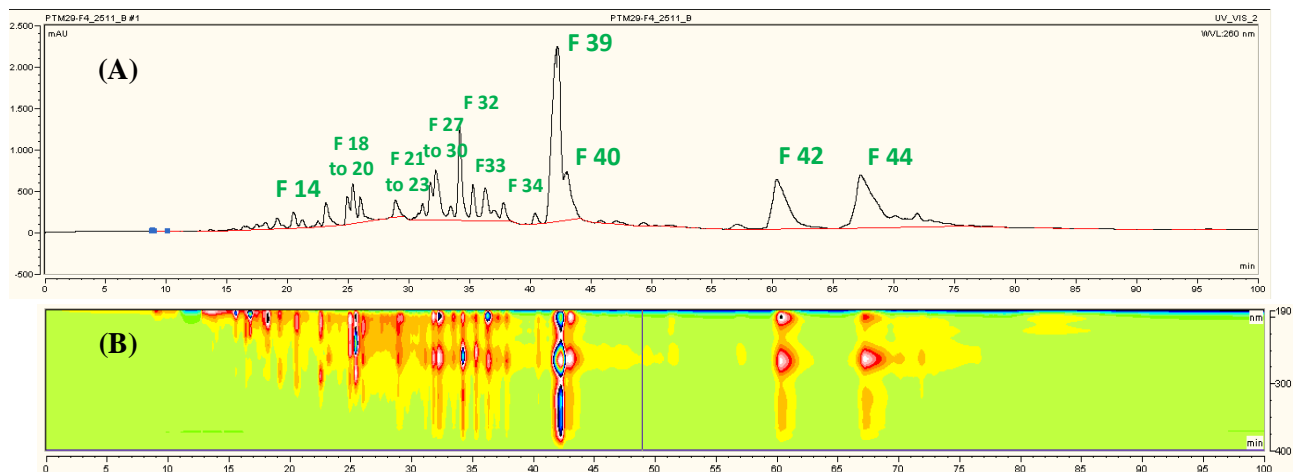
HPLC Chromatograms of PTM-029 fractions

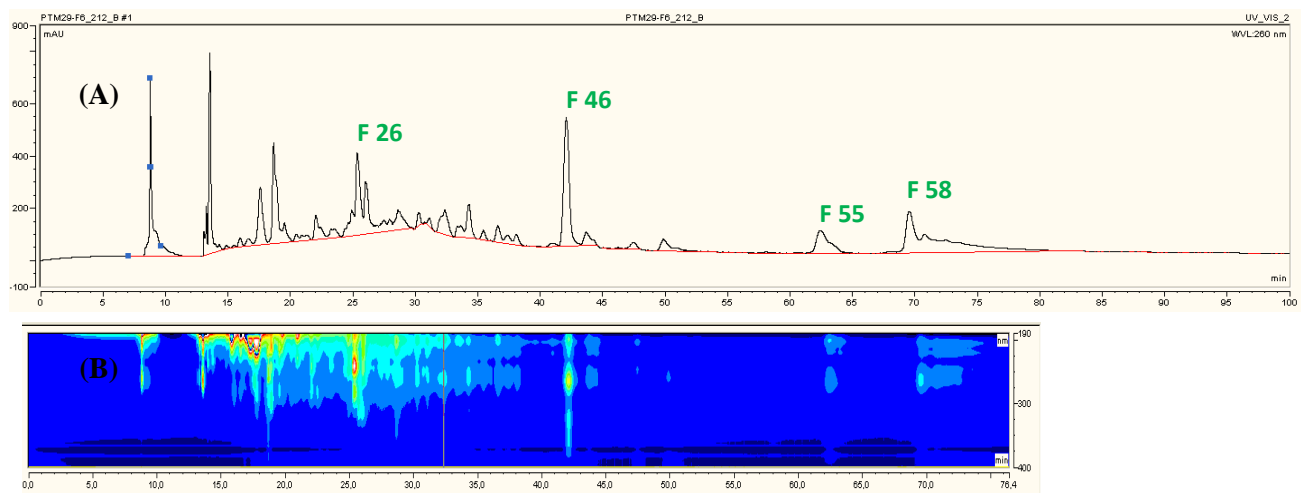


Chromatogram 1 - (A) Chromatographic profile at $\lambda = 260\text{nm}$ and (B) DAD of fraction 2 (F2) from PTM-029 performed by HPLC. Fractions in highlight are pure compounds belonging to the napyradiomycins family.

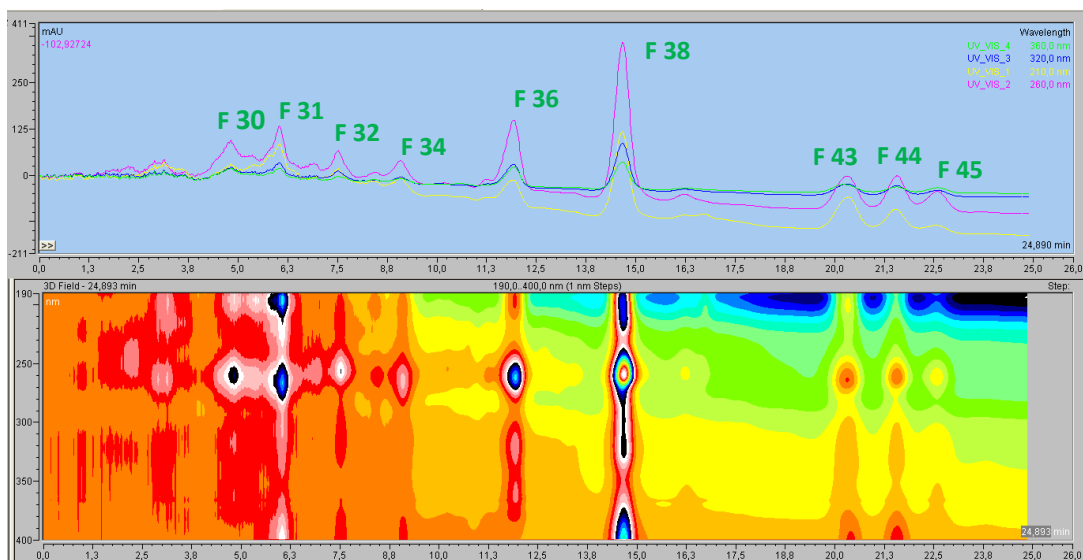
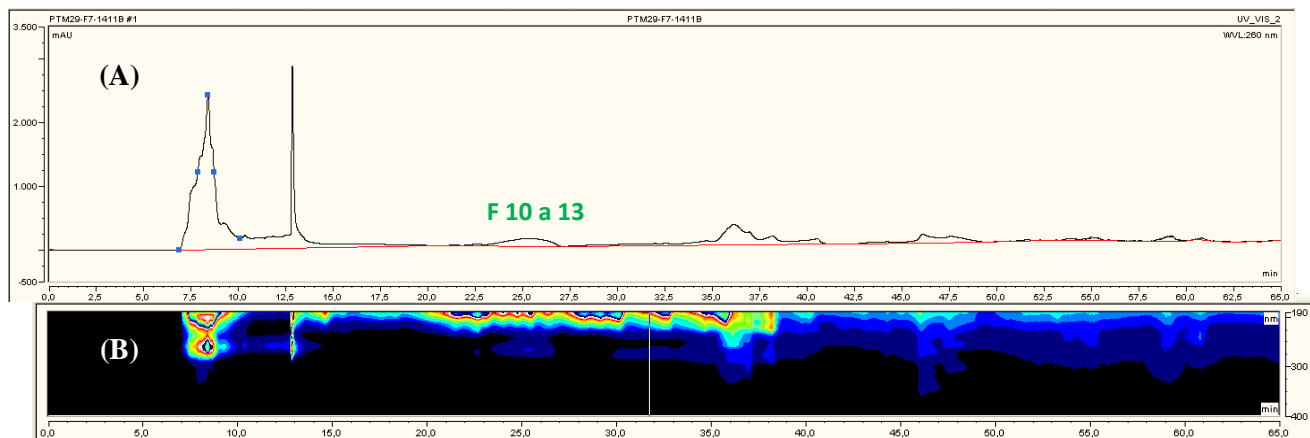


Chromatogram 2 - (A) Chromatographic profile at $\lambda = 260\text{nm}$ and (B) DAD of fraction 3 (F3) from PTM-029 performed by HPLC. Fractions in highlight are pure compounds belonging to the napyradiomycins family.

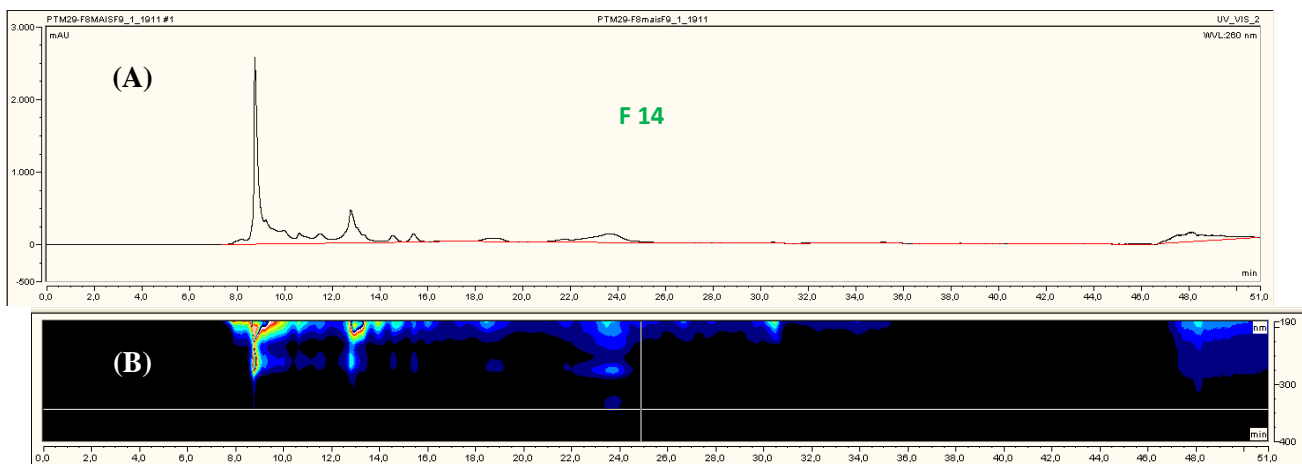




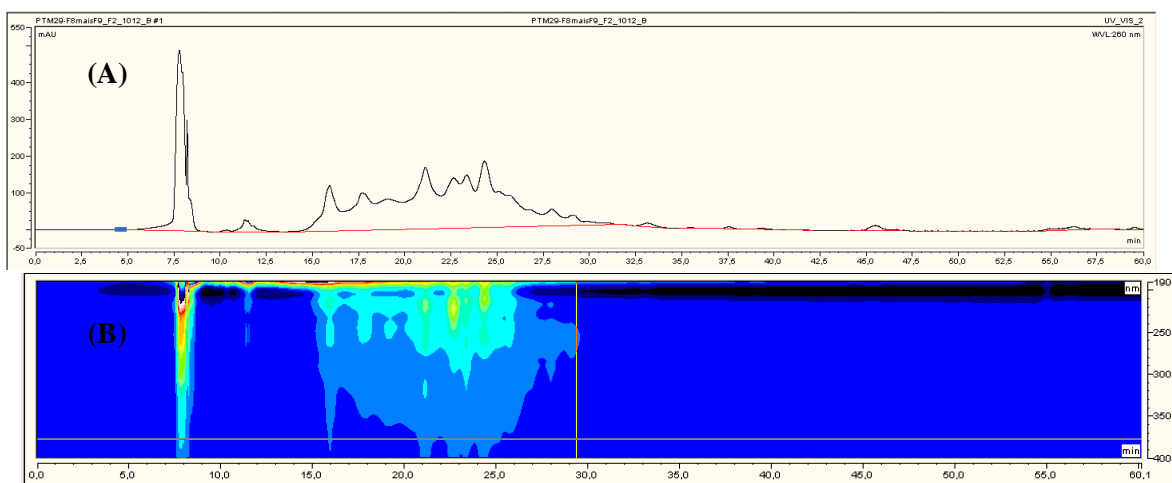
Chromatogram 5 - (A) Chromatographic profile at $\lambda = 260\text{ nm}$ and (B) DAD of fraction 6 (F6) from PTM-029 performed by HPLC. Fractions in highlight are pure compounds belonging to the napyradiomycin family.



Chromatogram 6 - (A) Chromatographic profile at $\lambda=260\text{nm}$ and (B) DAD of fraction 7 (F7) from PTM-029 performed by HPLC. Fractions in highlight are pure compounds belonging to the napradiomycins family.



Chromatogram 7 - (A) Chromatographic profile at $\lambda = 260\text{nm}$ and (B) DAD of fraction 8+9 (F8+9, F1) from PTM-029 performed by HPLC. Fractions in highlight are pure compounds belonging to the napyradiomycins family.



Chromatogram 8 - (A) Chromatographic profile at $\lambda = 260\text{nm}$ and (B) DAD of fraction 8+9 (F8+9, F2) from PTM-029 performed by HPLC.

Annex 4

Biological activity and respectively mass of pure compounds from PTM-029

F2

Table 1 – Antibacterial activity and respectively mass of pure compounds of F2 from PTM-029. * and ** peaks correspond of pure uncharacterized compounds and pure compounds belonging to napyradiomycin family, respectively.

Sample	Peak	Sample mass (mg)	MIC ($\mu\text{g/mL}$)	
			MRSA	VRE EF82
PTM-29 F2, F1		2.1		
PTM-29 F2, F2		0.2		
PTM-29 F2, F3		0.3		
PTM-29 F2, F4		0.6		
PTM-29 F2, F5	*	0.6	0	0
PTM-29 F2, F6		0.3		
PTM-29 F2, F7		0.1		
PTM-29 F2, F8		0.3		
PTM-29 F2, F9		0.3		
PTM-29 F2, F10		0.1		
PTM-29 F2, F11		0.3		
PTM-29 F2, F12		0.4		
PTM-29 F2, F13	*	0.6	0	0
PTM-29 F2, F14		0.3		
PTM-29 F2, F15		0.2		
PTM-29 F2, F16	*	0.5	0	0
PTM-29 F2, F17	*	0.6	0	0
PTM-29 F2, F18	*	0.6	0	0
PTM-29 F2, F19		0.3		

PTM-29 F2, F20	**	7.4	0.98	0.98
PTM-29 F2, F21		1.2		
PTM-29 F2, F22	**	0.6	31.25	31.25
PTM-29 F2, F23		1		
PTM-29 F2, F24	*	1.1	31.25	31.25
PTM-29 F2, F25		0.5		
PTM-29 F2, F26	*	1	125	0
PTM-29 F2, F27	**	1.7	62.50	31.25
PTM-29 F2, F28		0.5		
PTM-29 F2, F29	**	6.8	7.81	1.95
PTM-29 F2, F30		0.5		
PTM-29 F2, F31	**	1.4	15.63	3.91
PTM-29 F2, F32		1.3		
PTM-29 F2, F33	*	1	250	0
PTM-29 F2, F34		8.3		

F3

Table 2 – Antibacterial activity and respectively mass of pure compounds of F3 from PTM-029. * and ** peaks correspond of pure uncharacterized compounds and pure compounds belonging to napyradiomycin family, respectively.

Sample	Peak	Sample mass (mg)	MIC ($\mu\text{g/mL}$)	
			MRSA	VRE EF82
PTM-29 F3, F1		1.3		
PTM-29 F3, F2		0.9		
PTM-29 F3, F3		0.6		
PTM-29 F3, F4		0.8		
PTM-29 F3, F5		0.6		
PTM-29 F3, F6		0.5		
PTM-29 F3, F7		0.8		
PTM-29 F3, F8		0.7		
PTM-29 F3, F9		0.7		
PTM-29 F3, F10		0.5		
PTM-29 F3, F11		1.2		
PTM-29 F3, F12		0.6		
PTM-29 F3, F13		0.7		
PTM-29 F3, F14		0.5		
PTM-29 F3, F15	*	0.7	0	0
PTM-29 F3, F16		0.5		
PTM-29 F3, F17	*	0.6	0	0
PTM-29 F3, F18		1		
PTM-29 F3, F19		0.5		
PTM-29 F3, F20	*	1		
PTM-29 F3, F21		0.6		
PTM-29 F3, F22	*	1.1	0	0
PTM-29 F3, F23	*	0.7		
PTM-29 F3, F24	*	0.9		
PTM-29 F3, F25		0.7		
PTM-29 F3, F26	*	1		
PTM-29 F3, F27	*	0.7		
PTM-29 F3, F28	*	1		
PTM-29 F3, F29		0.8		
PTM-29 F3, F30		0.7		
PTM-29 F3, F31	*	1.1	125	125
PTM-29 F3, F32	*	0.6	0	0

PTM-29 F3, F33		0.8		
PTM-29 F3, F34	*	0.8		
PTM-29 F3, F35	*	1.1	31.25	62.50
PTM-29 F3, F36	**	1.6	31.25	15.63
PTM-29 F3, F37	**	1.9	31.25	31.25
PTM-29 F3, F38	*	1.1	62.50	31.25
PTM-29 F3, F39	**	3.5	31.25	0
PTM-29 F3, F40	*	0.7		
PTM-29 F3, F41	**	1.5	31.25	31.25
PTM-29 F3, F42		2.9		
PTM-29 F3, F43	**	1.9	31.25	15.63
PTM-29 F3, F44		1.7		
PTM-29 F3, F45	*	1.2	31.25	7.81
PTM-29 F3, F46	*	1.9	3.91	1.95
PTM-29 F3, F47	**	0.4	15.63	7.81
PTM-29 F3, F48	*	17.6	3.91	1.95
PTM-29 F3, F49		1.4	62.50	15.63
PTM-29 F3, F50	*	0.9	15.63	7.81
PTM-29 F3, F51	*	1	125	31.25
PTM-29 F3, F52	*	0.8	62.5	15.63
PTM-29 F3, F53		0.9		
PTM-29 F3, F54	*	3	62.5	15.63
PTM-29 F3, F55		1.2		
PTM-29 F3, F56	**	0.6	62.50	15.63
PTM-29 F3, F57		4.9		
PTM-29 F3, F58	*	0.9	62.5	15.63
PTM-29 F3, F59	**	1.1	31.25	15.63
PTM-29 F3, F60		5		
PTM-29 F3, F61	*	3.2	7.81	3.91
PTM-29 F3, F62		1.2		
PTM-29 F3, F63		9.3		

F4

Table 3 – Antibacterial activity and respectively mass of pure compounds of F4 from PTM-029. * and ** peaks correspond of pure uncharacterized compounds and pure compounds belonging to napyradiomycin family, respectively.

Sample	Peak	Samples mass (mg)	MIC ($\mu\text{g/mL}$)	
			MRSA	VRE EF82
PTM-29 F4, F1		1.4		
PTM-29 F4, F2	*	0.3	0	0
PTM-29 F4, F3		1.1		
PTM-29 F4, F4	*	0.9	0	0
PTM-29 F4, F5	*	1.3	0	0
PTM-29 F4, F6	*	0.9	0	0
PTM-29 F4, F7		0.8		
PTM-29 F4, F8	*	1	0	0
PTM-29 F4, F9	*	0.8	0	0
PTM-29 F4, F10	*	0.8	0	0
PTM-29 F4, F11	*	0.6	0	0
PTM-29 F4, F12	*	0.7	0	0
PTM-29 F4, F13	*	0.9	0	0
PTM-29 F4, F14	**	1.4	0	0
PTM-29 F4, F15	*	1.2	0	0
PTM-29 F4, F16	*	1.5	0	0
PTM-29 F4, F17	*	1.1	0	0
PTM-29 F4, F18	**	1.2	0	250
PTM-29 F4, F19	**	1.2	0	0
PTM-29 F4, F20	**	1.3	0	0
PTM-29 F4, F21	**	1	0	0
PTM-29 F4, F22	**	1.5	0	0
PTM-29 F4, F23	**	1.5	0	0
PTM-29 F4, F24		1.5		
PTM-29 F4, F25		1		

PTM-29 F4, F26		0.8		
PTM-29 F4, F27	**	2	62.50	125
PTM-29 F4, F28	**	2.8	31.30	0
PTM-29 F4, F29	**	2.6	62.50	62.50
PTM-29 F4, F30	**	2.5	62.50	62.50
PTM-29 F4, F31	*	2	31.30	15.60
PTM-29 F4, F32	**	3.1	250	0
PTM-29 F4, F33	**	2.6	31.25	250
PTM-29 F4, F34	**	2.4	62.5	125
PTM-29 F4, F35	*	1.2	31.30	15.60
PTM-29 F4, F36	*	3.1	62.50	250
PTM-29 F4, F37	*	1.4	62.50	15.60
PTM-29 F4, F38	*	1.8	3.91	0.244
PTM-29 F4, F39	**	13.2	1.95	1.95
PTM-29 F4, F40	**	3.4	3.91	0.98
PTM-29 F4, F41		6.3		
PTM-29 F4, F42	**	5.3	3.91	0.98
PTM-29 F4, F43		2.4		
PTM-29 F4, F44	**	6.1	3.91	0.98
PTM-29 F4, F45	*	3.4	3.91	1.95
PTM-29 F4, F46	*	1.6	15.60	7.81
PTM-29 F4, F47	*	2.1	15.60	7.81
PTM-29 F4, F48		7.3		
PTM-29 F4, F49		7		

F5

Table 4 – Antibacterial activity and respectively mass of pure compounds of F5 from PTM-029. * and ** peaks correspond of pure uncharacterized compounds and pure compounds belonging to napyradiomycin family, respectively.

Sample	Peak	Sample mass (mg)	MIC ($\mu\text{g/mL}$)	
			MRSA	VRE EF82
PTM-29 F5, F1		0.11		
PTM-29 F5, F2		0.04		
PTM-29 F5, F3	*	0.16		
PTM-29 F5, F4		0.15		
PTM-29 F5, F5	*	0.1		
PTM-29 F5, F6	*	0.16		
PTM-29 F5, F7		0.06		
PTM-29 F5, F8		0.01		
PTM-29 F5, F9	*	0.11		
PTM-29 F5, F10	*	0.05		
PTM-29 F5, F11	*	0.06		
PTM-29 F5, F12		0.05		
PTM-29 F5, F13	*	0.07		
PTM-29 F5, F14	*	0.09		
PTM-29 F5, F15	*	0.24		
PTM-29 F5, F16		0.5		
PTM-29 F5, F17	**	3.84	7.81	0
PTM-29 F5, F18	*	0.2	0	0
PTM-29 F5, F19		1.6		
PTM-29 F5, F20	*	0.6	62.50	62.50
PTM-29 F5, F21	*	0.27		
PTM-29 F5, F22	*	1.12		
PTM-29 F5, F23	*	0.22		
PTM-29 F5, F24	*	0.71	31.30	31.30
PTM-29 F5, F25	*	0.69	31.30	31.30

PTM-29 F5, F26	*	1.01	125	31.30
PTM-29 F5, F27	**	0.97	125	7.81
PTM-29 F5, F28		0.55		
PTM-29 F5, F29	*	0.59	62.50	15.60
PTM-29 F5, F30	*	0.83	125	7.81
PTM-29 F5, F31	*	0.63	125	15.60
PTM-29 F5, F32	*	0.67	62.50	15.60
PTM-29 F5, F33	*	1.42	1.95	0.49
PTM-29 F5, F34	**	3.5	0	1.95
PTM-29 F5, F35		0.74		
PTM-29 F5, F36	**	1.28	7.81	3.91
PTM-29 F5, F37		9.59		
PTM-29 F5, F38	**	1.76	0.49	0.0076
PTM-29 F5, F39	*	0.91	0.02	0.0076
PTM-29 F5, F40		1.5		
PTM-29 F5, F41	**	1.87	1.95	0.49
PTM-29 F5, F42	*	1.21	1.95	0.24
PTM-29 F5, F43	*	0.73	7.81	0.24
PTM-29 F5, F44		3.86		
PTM-29 F5, F45		2.49		
PTM-29 F5, F46		2.46		

F6

Table 5 – Antibacterial activity and respectively mass of pure compounds of F6 from PTM-029. * and ** peaks correspond of pure uncharacterized compounds and pure compounds belonging to napyradiomycin family, respectively.

Sample	Peak	Sample mass (mg)	MIC ($\mu\text{g/mL}$)	
			MRSA	VRE EF82
PTM-29 F6, F1		0.8		
PTM-29 F6, F2		0.8		
PTM-29 F6, F3	*	0.9		250
PTM-29 F6, F4		0.9		
PTM-29 F6, F5		0.8		
PTM-29 F6, F6		1.1		
PTM-29 F6, F7	*	1.1	0	0
PTM-29 F6, F8	*	0.8	0	0
PTM-29 F6, F9	*	0.7	0	0
PTM-29 F6, F10		0.8		
PTM-29 F6, F11		0.8		
PTM-29 F6, F12	*	1.4	0	0
PTM-29 F6, F13	*	1.2	0	0
PTM-29 F6, F14		7.5		
PTM-29 F6, F15	*	4.1	0	0
PTM-29 F6, F16	*	1.2	0	0
PTM-29 F6, F17	*	0.8	0	250
PTM-29 F6, F18		0.6		
PTM-29 F6, F19	*	0.9	0	0
PTM-29 F6, F20	*	0.7	0	0
PTM-29 F6, F21	*	1.4	0	0
PTM-29 F6, F22	*	0.9	125	31.30
PTM-29 F6, F23	*	1.6	0	250
PTM-29 F6, F24		1		
PTM-29 F6, F25	*	1.1	0	250

PTM-29 F6, F26	**	1.4	0	250
PTM-29 F6, F27		0.9		
PTM-29 F6, F28	*	1.1	0	250
PTM-29 F6, F29		1.1		
PTM-29 F6, F30	*	1.5	0	250
PTM-29 F6, F31	*	1.3	0	250
PTM-29 F6, F32		0.9		
PTM-29 F6, F33	*	1	250	125
PTM-29 F6, F34		0.6		
PTM-29 F6, F35	*	1.5	250	125
PTM-29 F6, F36	*	1.8	125	125
PTM-29 F6, F37	*	1.5	250	250
PTM-29 F6, F38	*	1.3	125	125
PTM-29 F6, F39		0.6		
PTM-29 F6, F40	*	1	125	15.60
PTM-29 F6, F41	*	1.1	125	15.60
PTM-29 F6, F42	*	0.6	250	125
PTM-29 F6, F43	*	0.6	250	125
PTM-29 F6, F44	*	1.2	125	125
PTM-29 F6, F45	*	1.7	7.81	0.49
PTM-29 F6, F46	**	2.3	7.81	3.91
PTM-29 F6, F47	*	1.3	31.30	7.81
PTM-29 F6, F48	*	0.8	62.50	7.81
PTM-29 F6, F49		0.8		
PTM-29 F6, F50		1		
PTM-29 F6, F51	*	0.7	125	31.30
PTM-29 F6, F52		1.1		
PTM-29 F6, F53	*	0.9	125	62.50
PTM-29 F6, F54		6		
PTM-29 F6, F55	**	1.3	0.49	0.0076
PTM-29 F6, F56	*	1.1	0.12	0.0076
PTM-29 F6, F57		1.3		
PTM-29 F6, F58	**	1.4	7.81	0.98
PTM-29 F6, F59		3		

PTM-29 F6, F60	*	0.9	31.30	0
----------------	---	-----	-------	---

F7

Table 6 – Antibacterial activity and respectively mass of pure compounds of F7 from PTM-029. * and ** peaks correspond of pure uncharacterized compounds and pure compounds belonging to napyradiomycin family, respectively.

Sample	Peak	Sample mass (mg)	MIC ($\mu\text{g/mL}$)	
			MRSA	VRE EF82
PTM-29 F7, F1		21.90		
PTM-29 F7, F2	*	3	0	0
PTM-29 F7, F3	*	3.60	0	0
PTM-29 F7, F4	*	3.20	0	0
PTM-29 F7, F5		2.20		
PTM-29 F7, F6		3.10		
PTM-29 F7, F7	*	8.40	0	0
PTM-29 F7, F8	*	3.30	0	0
PTM-29 F7, F9	*	2.80	0	0
PTM-29 F7, F10	*	3.40	0	0
PTM-29 F7, F11	*	2.60	0	0
PTM-29 F7, F12	*	3.80	0	0
PTM-29 F7, F13	*	2.60	250	0
PTM-29 F7, F14	*	1.70	0	0
PTM-29 F7, F15	*	6.80	0	0
PTM-29 F7, F16	*	4.60	0	0
PTM-29 F7, F17	*	6.70	0	0
PTM-29 F7, F18	*	7.40	0	0
PTM-29 F7, F19	*	8.90	0	0
PTM-29 F7, F20	*	3.10	0	0
PTM-29 F7, F21	*	3.30	0	0
PTM-29 F7, F22	*	2.40	0	0

PTM-29 F7, F23		6.70		
PTM-29 F7, F24	*	5.40	0	0
PTM-29 F7, F25	*	9.80	0	0
PTM-29 F7, F26		4.10		
PTM-29 F7, F27	*	3.50	0	0
PTM-29 F7, F28	*	7.10	250	31.25
PTM-29 F7, F29	*	7.80		
PTM-29 F7, F30	**	4.30	125	250
PTM-29 F7, F31	**	1.80	250	250
PTM-29 F7, F32	**	2.90	250	250
PTM-29 F7, F33		1.90		
PTM-29 F7, F34	**	2.30	62.50	250
PTM-29 F7, F35		2.80		
PTM-29 F7, F36	**	1.60	250	7.82
PTM-29 F7, F37		2.20		
PTM-29 F7, F38	**	2.40	62.50	250
PTM-29 F7, F39		2.90		
PTM-29 F7, F40		1.70		
PTM-29 F7, F41		1.30		
PTM-29 F7, F42		1.80		
PTM-29 F7, F43	**	2.10	125	15.63
PTM-29 F7, F44	**	1.50	62.50	31.25
PTM-29 F7, F45	**	1.50	0	15.63
PTM-29 F7, F46		3.90		

F8+9, F1

Table 7 – Antibacterial activity and respectively mass of pure compounds of F8+9, F1 from PTM-029. * and ** peaks correspond of pure uncharacterized compounds and pure compounds belonging to napyradiomycin family, respectively.

Sample	Peak	Sample mass (mg)	MIC ($\mu\text{g/mL}$)	
			MRSA	VRE EF82
PTM-29 F8+F9, F1, F1		2.1		
PTM-29 F8+F9, F1, F2	*	18.6	0	0
PTM-29 F8+F9, F1, F3	*	1.9	0	0
PTM-29 F8+F9, F1, F4	*	3.5	0	0
PTM-29 F8+F9, F1, F5	*	1	0	0
PTM-29 F8+F9, F1, F6		0.8		
PTM-29 F8+F9, F1, F7	*	3.8	0	0
PTM-29 F8+F9, F1, F8	*	1.6	0	0
PTM-29 F8+F9, F1, F9	*	1	0	0
PTM-29 F8+F9, F1, F10	*	0.5	0	0
PTM-29 F8+F9, F1, F11	*	1.2	0	0
PTM-29 F8+F9, F1, F12	*	4.7	0	0
PTM-29 F8+F9, F1, F13	*	0.6	0	0
PTM-29 F8+F9, F1, F14	**	2.6	0	0
PTM-29 F8+F9, F1, F15	*	1.6	0	0
PTM-29 F8+F9, F1, F16	*	1.5	0	0
PTM-29 F8+F9, F1, F17		1.3		
PTM-29 F8+F9, F1, F18	*	1.7	0	0
PTM-29 F8+F9, F1, F19	*	1.2	0	0
PTM-29 F8+F9, F1, F20		0.64		
PTM-29 F8+F9, F1, F21	*	2.7	0	0
PTM-29 F8+F9, F1, F22		2.8		
PTM-29 F8+F9, F1, F23	*	1.9	0	0
PTM-29 F8+F9, F1, F24		2.3		
PTM-29 F8+F9, F1, F25		1.7		

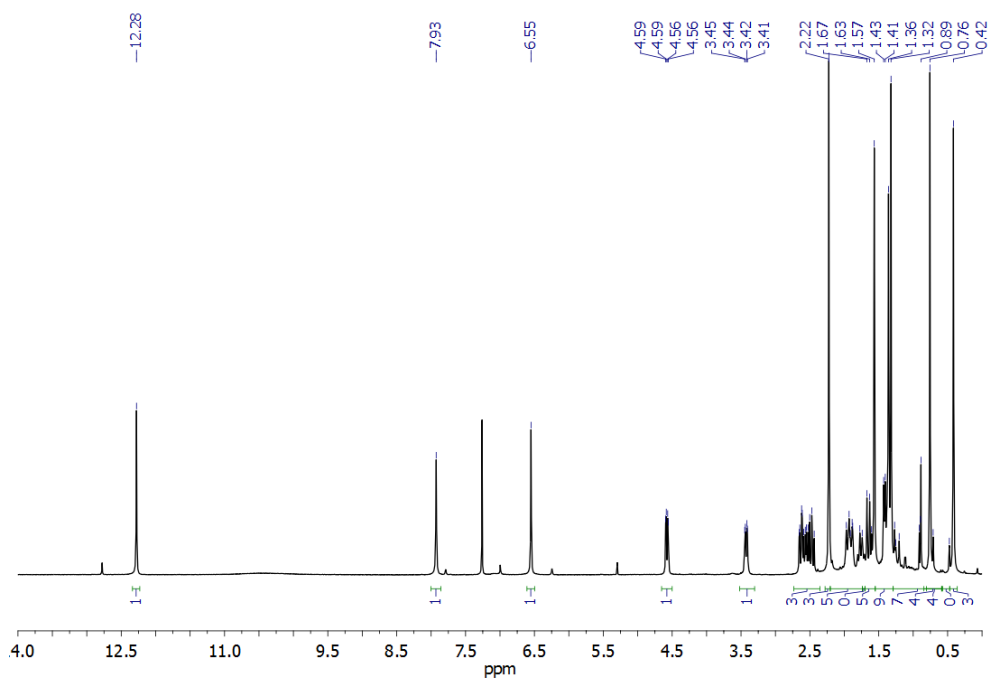
F8+9, F2

Table 8 – Antibacterial activity and respectively mass of pure compounds of F8+9, F2 from PTM-029. * and ** peaks correspond of pure uncharacterized compounds and pure compounds belonging to napyradiomycin family, respectively.

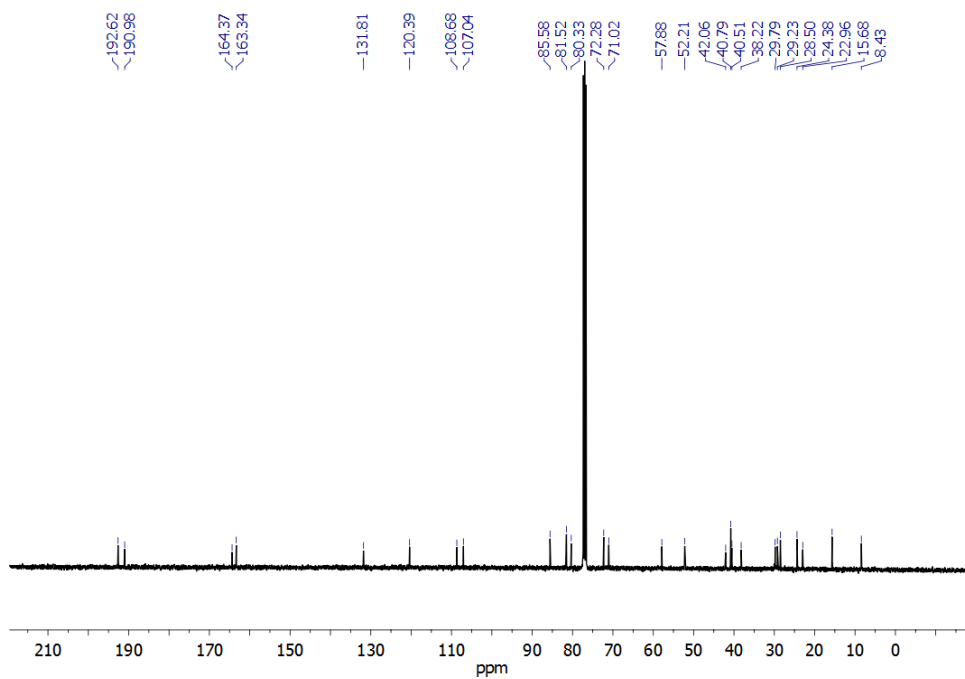
Sample	Peak	Sample mass (mg)	MIC ($\mu\text{g/mL}$)	
			MRSA	VRE EF82
PTM-29 F8+F9, F2, F1		0.3		
PTM-29 F8+F9, F2, F2		0.5		
PTM-29 F8+F9, F2, F3		0.2		
PTM-29 F8+F9, F2, F4	*	0.7	0	0
PTM-29 F8+F9, F2, F5	*	2	0	0
PTM-29 F8+F9, F2, F6	*	1.4	0	0
PTM-29 F8+F9, F2, F7		1.2		
PTM-29 F8+F9, F2, F8	*	1	0	0
PTM-29 F8+F9, F2, F9		1.3		
PTM-29 F8+F9, F2, F10	*	1.2	0	0
PTM-29 F8+F9, F2, F11				
PTM-29 F8+F9, F2, F12	*	1.3	0	0
PTM-29 F8+F9, F2, F13	*	1.4	0	0
PTM-29 F8+F9, F2, F14	*	0.7	0	0
PTM-29 F8+F9, F2, F15	*	1.2	0	0
PTM-29 F8+F9, F2, F16	*	1	0	0
PTM-29 F8+F9, F2, F17	*	1.2	0	0
PTM-29 F8+F9, F2, F18		1.7		
PTM-29 F8+F9, F2, F19	*	1.1	0	0
PTM-29 F8+F9, F2, F20		1.2		
PTM-29 F8+F9, F2, F21		1.2		
PTM-29 F8+F9, F2, F22		1.3		
PTM-29 F8+F9, F2, F23	*	1.4	125	7.81
PTM-29 F8+F9, F2, F24		5.2		

Annex 5

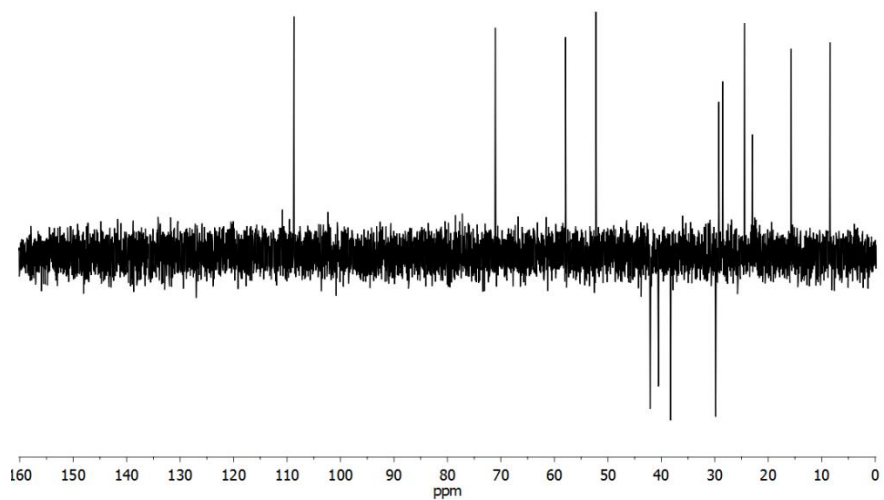
NMR and Mass data of PTM-029, F4, F39



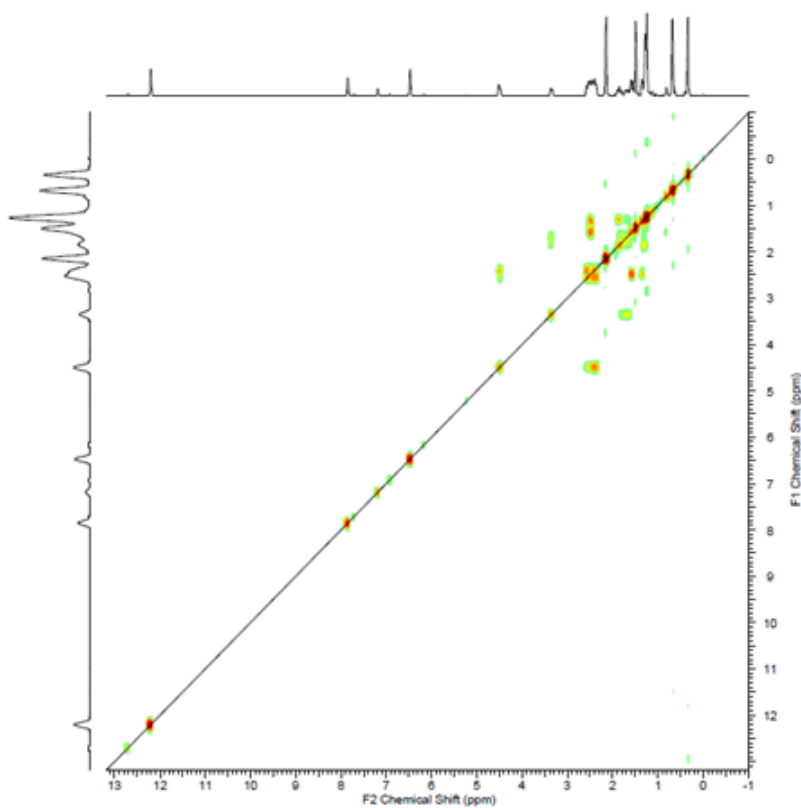
Annex 5. 1 - ^1H -NMR spectrum of PTM-029, F4, F39 in CDCl_3 .



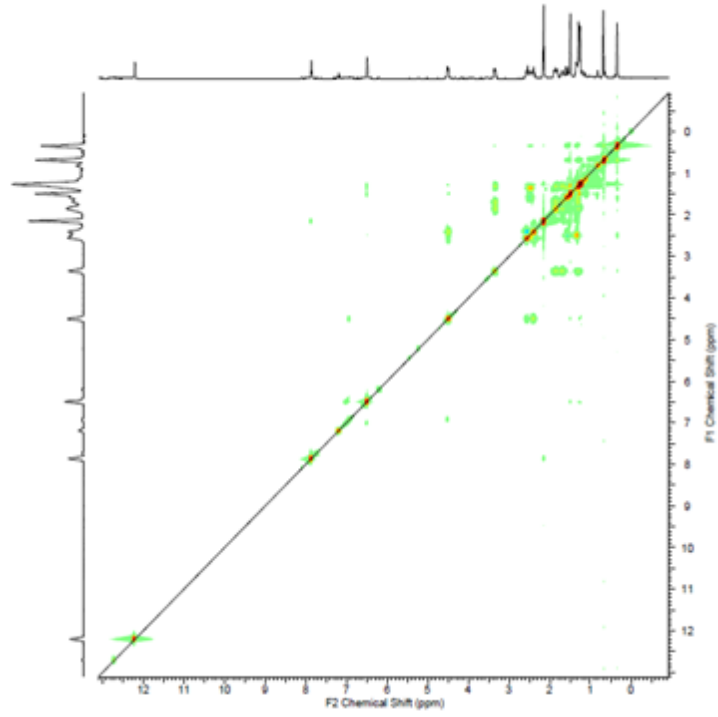
Annex 5. 2 - ^{13}C -NMR spectrum of PTM-029, F4, F39 in CDCl_3 .



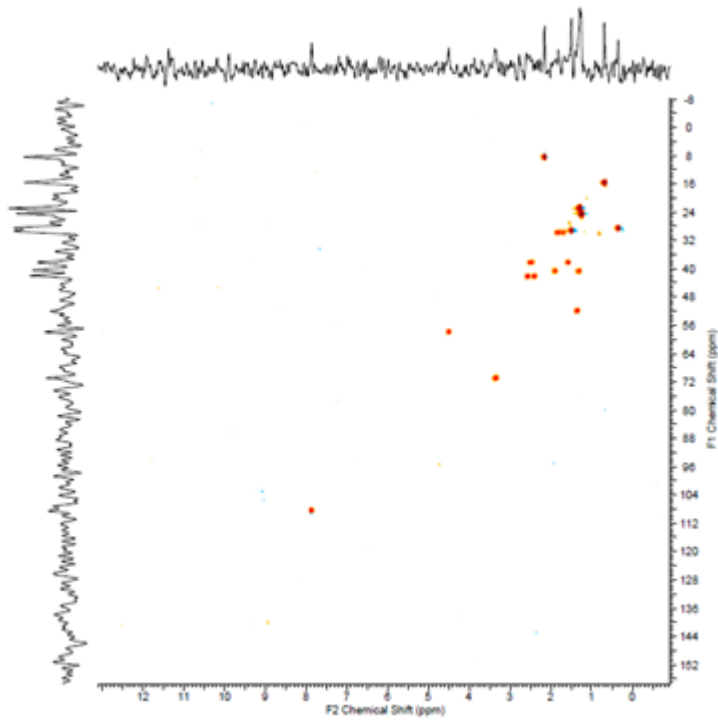
Annex 5. 3 - ^{13}C -NMR DEPT 135 spectrum of PTM-029, F4, F39 in CDCl_3 .



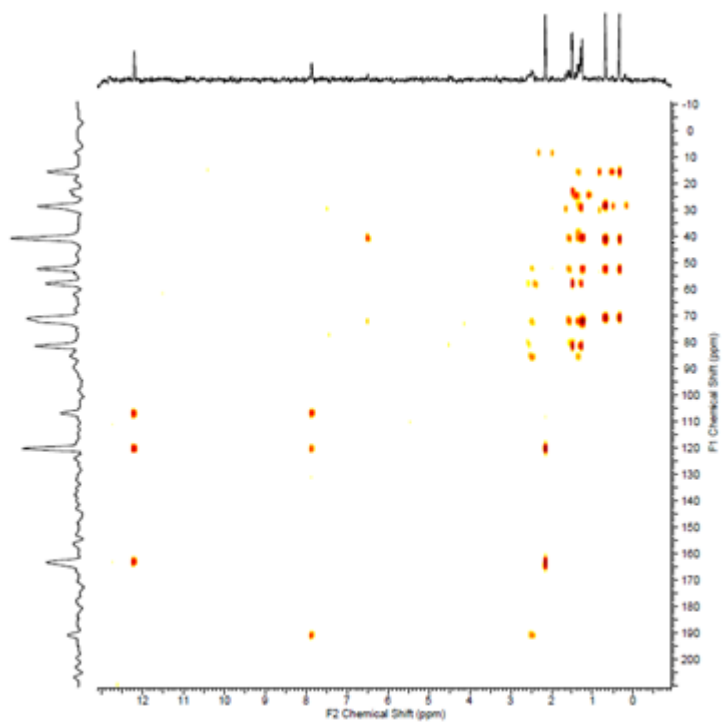
Annex 5. 4 - COSY spectrum of PTM-029, F4, F39.



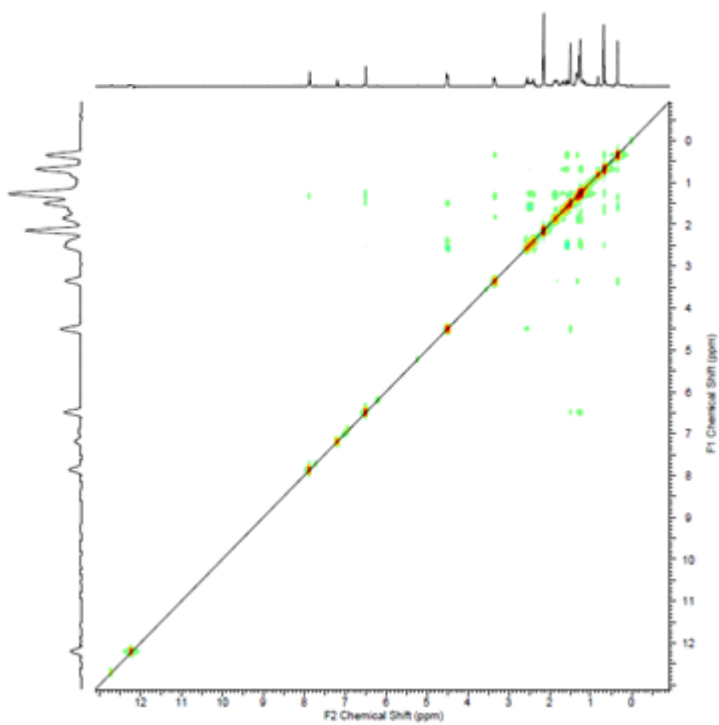
Annex 5. 5 - TOCSY spectrum of PTM-029, F4, F39.



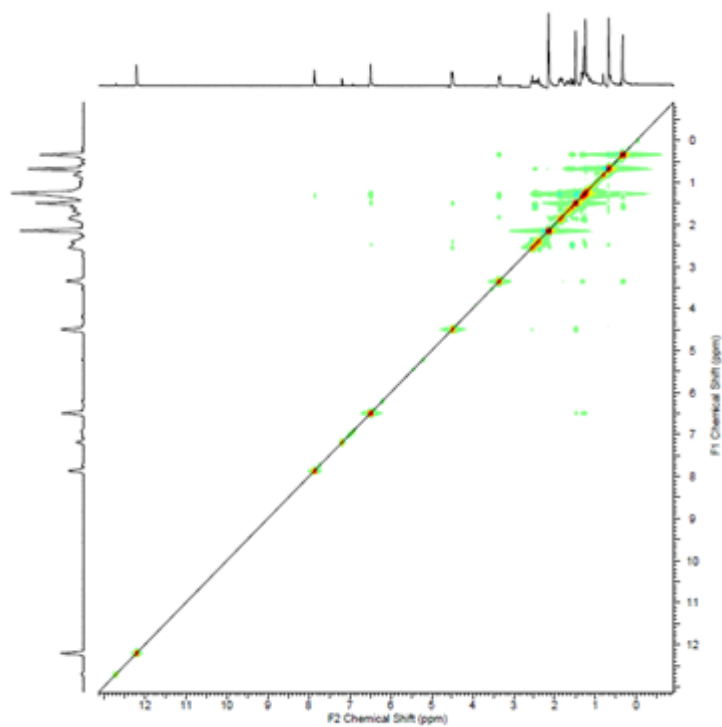
Annex 5. 6 - HSQC spectrum of PTM-029, F4, F39.



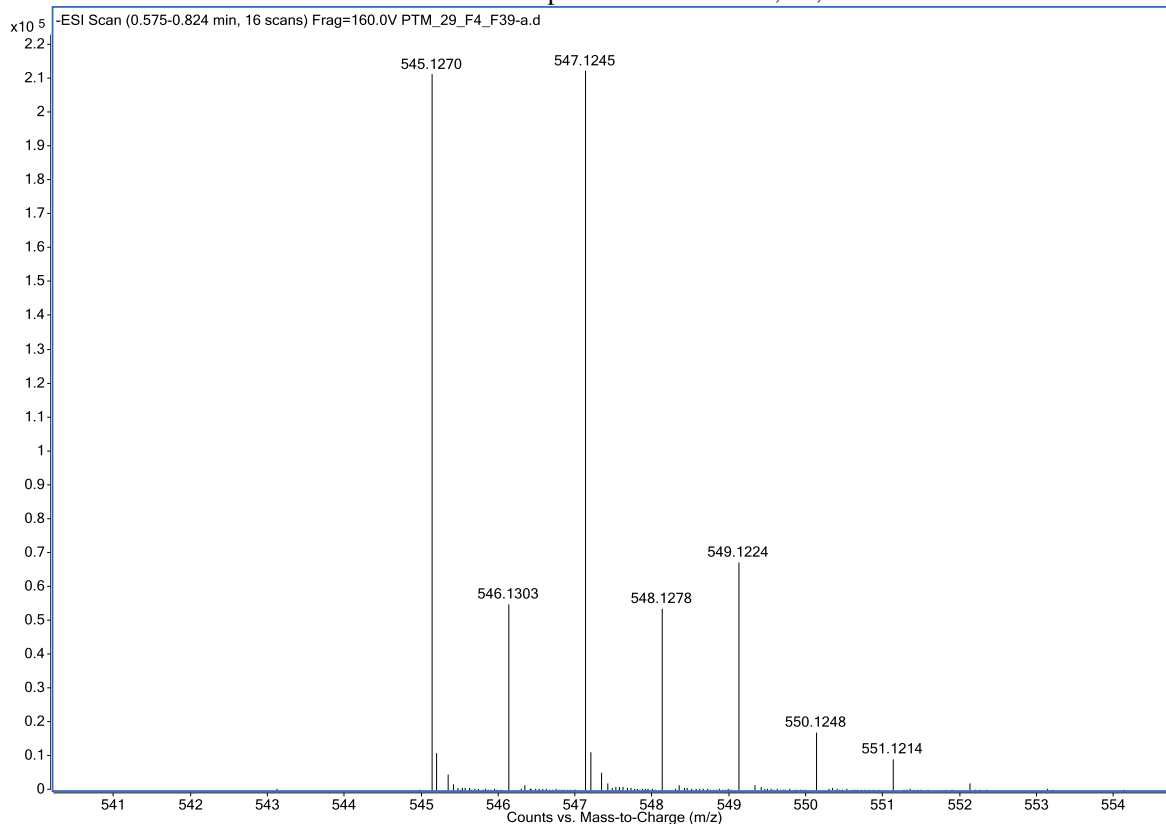
Annex 5. 7 - HMBC spectrum of PTM-029, F4, F39.



Annex 5. 8 - NOESY spectrum of PTM-029, F4, F39.



Annex 5. 9 - ROESY spectrum of PTM-029, F4, F39.



Annex 5. 10 - HR-Mass spectrum of PT M-029.

Part II - Dry powder formulations containing encapsulated bioactive-agent by supercritical assisted spray-drying (SASD)

1. Introduction

Drug delivery, much like drug discovery, is focused on improving health. Controlled drug delivery strategies include both sustained (over days/weeks/months/years) and targeted (e.g. to a tumor, diseased blood vessel, etc.) delivery on a one-time or sustained basis.³⁰

The route of administration significantly influences the therapeutic income of a drug. A drug delivery system should assure protection of a drug against degradation and ensure that the drug reaches proper permeability properties to subsequently, provide a complex transportation and protection system against the natural barriers.³¹ Even though the oral route is simple and the most common one, it has a risk of drug decomposition by digestive system. The transdermal route is also simple, but an adsorption efficiency of drugs is generally low in this method. Injections result in high adsorption efficiency, an early effect of injected drugs' pharmacological actions, and no risk of drug decomposition by digestive organs. However, because this is an invasive method, it provokes discomfort to patients.³²

Recently, there has been an increasing interest in developing systems for the controlled delivery of therapeutic molecules to the lungs since it provides excellent advantages. The local application of drugs to the respiratory tract via inhalation facilitates a site specific treatment of lung diseases (asthma, chronic obstructive pulmonary disease (COPD)) with lower systemic exposure and consequently, reduced side effects. Yet again, it is also an advantageous route for systemic drug delivery since it shows a high solute permeability, due to its very thin absorption membrane (0.1-0.2 μm), to its elevated blood flow (5L/min) and to the highly vascularized alveolar epithelium constituted by a single layer of cells, which offers a large absorptive surface (80–100 m^2). All this facilitates the distribution of the molecules throughout the body.^{33,34} It also has an easy administration, shows early effects of drugs' pharmacological actions and has no risk of drug decomposition.³⁵ The absorption of macromolecules via the pulmonary route is rapid and facilitated by the highly vascularized alveolar epithelium. Also, unlike the oral route, it is not subject to first

pass metabolism which is especially important to macromolecules (i.e. peptides and proteins) that are easily degraded by enzymes.

However, the short duration of drug action in the lung is considered a significant disadvantage of conventional inhalation therapy. Therefore, the development of pulmonary controlled release formulations would be highly beneficial for patients suffering from lung diseases. Controlled drug release systems composed of polymeric materials with particular characteristics, such as biocompatibility and degradability, have been shown to improve the pharmacokinetic and pharmacodynamic profiles of encapsulated drugs in the lung.^{32,35}

The inhalation technology has two main areas: the development of inhalation devices, by designing more sophisticated inhalers, however these devices are complex and costly; and the other by using particle engineering.³⁶ From the formulations available for inhalation, the dry powders as drug delivery systems has been increasingly considered as a treatment option, even though it brings out concerns related to respiratory tract anatomy, breathing pattern and particle size.³⁷ Ideally, dry powders should have high dispersibility, drug stability, narrow size distribution and sustained release. Above all, there is a need to control both size and morphology of the particles since those are the characteristics that affect drug deposition. There is also a need to make sure that the particles have a physical stability in order to prevent unfavorable solid-state transitions.³¹

1.1 Dry Powder Inhalers

Dry powder inhalers, to be a good aerosol delivery device, should generate an aerosol of a suitable size (1-5 μm) with a reproducible drug dosing that makes sure the drug chemical stability and activity are intact. Besides, this device should be simple, easy to use, inexpensive and portable.³⁴ Table II. 1 represents a comparison between the three existing inhalers, taking into account the described characteristics.

Table II. 1 – Comparison between the different inhalers relatively to different characteristics.

	Nebulizers	pDMI	DPI
Delivery efficiency	+	-	+
Ease of use	-	-	+
Portability	-	+	+
Drug stability	-	-	+

The first inhalers to be developed and to appear on the market were the nebulizers, in which the drug is dissolved in a polar liquid. However, they showed some disadvantages such as low efficiency and reproducibility, the required time to the administration was about 30 minutes and their use was confined to hospitals or home, given that they were not portable.^{33,34}

To surpass these issues, the pressurized metered dose inhalers (pMDIs) were developed since they show greater efficiency and reproducibility, they are faster to use and also portable. Despite that, they also show some drawbacks since they require the use of compressed volatile liquids as propellants (i.e. chlorofluorocarbon), making them environmentally unfriendly.³⁸

In order to overpass these problems, the inhalers were improved, and dry powder inhalers (DPIs) appeared (Figure II. 1). Besides being easy to use and portable, they are also propellant-free, making them environmentally friendly. Also, since the aerosols are in a dry state they assure the stability of the drug, needing no special condition storage and distribution.³⁹ However, they are expensive, complex to develop and the uniformity of the doses depends on the patient's inspiratory flow since it is what set the particles in motion, provoking turbulence and shear in order to generate the aerosol. The particles then enter the patients airways and are carried to the deep lung.⁴⁰ These devices are divided in "single-dose" DPIs, which use a single dose capsule, in "multiple unit dose" DPIs, which contains small doses separated in several capsules or blisters and in "multidose" DPIs that contain an amount of powder that is then delivered in several metered doses.⁴¹

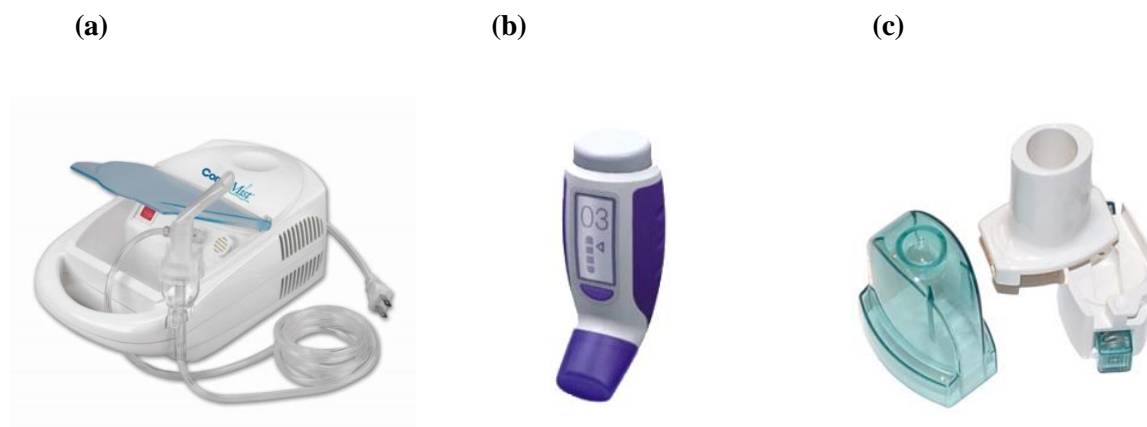


Figure II. 1 - Example of different inhalers (a) is a nebulizer, (b) a pMDI and (c) a dry powder inhaler.⁴²

1.2 Characterization of inhaled particles

Particle engineering using appropriate processes and excipients is required to produce particles of optimal size, morphology, and surface properties that would enhance aerosol flowability efficiency. As a consequence, the preparation of drug microparticles with a controlled particle sized distribution has become an important step for the development of aerosol delivery formulations. DPI's for aerosol delivery require a particle aerodynamic diameter distribution ranging between 1 and 5 μm to avoid impaction and/or sedimentation in the upper airways.^{43,44}

In order to understand where particles with different size deposit in the respiratory tract, the aerodynamic diameter (d_a) it has to be taken into account and is defined by the equation (1).

$$d_a = d_g \sqrt{\frac{\rho_p}{\rho_0 x}} \quad (1)$$

Where ρ is the mass density of the particle, ρ_0 is the unit density, d_g is the geometric diameter and x the particle dynamic shape factor.⁴⁴

Though some conflicts regarding the range for optimal d_a to efficiently reach the deep lungs may exist, the most recent works states that the aerodynamic diameter of aerosol particles should be between 1 and 5 μm since these size range is the one that gets to the deep lungs (Figure II. 2). While smaller particles may fail to deposit and are exhaled, bigger ones may accumulate in the mouth and throat by inertial impaction. The particles in between should deposit in the deep lung by inertial impaction and sedimentation.^{43,44}

Moreover, smaller particles are more likely phagocytized and have the tendency to aggregate due to van der Waals and electrostatic forces⁴⁵, making large porous particles with low density suitable for lung delivery⁴⁶. Large porous particles have a mean diameter bigger than 5 μm and an associated low mass density, so even though these particles have large geometric diameters, they exhibit aerodynamic diameters comparable to smaller particles due to their low density. Since they have large sizes, these particles will avoid clearance by alveolar macrophages, enabling sustained drug delivery through the lungs. Furthermore, increasing the geometric diameters would increase the dispersibility and entrainment of the drug particles from the inhaler and finally they would tend to de-aggregate much easier than small non-porous particles.³¹

Andersen Cascade Impactor (ACI) is generally used for testing both the development and quality control of inhaler products since both the differential pressure over the inhaler and airflow rate can be controlled and, alongside with the Next Generation Impactor (NGI), is recommended in

both the European and United States pharmacopoeia. ACI is a sizing sampler containing 8 aluminum stages, each with a collection plate and a filter, and an induction port with a suitable mouth piece adapter. At times a pre-separator is used to collect large masses of non-respirable powders. The air flow rate should provide a pressure drop of 4 KPa with a defined time that allows the passage of 4 liters of air through the ACI. The inhaled aerosol will be fractionated into different stages that have a decrease in the nozzles' diameter throughout the apparatus (Figure II. 2). The particles deposition on each collection plate will depend on their size and density, and subsequently their inertia, being the particles with larger d_a collected in the early stages and the smaller ones on the last.

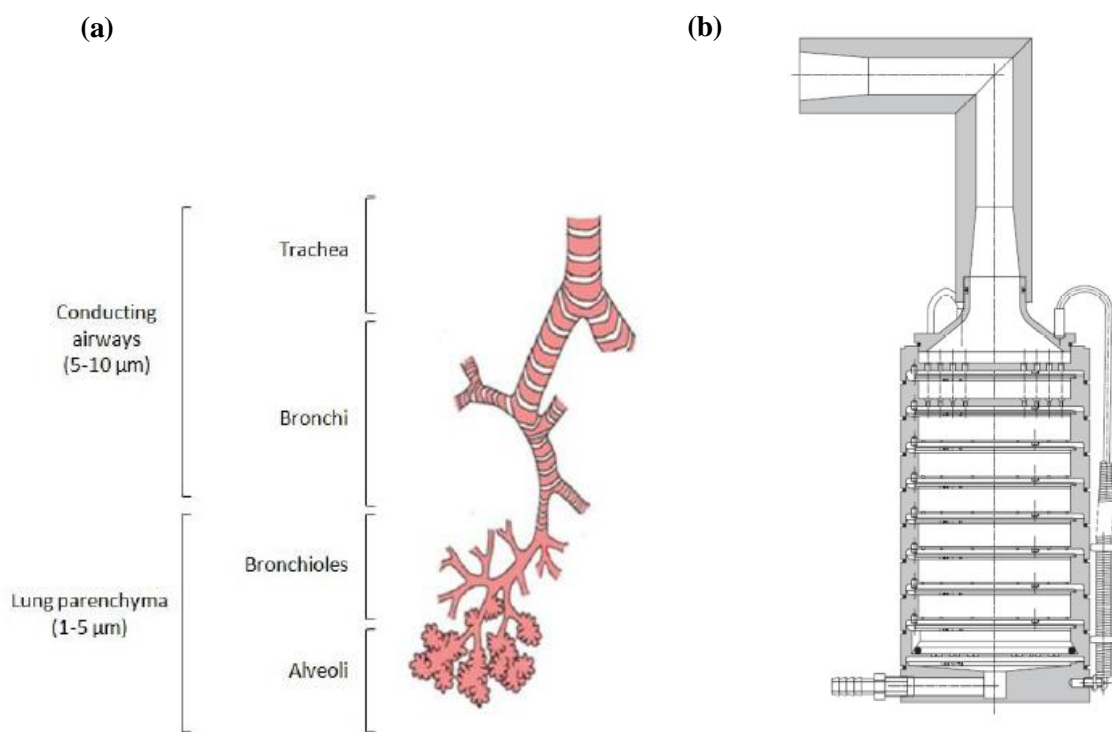


Figure II. 2 - (a) Representation of the different stages of the respiratory tract and the particles' deposition according to size. (b) Schematic representation of the Andersen Cascade Impactor, adapted from the European pharmacopoeia.

ACI provide important parameters to evaluate the aerodynamic performance of a DPI, like the mass median aerodynamic diameter (MMAD), which is the particle diameter that can be obtained with the use of an *in vitro* aerosolization study such as a multistage cascade impactor, and it corresponds to 50% of the cumulative distribution. With the same apparatus it is possible to calculate the fine particle fraction (FPF) that is the mass of particles under a cut-off diameter of

around 5 μm and with the use of a dosage unit sampling apparatus (DUSA) the shot weight can be determined, which is the proportion of powder that exits the capsule.⁴⁷

To provide a sustained controlled release, drug-polymer systems were produced and the release of the drug is dependent not only in the diffusion rate from the non-degraded polymer, but also by its swelling and erosion. By modeling the drug release using mathematical equations, important information regarding mass transport and chemical processes relatively to the drug delivery system can be acquired, coupled with the effect of the parameters, for instance particle geometry or drug loading.⁴⁸

When it comes to model the drug release out of polymeric matrices, the most used is the Korsmeyer-Peppas equation (2), even though it stands on a method to study only the importance of the diffusional exponent, n , which indicates the transport mechanism. The mechanism can either be due to the Fickian diffusional release ($n=0.43$) or polymer's swelling ($n=0.85$). It also considers the constant k , which incorporates characteristics of the macromolecular network system of the drug.⁴⁹ It is only valid to the first 60% of the release, since the further release is dependent on other factors that are not taken into account, such as particles degradation.

$$\frac{M_t}{M_\infty} = kt^n \quad (2)$$

1.3 Cholesterol and Chitosan excipients

In the last decades lipid based carrier systems have captured attention since they are made up of physiological, biodegradable and biocompatible lipid materials. The most commonly employed lipid materials, in drug carriers development, is cholesterol (CLT) (Figure II. 3).^{44,50}

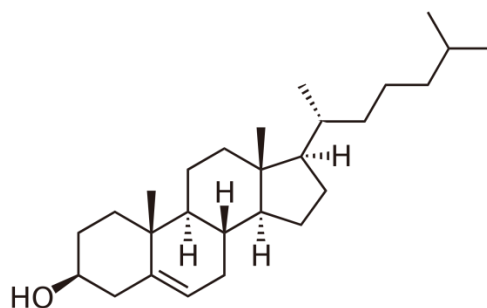


Figure II. 3 - Cholesterol structure.

Cholesterol offer a good tolerance in the pulmonary tract as it constitutes a significant portion of the naturally occurring pulmonary surfactant pool.⁵¹ Both lung tissue and lung airway fluid contain significant amounts of cholesterol, representing ~16–22% of the total lipids in human lung tissue and ~5–6% of the total lipids in lung surfactant.⁵⁰ Use of excipients endogenous to the lungs, like cholesterol is interesting, once it is biocompatible to the lung and can easily be metabolized or cleared by direct absorption through the epithelial cells or uptake by the alveolar macrophages.⁵¹ Nevertheless, a careful balance should be maintained between exogenous and endogenous components. Use of lipids for coating drug particles or incorporated in a matrix, seems to be very promising as an excipient in the future development of sustained dry powder formulations, for pulmonary delivery of drugs. Moreover, their ability to modify the surface properties of particles through coating reduces the agglomeration tendency of a powder and increases the fine particle fraction, due to the hydrophobic nature of lipids, especially of neutral lipids, which reduces the absorption of the ubiquitous vapor onto particles during inhalation, limiting aggregation and adhesion phenomena.³⁴

Chitosan (CHT) is a cationic linear polysaccharide (Figure II. 4). It is a co-polymer comprising N-acetyl-2-amino-2-deoxy-D-glucopyranose and 2-amino-2-deoxy-D-glucopyranose, being obtained by partial deacetylation of chitin and is already being used in cosmetics. Many applications of CHT have been proposed for therapy and theranostics, such as for the delivery of therapeutic agents, bioimaging, tissue engineering, and wound healing and stimuli-responsive materials.^{52,53}

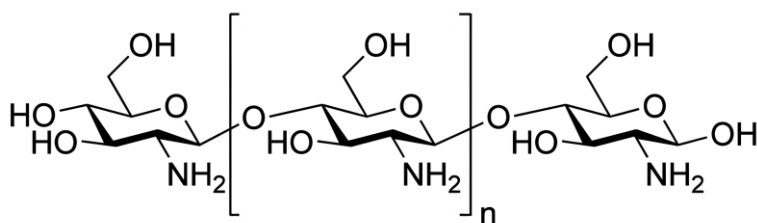


Figure II. 4 - Chitosan structure, where n is related to the DD % and m to $(100 - DD \%)$. Ideal chitosan would have $m=0$ and chitin would have $n=0$. Adapted from M. Dash et al.⁵⁴ and J. Kumirska et al.⁵³

For the delivery of therapeutic agents, CHT has been successfully applied to gene delivery, growth factor hormones, BSA, IBP, doxorubicin, dopamine and paclitaxel.^{55,56,57} Chitin is the second most occurring polysaccharide in nature, next to cellulose and is present in crustaceous

shells. Several millions of tons of chitin are harvested each year as the shell waste of crustaceans, making it a relatively cheap and readily available source of crustaceans, making it a relatively cheap and readily available source.^{54,58}

CHT can be eliminated by renal clearance, unless its MW is too large. If that is the case, then CHT must be degraded by enzymes capable to hydrolyze glucosamine-glucosamine, glucosamine-N-acetyl-glucosamine and N-acetyl-glucosamine-N-acetyl-glucosamine linkages, such as lysozyme, which is also present in the lung mucosa.^{54,59} Since it is biodegradable, biocompatible and non-toxic, CHT is an interesting choice to be used as a drug carrier, protecting the drug against enzymatic degradation. Also, clinical tests made CHT-based biomaterials show that there are no inflammatory or allergic reactions due to its application and possesses a LD₅₀ in laboratory mice similar to sugar and salt. It is characterized by molecular attractive forces due to electrostatic interactions between positively charged CHT and negatively charged mucosal surfaces, promoting drug transmucosal absorption.⁵⁴ CHT microparticles can be used as carriers, the drug is released due to the gelling ability of CHT because when it contacts with aqueous solutions, the polymeric chain begins to swell as water enters the small holes between each chain. Also, it has recently been confirmed that CHT has a drug adsorption-enhancing effect in pulmonary tissues by opening of the intercellular junction of the lung epithelium, as well as improving drug targeting and dissolution rate of drugs. Since CHT is soluble in weak acidic solutions, the production of microparticles offers the possibility of avoiding hazardous organic solvents. Also, CHT has a good ability to control the release of APIs, making it a material of interest to produce and develop drug release systems.

1.4 PLGA

Poly (lactic-co-glycolic acid) (PLGA) (Figure II. 5) is used as a biodegradable slow-release polymer, it is physically strong, highly biocompatible and bioabsorbable and also allows an effective encapsulation of all kinds of drugs, proteins, various other macromolecules such as DNA, RNA and peptides and besides, it is FDA (Food and Drug Administration) approved.⁶⁰

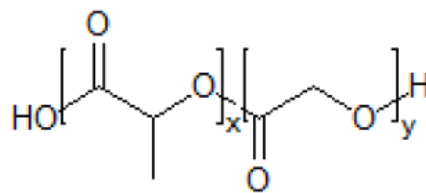


Figure II. 5 - PLGA structure, with the lactic acid between the left-side brackets and the glycolic acid between the right-side brackets. x and y represent the number of times the unit it repeated.

A main influence on the release is the polymer biodegradation. PLGA's ester backbone undergoes hydrolysis in aqueous environments, such as body fluids, and the polymer eventually degrades to lactic and glycolic acid monomers with well-established compatibility and safety profile since the products are nontoxic, noncarcinogenic, and nonteratogenic.^{61,62} The presence of a drug may change the mechanism from bulk erosion to surface degradation. In general, the PLGA degradation and the drug release rate can be accelerated by greater hydrophilicity, increase in chemical interactions among the hydrolytic groups, less crystallinity and larger volume to surface ratio of the particles. The T_g (glass transition temperature) of the PLGA copolymers are reported to be above the physiological temperature of 37 °C and hence are glassy in nature, exhibiting fairly rigid chain structure. It is known that the T_g decrease with a decrease of lactide content in the copolymer composition and with a decrease in molecular weight. The glass transition temperature for 50:50 ratio of PLA/PGA is between 45 and 50 °C.⁶³

1.5 *Living polymer end-capped with different compounds*

Poly(2-ethyl-2-oxazoline)-based lipid conjugates have been proposed⁶⁴ as alternative to PEG-based materials, the most extensively described polymer for conjugation in drug delivery. Mero *et al.*⁶⁵ reported in their work that the properties of polyoxazolines-conjugates could be compared with those of similar PEG-conjugates.⁶⁶

Oxazoline-based polymers are, relatively non-toxic and generally water soluble and biodegradable. Due to their versatility and ability to form functional materials, this class of polymer are interesting candidates for use in a large number of applications, such as smart materials, membrane structures, drug carriers, synthetic vectors for DNA or RNA delivery and antimicrobial agents.⁶⁷ Polyoxazolines of various architectures and chemical functionalities can be prepared in a

living and controlled manner via cationic ring-opening polymerization (CROP). The name of “living” polymerization is due to the polymeric chain ends, which remain active until a direct termination occurs.^{65,66}

Although, 2-oxazoline-based polymers have not found widespread commercial application due, in part, to their polymerization times ranges (reactions times can vary from several hours to several days). This method leads to less side reactions and maintain the *living* character of the reaction, using a higher temperature and pressure.⁶⁶

The polymerization starts with a nucleophilic attack of the lone pair of the 2-oxazoline ring onto the formed oxazolinium species leads to the ring opening by cleavage of the C-O bond (Figure II. 6). Due to the absence of chain-transfer or termination reactions under the appropriate conditions, the polymerization occurs in a *living* manner until all monomer is consumed or an end-capping agent is added. The interest in this class of polymers is increasing due to their particular characteristics and extensive applications in chemistry, biochemistry and pharmacology.^{65,68}

In this work, the obtained *living polymer*, 2-ethyl-2-oxazoline was later end-capped with different compounds like water, (*S*)-(+)-Ibuprofen Salt and a bioactive compound from marine *Actinobacteria* PTM-029, F4, F39, produced in Part I.

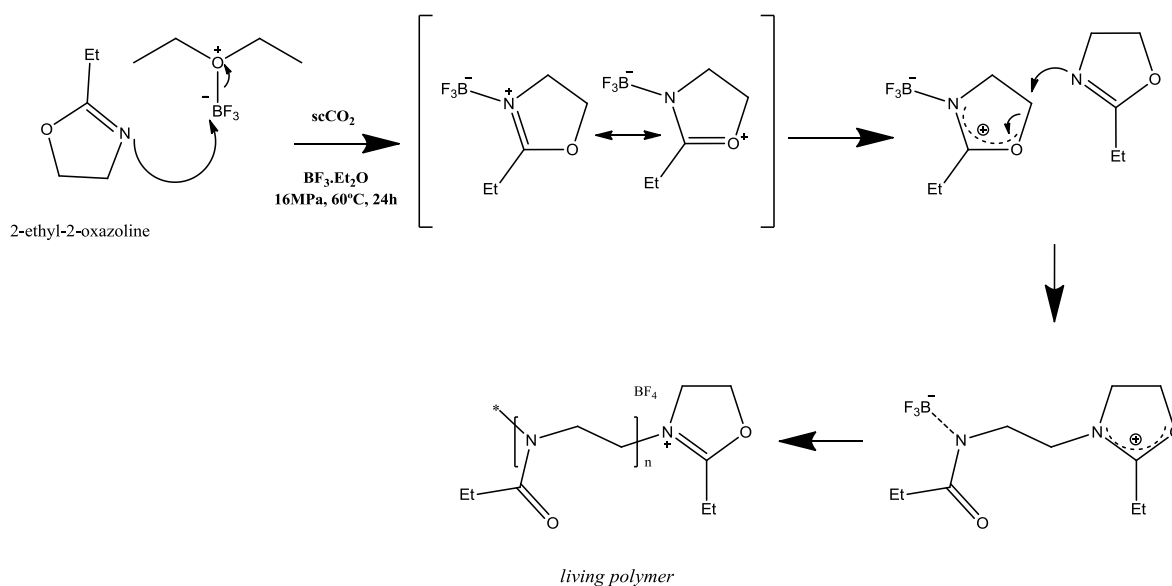


Figure II. 6 - Mechanism of the living cationic ring-opening polymerization of 2-ethyl-2-oxazoline.⁶⁸

1.6 Particle Production

The majority of currently commercially available inhalation products consist of a micronized drug in either agglomerated or blended form.³⁶

There are several known methods to produce particles for inhalation and those can be divided into two groups: the top-down (large particles are mechanically broken down to smaller ones) and the bottom-up (particles are formed from the molecular level).

Top down approach is based in milling since it consists on the grinding of bulk crystallized particles into small ones with the use of mechanical forces such as pressure, friction, attrition, impact or shear.⁶⁹ In order to produce particles for inhalation, there are three types of mills that can be used, fluid-energy mills (jet-milling), high-peripheral-speed mills (pin-mill) and ball mills. The most used technique is jet-milling where high-pressure nitrogen is used to provide a sonic velocity to solid particles, which makes them collide and fracture into particle down to 1 μ m. Even though it is considered a traditional particle production technique with a low cost associated, it is inadequate when it comes to particle production since the control of size distribution is limited.⁷⁰ Also the process might change the physicochemical properties of the material, turning the surface of fractured crystals amorphous.⁴¹

The bottom-up processes tend to be more sophisticated and complex, and produce particles with a better control of its characteristics. In this case, the manufacturing methods involve the use of an antisolvent or are based on solvent evaporation as is spray-drying, the most used and studied solvent evaporation technique.⁷¹ Spray drying is very rapid, convenient and has very few processing parameters, making it suitable for industrial scalable processing and it also provides stability and biological activity for the active pharmaceutical ingredient (API). In this process, drug/protein/peptide loaded microspheres are prepared by the means of an atomization of the feed solution into a spray, which later enters in contact with heated air in a drying chamber forming a dry powder. The nature of solvent used, temperature of the solvent evaporation and feed rate affect the morphology of the microspheres. The disadvantages of this process are the adhesion of the microparticles to the inner walls of the spray-dryer, turning the yields insufficient, and the possible degradation of heat-sensitive drugs.⁷²

1.7 Supercritical Fluid Technology

More recently, alternative particle production methods using supercritical fluids, especially supercritical CO₂ (scCO₂), have been proposed to overcome some limitations. Conventional methods usually require large amounts of organic solvents and thus require additional extensive purification steps to remove the residual solvent. When it comes to using scCO₂, organic solvents can be minimized or eliminated easily, since scCO₂ has a high affinity for them which enables their removal. A rapid expansion of the CO₂ using a pressure drop leads to the clustering of CO₂ molecules inside the liquid polymer, expanding it and inducing pore formation, making the system suitable for drug delivery. Moreover, the morphology and porosity can be easily altered by changing operation parameters such as pressure, temperature and gas release rate.⁷³

Supercritical Fluids (SF) are gases or liquids that are above their critical temperature and pressure, and that present characteristics of both states. In one hand they have the density of a liquid, which shows advantageous solvation power, while in the other hand they have the viscosity of a gas with an associated high diffusivity. Since these aspects are very changeable near the critical point, it is easy to control both of them by a slight change in pressure/temperature.⁷⁴ Also, near the critical point the compressibility and the heat capacity are much higher than in other conditions.

Carbon dioxide is the most used gas as a SF, since it is nontoxic, nonflammable, inexpensive and readily available in high purity from a variety of sources. Because it is a gas at normal pressure by simply reducing the pressure of the system, it is possible to easily separate the solvent and residues from the polymer, leading to highly pure materials. Besides, it has a low critical point (31.1°C/73.8 bar) (Figure II. 7), which is suitable to use with heat-sensitive materials and can reduce manufacturing complexity and energy.³⁶

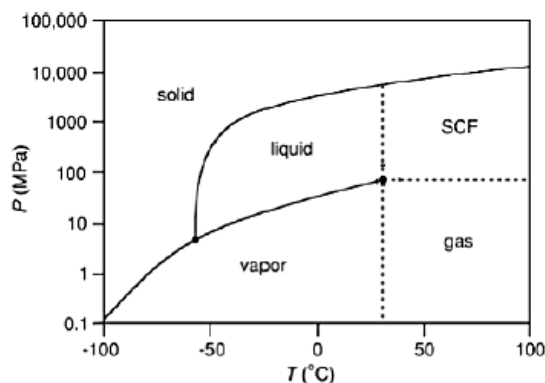


Figure II. 7 - Phase diagram of CO₂, adapted from W. Leitner et al.⁸⁴

There are several particle production techniques that use supercritical fluids, such as supercritical fluid extraction where particles are produced when a solution is brought into contact with scCO₂ in a semi-continuous method^{75,76}, rapid expansion of supercritical solutions (RESS) where the solid material is dissolved in scCO₂ and the solution is expanded by depressurization, leading to a fast decrease of temperature that will induce supersaturation and consequently microparticle formation and particles from gas saturated solutions (PGSS)^{70,70} that consists in two steps: the saturation of a solution with CO₂ and the mixture's expansion through a nozzle into a spray tower.

1.8 Supercritical Assisted Spray-Drying (SASD)

Supercritical Assisted Spray-Drying (SASD) is a process similar to the patented one by E. Reverchon in US 7276190B2 under the name “Process for the production of micro and/or nano particles”, and is based on the solubilization of controlled quantities of scCO₂ in liquid solutions. SASD offers many advantages over conventional methods, the possibility of operating in a continuous method in mild operating conditions and being able to use both organic and inorganic solvents while at the same time providing a good control over particle size and distribution.⁷⁷

The SASD apparatus mainly consists of two pumps to deliver liquid CO₂ and the liquid solution, a saturator, a precipitator and a condenser. The pumps are used to deliver the liquid solution to the saturator and to pump liquid CO₂, attained through a cryostat. Liquid CO₂ is then heated and the pressure is raised until supercritical conditions are reached. The mixing takes place in a saturator containing high-surface packing and ensuring long residence times in order to achieve near-equilibrium conditions. The solution will then be atomized through a nozzle by a two-step atomization: first primary droplets are obtained due to pneumatic atomization at the nozzle exit; then a secondary atomization process takes place by decompressive atomization due to CO₂ expansion from inside the primary droplets, shown Figure II. 8. This implies that the smallest particle size that can be achieved is the size of the smallest droplet achieved during the first atomization. The droplet size is determined by viscosity, surface tension and the amount of scCO₂ dissolved in the liquid solution, while temperature and chemical characteristics of the solute determines whether the particle is crystalline or amorphous.^{62,78}

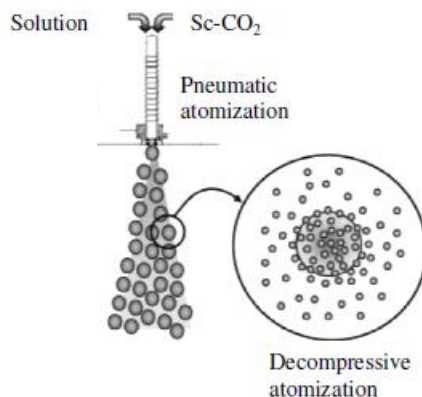


Figure II. 8 - Representation of the atomization mechanism, adapted from E. Reverchon et al.⁷⁸

The solubility of $scCO_2$ depends on the properties of the solvent and on operating temperature and pressure, being related to high-pressure vapor liquid equilibria (VLEs) of the system. Since there are only small amounts of acetic acid (1 % v/v) it became convenient to see where the operating conditions fall in the VLE for the ternary system water-ethanol- CO_2 . However, the possibility that acetic acid can influence the VLE must be taken into account. Fixing pressure and temperature, the mass flow ratio between CO_2 and the solvent determines the operating point the ternary system (Figure II. 9).^{79,80}

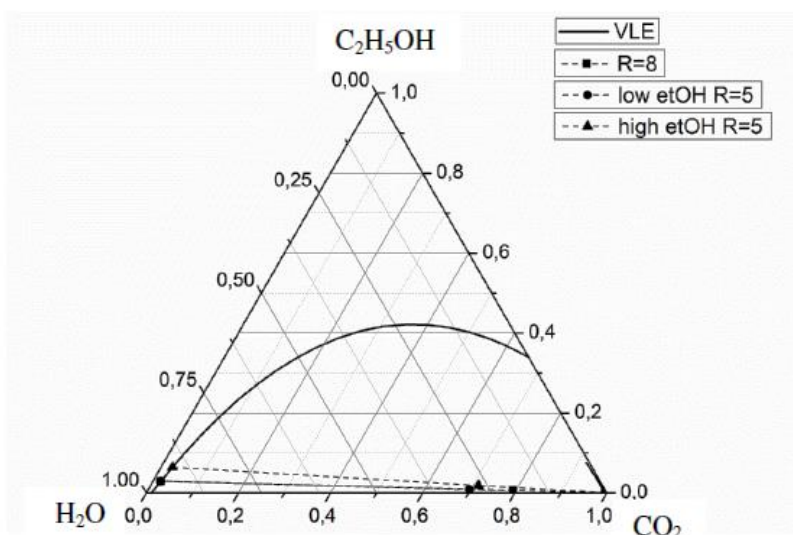


Figure II. 9 – VLE of water- CO_2 -ethanol system, adapted from C. Duarte et al.⁸⁰

At relatively low pressures and temperatures, the solubility of CO₂ in aqueous solutions is low, and the operating point always falls in a two-phase gas-liquid region. However, using small amounts of ethanol as co-solvent may significantly improve the miscibility of scCO₂ in water increasing the process efficiency. Although this improves the solubility of scCO₂ in aqueous solutions, the operating point still falls in a two-phase region, so there is no effect of the gas to liquid ratio on the composition of the phases. During particle formation, dissolved CO₂ reduces the viscosity and surface tension of the solution, while non-dissolved CO₂ enhances the pneumatic effect, improving primary atomization.^{81,82}

In this work, supercritical assisted spray-drying was used to produce CLT and CHT microparticles. These microparticles were blended with a *living polymer* end-capped with different compounds namely, water and IBP salt, a model drug. The microparticles with the best aerosol characteristics for pulmonary delivery were encapsulated with a marine bioactive compound, PTM-029, F4, F39, produced in Part I. Furthermore, the new dry powder formulations were properly characterized to assess if the microparticles were suitable for pulmonary delivery.

2. Experimental Section

2.1 Materials

All components were used as received without any further purification. Poly(D-L-lactide-co-glycolide) (PLGA, PURASORB® PDLG 5002A, molar ratio: 50/50, inherent viscosity 0.21dl/g) was purchased from PURAC (Gorinchem, Netherlands). Chitosan (viscosity 5-20mPa.s) was purchased from Tokyo Chemical Industry. Cholesterol (94% purity), (s)-(+)-Ibuprofen (IBP, 99% purity), *N,N*-Dimethylformamide (DMF) (anhydrous, $\geq 99,8\%$ purity), the monomer 2-ethyl-2-oxazoline (EtOx, $\geq 99\%$ purity), boron trifluoride diethyl etherate ($\text{BF}_3\cdot\text{OEt}_2$), acetone (99.8% purity), acetonitrile (ACN, 99.9% purity), acetic acid glacial (99.7% purity) and sodium bicarbonate were obtained from Sigma-Aldrich. Ethanol (EtOH) (96% purity) was purchased in Panreac. Diethyl ether was purchased from LabChem. Dimethyl Sulfoxide (DMSO, 99.9% purity) was purchase from Cambridge Isotope Lab. Industrial carbon dioxide (CO_2 , purity $\geq 99.93\%$) was obtained from Air Liquide.

2.2 Polymer synthesis in scCO_2

2.2.1 Synthesis of the *living polymer*

The *living polymer* synthesis followed the reported protocol in ⁶⁸. Typically, polymerization reactions were carried out in an 33 mL stainless-steel reactor that was loaded with, 2-ethyl-2oxazoline 2.4 mL of EtOx (23 mmol), the 2-substituted oxazoline monomer, and 0.237 mL of the initiator $\text{BF}_3\cdot\text{Et}_2\text{O}$ (1.92 mmol) under stirring conditions. The monomer/initiator ratio used to the polymerizations was $[\text{M}]/[\text{I}]=12$ according to the results previously reported in the literature.⁶⁷

The reactor was then closed with two aligned sapphire windows in both tops stamped with Teflon o-rings, connected to the CO_2 line charged with gas to approximately 0.1 MPa and placed in a thermostated water bath at 60 °C to assure control and avoid gas leakage from the reactor. After that, the pressure was finally adjusted to 16 MPa by addition of further CO_2 to ensure that the substrates were solubilized. The reaction was allowed to proceed under a homogenous supercritical phase during 24 hours. At the end, the reactor is flushed with CO_2 during one hour and then slowly depressurized and cooled to room temperature. A viscous foam or a solid-*living polymer* is

obtained. The *living polymer* was later end-capped with three different compounds namely, water, (S)-(+)-Ibuprofen salt and the bioactive compound PTM-029, F4, F39, obtained previously in Part I.

2.2.2 *Living polymer end-capping with water*

Termination of the *living polymer* can be performed with the addition of a tenfold excess of water in relation to the added amount of initiator. The mixture was kept at room temperature under stirring during one hour. The final product was then extracted with diethyl ether and the aqueous phase, was dried under vacuum, and a yellow oil was easily obtained.

¹H NMR (400 MHz, DMSO-*d*6) δ /ppm= 3.58 – 2.90 (m, 4H, H₂₇), 2.43 – 1.98 (m, 2H, H₂₈), 1.09 – 0.86 (m, 3H, H₂₉). (Annex 1, Figure 1)

¹³C NMR (101 MHz, DMSO-*d*6) δ /ppm= 173.54, 173.17, 172.94, 60.42, 44.41, 41.39, 28.44, 26.61, 24.94, 9.78, 9.43, 8.76. (Annex 1, Figure 2)

2.2.3 *Living polymer end-capping with (S)-(+)-ibuprofen salt*

Termination of the *living polymer* was performed with the addition of a (S)-(+)-ibuprofen salt. The (S)-(+)-Ibuprofen salt was obtained in a molar proportion 1:2 (S)-(+)-Ibuprofen:Sodium bicarbonate, dissolved in distilled water under stirring during one hour, until obtaining a clear solution and, after that, the water was removed under vacuum. In order to end-capped the *Living polymer*, under an inert atmosphere, the (S)-(+)-Ibuprofen salt dissolved in anhydrous DMF was added to PEtOx in a mass proportion 1:10 (S)-(+)-Ibuprofen salt:PEtOx. The mixture was kept at room temperature under stirring during one hour and after that dried under vacuum obtaining the final product

¹H NMR (400 MHz, DMSO-*d*6) δ /ppm= 7.16 (t, $J = 10.2$ Hz, 2H, H₆ and H₇), 7.08 (d, $J = 8.0$ Hz, 2H, H₅ and H₈), 3.63 – 3.50 (m, 4H, H₄), 3.50 – 3.13 (m, 36H, H₂₇), 2.40 (d, $J = 7.1$ Hz, 3H, H₉), 2.36 – 1.98 (m, 19H, H₂₈), 1.80 (dt, $J = 13.1, 6.6$ Hz, 1H, H₃), 1.32 (d, $J = 7.1$ Hz, 2H, H₉), 0.99 (dd, $J = 24.1, 6.1$ Hz, 28H, H₂₉), 0.85 (d, $J = 6.6$ Hz, 6H, H₁ and H₂). (Annex 1, Figure 3)

^{13}C NMR (101 MHz, DMSO-*d*6) δ/ppm = 176.29 (C=O from ester), 173.65, 173.42, 139.80, 139.45, 129.33, 129.12, 127.57, 63.95, 60.42, 48.05, 46.38, 45.22, 44.92, 44.69, 30.08, 28.92, 27.21, 25.41, 22.63, 19.17, 10.37, 10.25, 9.90, 9.42. (Annex 1, Figure 4)

2.2.4 Living polymer end-capping with bioactive compound PTM-029, F4, F39

The end-capping of the *living polymer* was performed by the addition of a bioactive compound PTM-029, F4, F39, obtained in thesis Part I. In order to do this, the new lead-like drug was solubilized in anhydrous DMF and added to the *Living polymer* under an inert atmosphere, in a mass proportion 1:10 PTM-029, F4, F39:PEtOx. The mixture was kept at room temperature under stirring during one hour and dried under vacuum obtaining the desired final product.

^1H NMR (400 MHz, DMSO-*d*6) δ/ppm = 8.06 – 7.65 (m, 3H), 6.52 (s, 2H), 4.29 – 4.14 (m, 4H), 3.67 – 2.95 (m, 132H, H₂₇), 2.42 – 1.92 (m, 26H, H₂₈), 1.14 (s, 1H), 1.10 – 0.74 (m, 38H, H₂₉). (Annex 1, Figure 5)

^{13}C NMR (101 MHz, DMSO-*d*6) δ/ppm = 173.70, 60.41, 52.13, 40.61, 40.40, 40.20, 27.11, 25.83, 25.45, 10.28, 9.94, 9.24. (Annex 1, Figure 6)

2.3 Microparticles preparation

2.3.1 CLT Microparticles

To produce CLT microparticles nine casting solutions with three different total solids concentration (0.25%, 0.5% and 1% (w/v), Table II. 2 were prepared. The solutions containing CLT-PLGA, PLGA were previously dissolved in acetonitrile and the CLT in acetone. All the remaining solutions were dissolved in ethanol.

Table II. 2 - Composition of casting solutions with various concentrations of 0.25%, 0.5% and 1% (w/v) of total solids used for the preparation of CLT microparticles.

Trials	Total solids concentration	Solution Components	Solvent of the solution
1	0.25% (w/v)	0.2495% (w/v) CLT	100% (v/v) EtOH
2		0.0005% (w/v) IBP	
3	0.5% (w/v)	0.4995% (w/v) CLT	
4		0.0005% (w/v) IBP	
5	0.5% (w/v)	0.2% (w/v) CLT	48.5% (v/v) Acetone
6		0.3% (w/v) PLGA	51.5% (w/v) ACN
6	0.5% (w/v)	0.25% (w/v) CLT	46.5% (v/v) Acetone
6		0.25% (w/v) PLGA	53.5% (w/v) ACN
7	1% (w/v)	1% (w/v) CLT	100% (v/v) EtOH
8		0.956 % (w/v) CLT	
9		0.044 % (w/v) PEtOx-OH	
9	1% (w/v)	0.956 % (w/v) CLT	100% (v/v) EtOH
9		0.040 % (w/v) PEtOx	
9		0.004 % (w/v) IBP	

2.3.2 CHT Microparticles

To produce 1% (w/v) CHT microparticles three solutions with different components (Table II. 3) were prepared. The CHT was previously dissolved in 1% (v/v) acidic water (acetic acid solution prepared with Milli-Q water) and in ethanol. All the solutions were filtrated in order to remove CHT insoluble remains.

Table II. 3 - Composition of casting solutions with 1% (w/v) of total solids used for the preparation of CHT microparticles.

Trials	Total solution concentration	Solution Components	Solvent of the solution
1	1% (w/v)	1% (w/v) CHT	80% (v/v) Acidic water 20% (v/v) EtOH
2		0.956 % (w/v) CHT 0.044 % (w/v) PEtOx-OH	
3		0.956 % (w/v) CHT 0.040 % (w/v) PEtOx 0.004 % (w/v) IBP	

2.3.3 SASD Apparatus

The laboratory scale SASD apparatus, represented in Figure II. 10 consists of two high-pressure pumps to deliver the liquid solution (HPLC pump 305 Gilson) and the CO₂ (HPLC pump K-501, Knauer) to the static mixer. Since the CO₂ pump is suitable for liquid solutions, there is a need to liquefy the CO₂ in a cryogenic bath. Before entering the static mixer the CO₂ is heated in an

oil bath. The static mixer (3/16 model 37-03-075 Chemier) is a high-pressure vessel with a 4.8 mm diameter, 191 mm length and 27 helical mixing elements that allows the solubilization of the CO₂ into the liquid solution due to its high surface packing. In order to control the temperature of the mixture, the static mixer is enrolled by heating tapes controlled by a shinko FCS-13A temperature controller (0.2°C resolution). The obtained mixture is then atomized into the precipitator in the form of a spray by the passage through a nozzle with an internal diameter of 150 μm. At the same time, a flow of previously heated compressed air enters the precipitator to evaporate the liquid solvent. The precipitator is a plastic vessel that operates at near-atmospheric conditions. After the precipitator there is a short plastic tube connected to a high-efficiency cyclone to make sure the flow remains at high temperatures, thus avoiding heat losses and consequent solvent condensation. The high-efficiency cyclone will help the separation between the particles and the CO₂-solvent flow, to collect the microparticles in a glass flask which is placed after the cyclone.

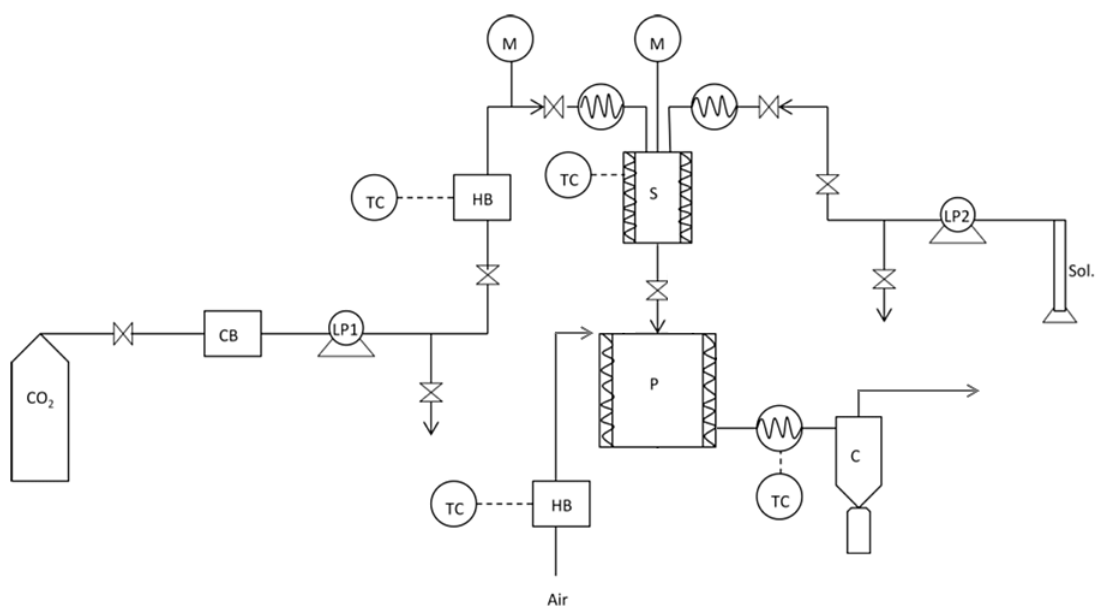


Figure II. 10 - Schematic representation of the SASD apparatus: (CB) cryogenic bath; (LP) liquid pump; (HB) heating bath; (TC) temperatute controller; (M) manometer; (S) saturator; (P) precipitator; (c) cyclone.

2.4 Microparticles Characterization

2.4.1 Particle Size Distribution

The particle size (PS) and the particle size distribution (PSD) were measured by a Morphologi G3 essentials, a particle analyzer system. In each particle size calculation around 30000 particles were considered. Also the span was calculated, a measure of the width of particle distribution, and it considers the $d_{v,10}$, $d_{v,50}$ and $d_{v,90}$ (particle diameter in volume corresponding to 10, 50 and 90% of the population) as represented in equation 3:

$$\text{Span} = \frac{d_{v,90} - d_{v,10}}{d_{v,50}} \quad (3)$$

2.4.2 Particles Morphology

The morphology of the produced particles was studied by Scanning Electron Microscopy (SEM) equipment from Hitachi, S-2400 instrument, with an accelerating voltage set to 15kV and at magnifications of 5K and 10K. All the samples were dispersed on carbon tape previously attached to an aluminum stub and were coated with gold before analysis.

2.4.3 Fourier Transform Infra Red (FT-IR)

FT-IR spectra were carried out on a PerkinElmer spectrum 1000 FTIR coupled with Opus Spectroscopy Software with potassium bromide (KBr) tablets containing 20% sample.

2.4.4 Water Content Determination

Karl Fischer coulometric titration was used for the determination of water content on the samples. An aliquot of the samples was transferred into the titration vessel and titrated with Karl Fischer reagent, which reacts quantitatively and selectively with water. The instrument was composed by the 831 KF Coulometer and a 728 stirrer both from Metrohm and by a Pt /-20...70 °C electrode.

2.4.5 Aerodynamic Properties

2.4.5.1 Emitted Fraction

To determine the shot weight, which is the amount of powder that is released from the capsules, the Dosage Unit Sampling Apparatus (DUSA) is used (Figure II. 11). The air is drawn by a High Controller Pump model HCP5 (Copley) that simulates inhalation and air flow was regulated in a Critical Flow Controller model TPK (Copley) until the P1 pressure achieves the 4kPa. The air flow (Q_{air}) was measured with a flow meter model DFM3 (Copley) in order to calculate the run time of each capsule using the equation 4:

$$t(s) = \frac{4L}{Q_{air} (L/min)} \times 60 (s/min) \quad (4)$$

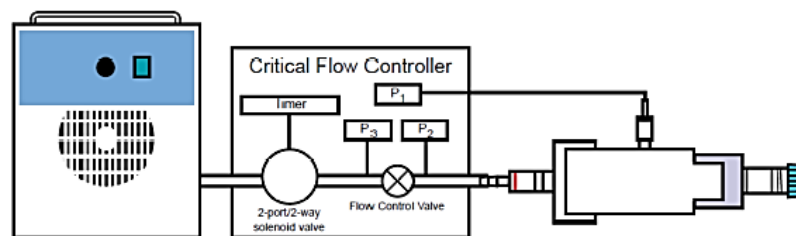


Figure II. 11 - Schematic representation of the DUSA, adapted from Copley Scientific.

Also, there is a need to ensure that $P3/P2 \leq 0.5$ in order to guarantee the critical flow. The assay consists on the release of 4 capsules (HPMC capsules n°3 Aerovaus) with 30 ± 2 mg of powder each from a dry powder inhaler (Plastique 60LPM – Mode 7) and it is performed in triplicate as reported in the European Pharmacopeia. The emitted fraction (EF) or emitted dose (ED) (%) uses the weights (mg) of the capsule before and after the assay (m_{full} and m_{empty} respectively) as represented in equation 5:

$$EF(\%) = \frac{m_{full} - m_{empty}}{m_{full}} \times 100\% \quad (5)$$

2.4.5.2 Andersen Cascade Impactor

The aerodynamic properties of fine particles were carried out using an aluminum Andersen Cascade Impactor apparatus (ACI)(Copley) (Figure II. 12). The assay is performed with the same instruments as the emitted fraction test, being the capsules prepared equally and the run time calculated using the same European Pharmacopeia protocol.

The assays were performed gravimetrically, so glass microfiber filters (80mm, Filter Lab) were placed in all the stages and were weighted before and after the capsules release. In order to obtain the drug concentration on each stage, the powder of each filter was then dissolved, the solution was centrifuged and its absorbance was read in an UV spectrophotometer (PerkinElmer Lambda 35). Each capsule was drawn through the induction port into the ACI at a flow rate of 62 ± 2 L/min for 3.9 ± 0.2 seconds. The effective cut-off aerodynamic diameter for each stage of the ACI were: stage -1, $8.6 \mu\text{m}$; stage -0, $6.5 \mu\text{m}$; stage 1, $4.4 \mu\text{m}$; stage 2, $3.2 \mu\text{m}$; stage 3, $1.9 \mu\text{m}$; stage 4, $1.2 \mu\text{m}$; stage 5, $0.55 \mu\text{m}$; stage 6, $0.26 \mu\text{m}$.

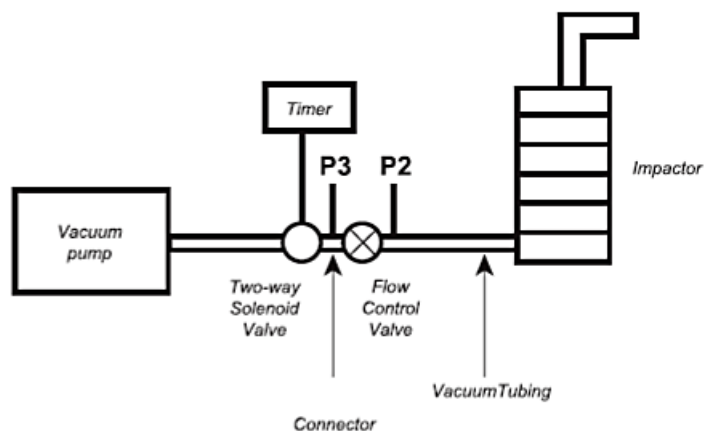


Figure II. 12 - Experimental set-up to perform ACI (adapted from European Pharmacopeia).

The fine particle fraction (FPF) was determined by the interpolation of the percentage of the particles containing less than 5 μm . The Mass Median Aerodynamic Diameter (MMAD) was determined as the particle diameter corresponding to 50% of the cumulative distribution. The Geometric Standard Deviation (GSD) was determined using the values of d_{84} and d_{16} , which represent the diameters of 84% and 16% of the cumulative distribution as in equation 6:

$$GSD = \sqrt{\frac{d_{84}}{d_{16}}} \quad (6)$$

2.4.6 Pharmacokinetic Studies

2.4.6.1 CLT and CHT Microparticles

The in vitro release studies were carried out in phosphate-buffered saline at pH 7.4 (PBS) and at 37 °C. 253.2 \pm 1.7 mg of sample was introduced in a SnakeSkin Dialysis Tubing (3.500 MWCO, 22 mm x 35 feet dry diameter, 34 mm dry flat width, 3.7 mL/cm, Thermo Scientific) that was suspended in 10 mL. Samples of 1 mL were taken at predetermined time points and other 1 mL of PBS was added to the suspension and the samples.

3. Results and Discussion

The production of microparticles as dry powder for pulmonary delivery was performed by SASD technique. PTM-029, F4, F39, the lead-like drug previously produced in Part I, of the present thesis, was available only in low quantities, thus it was necessary to conjugate it to a *living polymer*, the PEtOx to ensure that all drug was all blended with the excipients CLT and CHT. IBP, a nonsteroidal anti-inflammatory drug, was used as a model drug to optimize the end-capping of the PEtOx protocol. All solvents were chosen take into account their solubility in CO₂ and their “greener” character. CLT solutions were all processed with EtOH as a solvent with exception of CLT-PLGA solutions, where the chosen organic solvent to dissolve PLGA was acetonitrile. Since CHT is only soluble in 1% v/v acetic acid aqueous solution, all compounds were processed in it together with EtOH in a volume proportion 4:1, respectively.

3.1 CLT Microparticles

CLT-based formulations were developed with four different types of components: IBP, PLGA and PEtOx end-capped with water and (S)-(+)-ibuprofen salt. The chosen solvent was EtOH for all the formulations. Preceding the atomization of the CLT formulations, it was necessary to determine the best operating conditions for the production of the microparticles by changing one operating parameter, while maintaining the others unchanged. In this work, the changed operating parameters were the total solids concentration of the formulations, the gas to liquid ratio and, in CLT-PLGA microparticles, *i.e.* the mass ratio between CLT and PLGA. Important operating parameters like the static mixer temperature, the compressed air temperature or pressure were necessarily taken into count, in order to produce the microparticles. The operating temperature of the static mixer was fixed in 50°C due to the low T_g PLGA presents (45-50 °C). When the mixture occurs in the static mixer, the temperature needs to be below this value, but yet, it has to be above the CO₂'s critical temperature (31.1 °C) and so 50 °C was used as the set point, while the CO₂ was heated at 60 °C, to guarantee that it was at supercritical conditions. Another important operating parameter was the temperature of compress air, which is essential for drying the particles in the precipitator chamber due to acetonitrile and ethanol's boiling temperature which are 82 °C and 78.3 °C, respectively. The best temperature to be used in the precipitator was around 70 °C with

compressed air entering at nearly 100 °C. The used pressure was 10 MPa and the gas to liquid ratio ($R=Q_{CO_2}/Q_{sol}$) was calculated taking into account the volumetric flows and was varied between 5 and 12.5.

The performed assays are listed in Table II. 4 as well as the operating conditions used in each one of them. CLT-IBP microparticles prepared from casting solutions with higher total solids concentration and gas to liquid ratio were obtained with higher yields. The same was observed for CLT-PLGA microparticles where the increased yield might be due to the presence of a higher mass proportion of CLT, relatively to PLGA. From all CLT microparticles, 1% (w/v) CLT presented the lower yields, probably because the microparticles had a small size or a low density that they were vented. However, when added the *living polymer* in the formulations, the CLT-PEtOx microparticles showed a better yield when end-capped with IBP comparatively than end-capped with water.

Table II. 4 - Operating parameters of the CLT assays and the respective yields.

	Assay	Yield (%)	Tsm (°C)	TCO₂ (°C)	Tair (°C)	Pressure (MPa)	Q_{CO₂}/Q_{sol}^a
0.25% (w/v)	CLT-IBP	23.8	50	60	100	10	5
	CLT-IBP	27.3	50	60	100	10	8.3
	CLT-IBP	25.8	50	60	100	10	5
0.5% (w/v)	CLT-IBP	29.7	50	60	100	10	8.3
	CLT-PLGA (40:60)	24.6	50	60	100	10	5
	CLT-PLGA (50:50)	45.3	50	60	100	10	5
1% (w/v)	CLT	3.1	50	60	100	10	12.5
	CLT-PEtOx-OH	10.1	50	60	100	10	12.5
	CLT-PEtOx-IBP	16.6	50	60	100	10	12.5

Tsm – Temperature of the static mixer; TCO₂ – Temperature of the carbon dioxide; Tair – Temperature of the compressed air. ^aQCO₂/Qsol ratio takes into account volumetric flows.

3.1.1 Morphology

By analyzing the diameters obtained in Table II. 5, there is no obvious difference in the $D_{v,50}$, all the CLT particles have values between 5 and 6 μm with exception of the CLT-PLGA microparticles that has values slightly below 5 μm . Comparing the geometric and numeric diameters, there is a substantial difference justified by the existence of large agglomerates. Observing Table II. 5, smaller diameters are obtained with the increasing of Q_{CO_2}/Q_{sol} ratio in CLT-IBP microparticles and in CLT-PLGA microparticles with the decrease of CLT proportion in the formulations.

Table II. 5 - Properties of CLT microparticles.

	Assay	$D_{v,50}$ (μm)	$D_{n,50}$ (μm)	Span
0.25% (w/v)	CLT-IBP ($Q_{CO_2}/Q_{sol}=5$)	11.55	4.66	0.62
	CLT-IBP ($Q_{CO_2}/Q_{sol}=8.3$)	12.05	5	0.56
0.5 (w/v)	CLT-IBP ($Q_{CO_2}/Q_{sol}=5$)	11.63	5.4	0.64
	CLT-IBP ($Q_{CO_2}/Q_{sol}=8.3$)	11.97	5.59	0.58
	CLT-PLGA (40:60)	11.35	3.37	0.65
1% (w/v)	CLT-PLGA (50:50)	11.56	4.51	0.64
	CLT	12.81	5.60	0.91
	CLT-PEtOx-OH	12.41	6.44	0.49
	CLT-PEtOx-IBP	12.20	5.91	0.53

$D_{v,50}$ = Particle volumetric diameter of 50% cumulative distribution; $D_{n,50}$ – Particle number diameter of 50% cumulative distribution.

Also to prove that the $D_{v,50}$ is due to the presence of agglomerates SEM was performed and the results are shown in Figure II. 13 to 21. As can be seen in the top of the images (**A** (a), (b) and (c)) single particles do not have diameters much larger than $1\mu\text{m}$. In the other hand, they do not seem spherical, with exception of Figure II. 21 showing some spherical particles, probably due to the presence of IBP. Also by analyzing the images obtained by Morphologi G3 (Figure II. 13 to 21) it is possible to recognize the presence of agglomerates. In the images (**B** (a), (b) and (c)) of the CLT microparticles there is a confirmation that these big diameter particles are truly aggregates since their individual form is outlined.

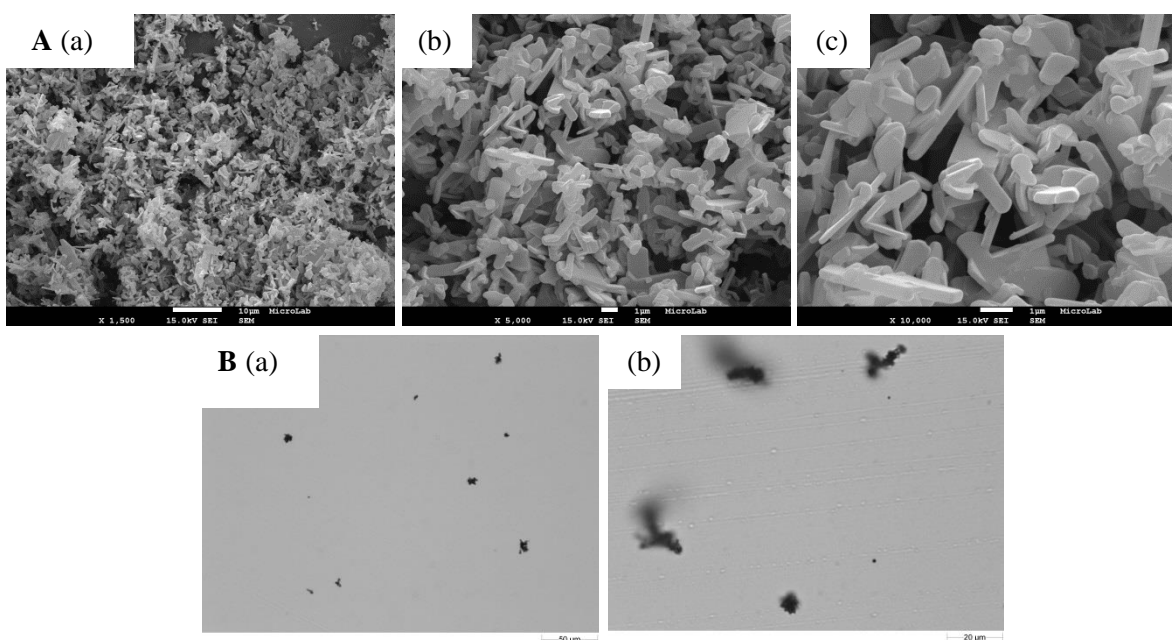


Figure II. 13 - 0.25% (w/v) CLT-IBP ($QCO_2/Q_{sol}=5$) microparticles. (**A**) SEM images of with a magnification of (a) 1,500x (b) 5,000x and (c) 10,000x and (**B**) Morphologi G3 images with magnification of (a) 20,000 and (b) 50,000 respectively.

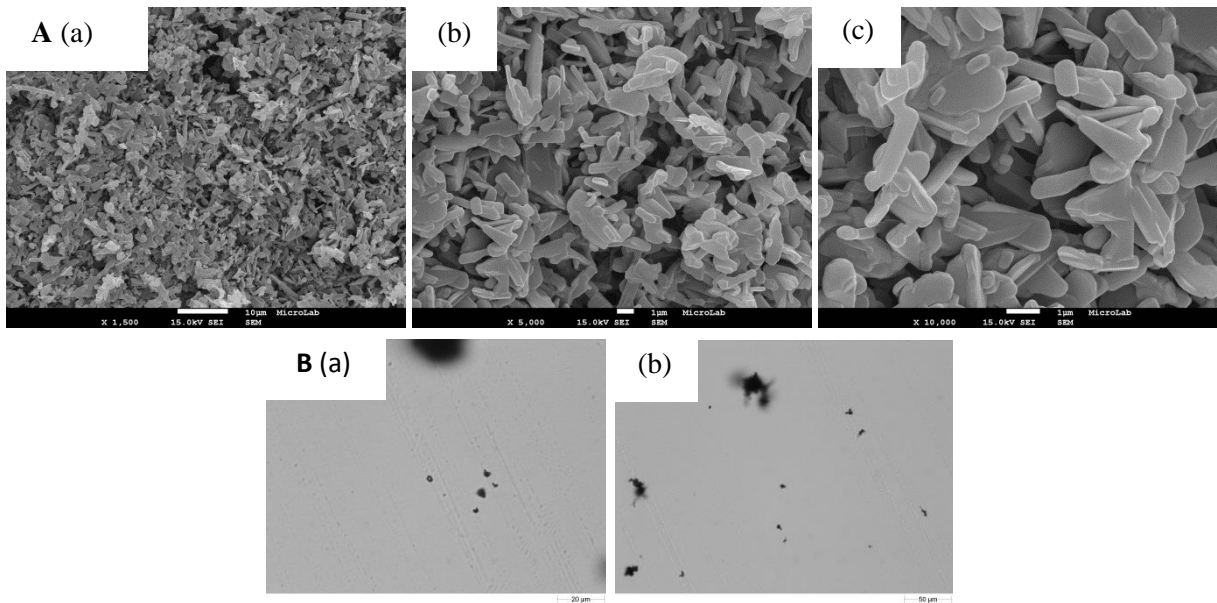


Figure II. 14 - 0.25% (w/v) CLT-IBP (QCO₂/Qsol=8.3) microparticles. (A) SEM images of with a magnification of (a) 1,500x (b) 5,000x and (c) 10,000x and (B) Morphologi G3 images with magnification of (a) 20,000 and (b) 50,000 respectively.

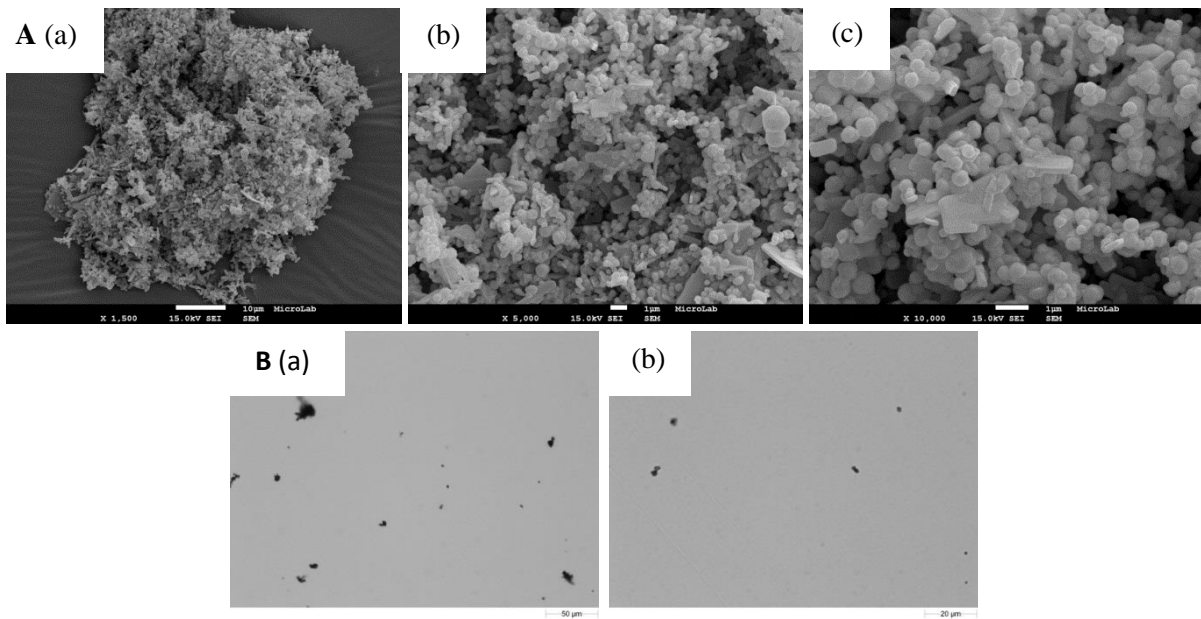


Figure II. 15 - 0.5% (w/v) CLT-IBP (QCO₂/Qsol=5) microparticles. (A) SEM images of with a magnification of (a) 1,500x, (b) 5,000x and (c) 10,000x and (B) Morphologi G3 images with magnification of (a) 20,000 and (b) 50,000 respectively.

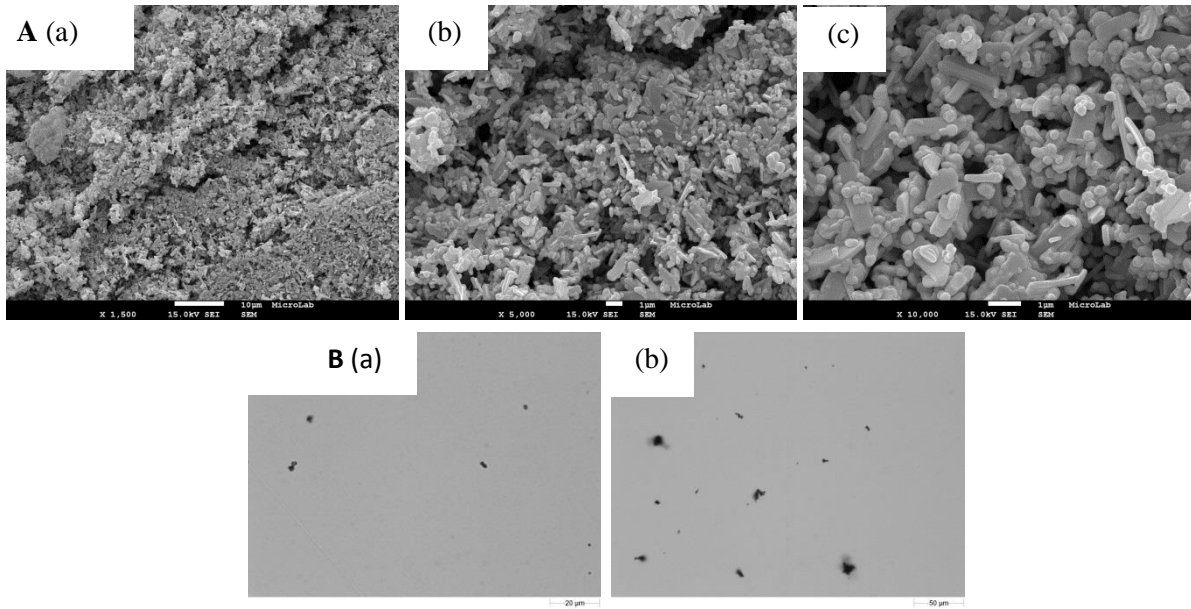


Figure II. 16 - 0.5% (w/v) CLT-IBP (QCO₂/Qsol=8.3) microparticles. (A) SEM images of with a magnification of (a) 1,500x, (b) 5,000x and (c) 10,000x and (B) Morphologi G3 images with magnification of (a) 20,000 and (b) 50,000 respectively.

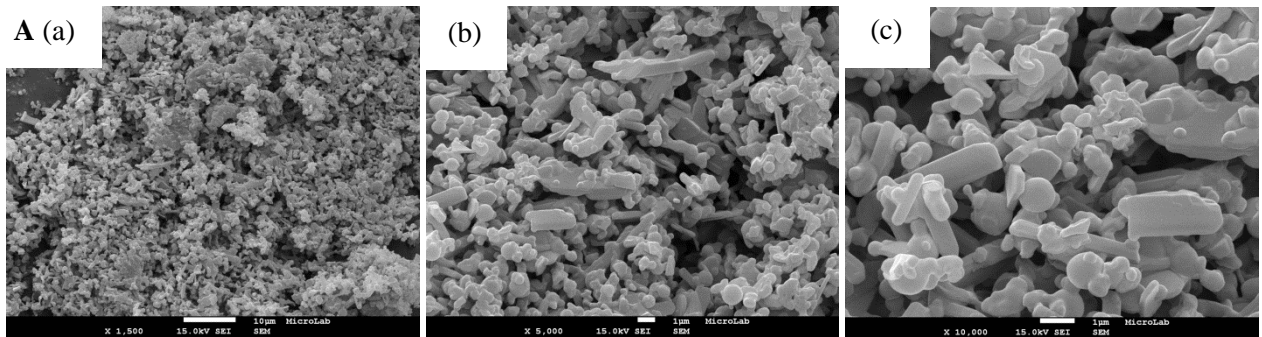


Figure II. 17 - 0.5% (w/v) CLT-PLGA (40:60) microparticles. (A) SEM images of with a magnification of (a) 1,500x, (b) 5,000x and (c) 10,000x.

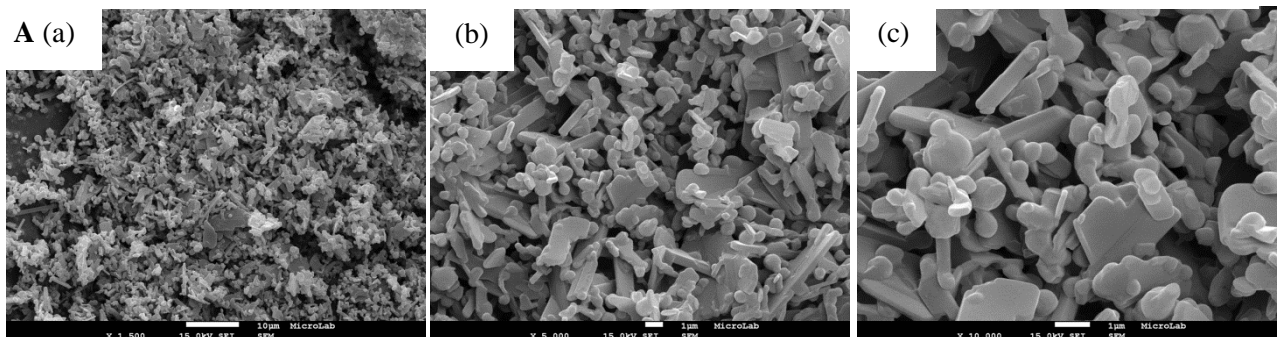


Figure II. 18 - 0.5% (w/v) CLT-PLGA (50:50) microparticles. (A) SEM images of with a magnification of (a) 1,500x, (b) 5,000x and (c) 10,000x.

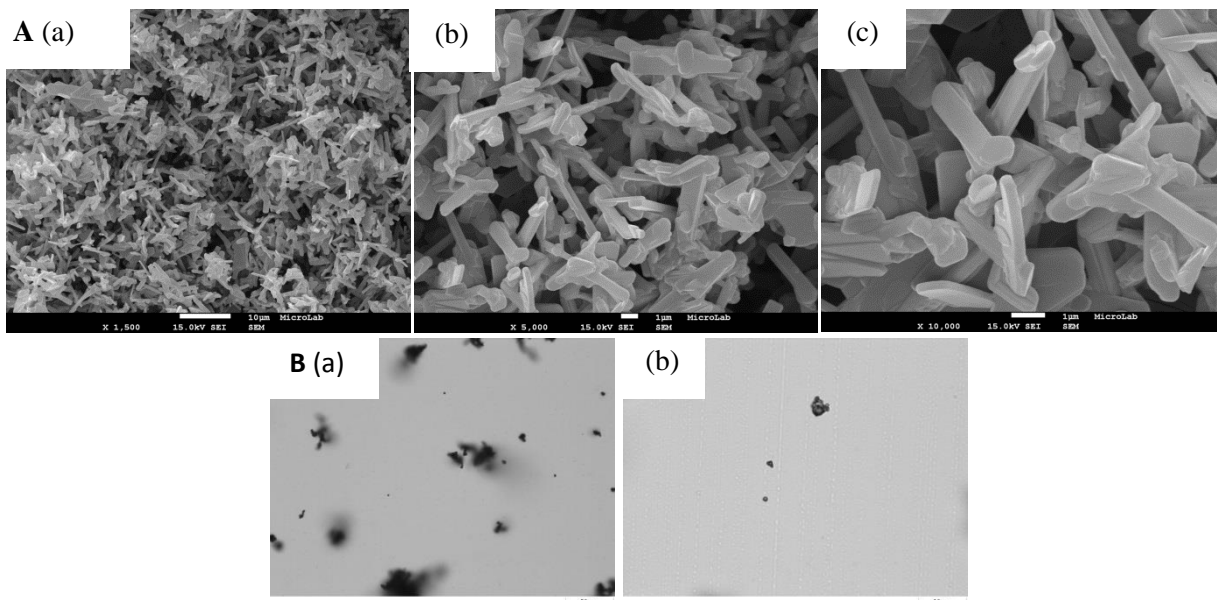


Figure II. 19 - Figure 3.7 - 1% (w/v) CLT microparticles. (A) SEM images of with a magnification of (a) 1,500x, (b) 5,000x and (c) 10,000x and (B) Morphologi G3 images with magnification of (a) 20,000 and (b) 50,000 respectively.

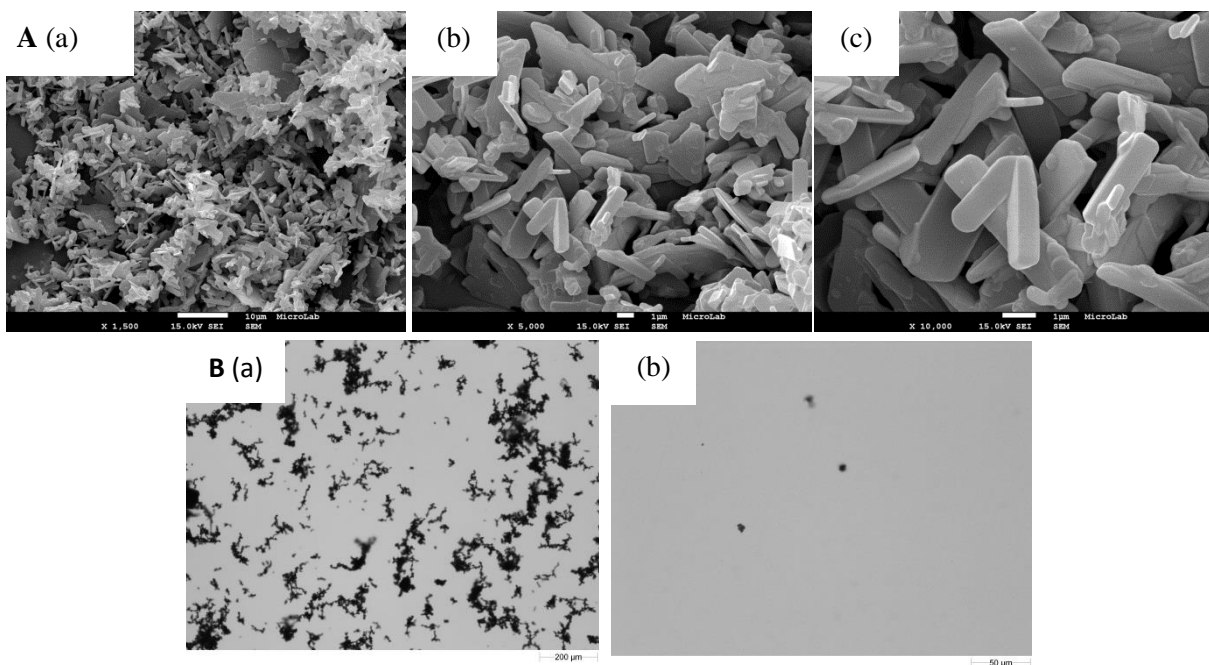


Figure II. 20 - 1% (w/v) CLT-PEtOx-OH microparticles. (A) SEM images of with a magnification of (a) 1,500x, (b) 5,000x and (c) 10,000x and (B) Morphologi G3 images with magnification of (a) 20,000 and (b) 50,000 respectively.

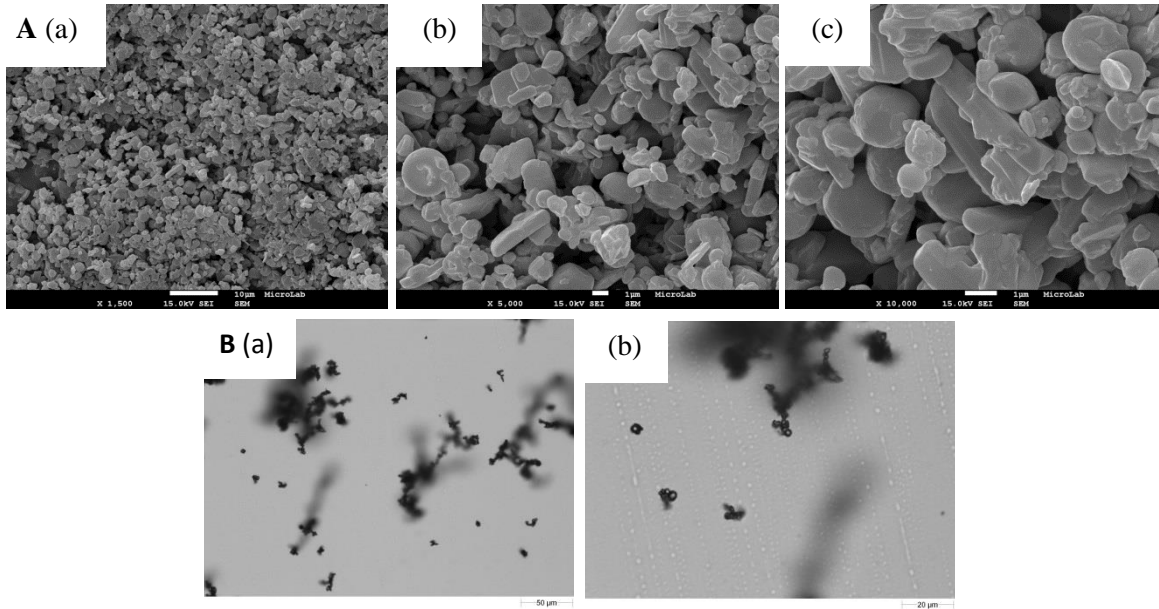


Figure II. 21 - Figure 3.9 - 1% (w/v) CLT-PEtOx-IBP microparticles. (A) SEM images of with a magnification of (a) 1,500x, (b) 5,000x and (c) 10,000x and (B) Morphologi G3 images with magnification of (a) 20,000 and (b) 50,000 respectively.

3.1.2 Aerodynamic Performance

As already mentioned, the MMAD is an important parameter considering the production of particles for inhalation purposes, and it is determined by cascade impaction measurements. The obtained result regarding the powders distribution is represented in Figure II. 22.

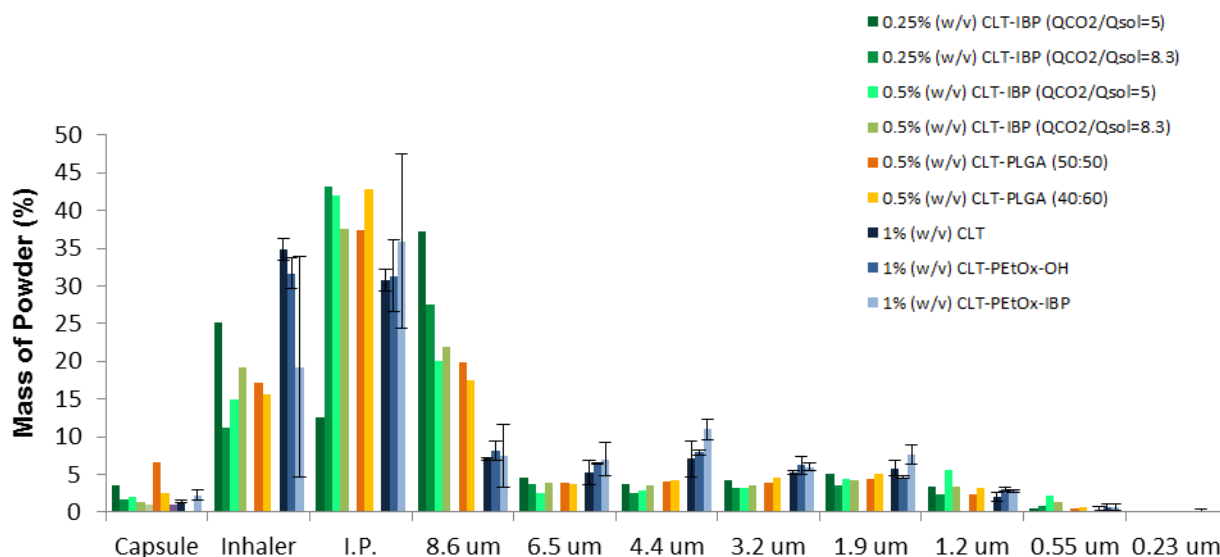


Figure II. 22 - Graphical representation of the powder distribution in the ACI stages for the CLT microparticles. (I.P. represents the induction port).

By observing Figure II. 22 it is clear that most of the dry powder deposits in the induction port (I.P.), which is representing the upper airways, probably because of the aggregates presence and the formation of turbulent eddies in the curving zone of the tube, that has as a consequence the aggregates impaction. Besides the MMAD, there are other important values obtained through the ACI, such as the FPF and GSD. Recurring to the use of DUSA, the ED is also calculated and all these values are included in Table II. 6.

MMAD for particles with 0.25% (w/v) of the total solids concentration shows values around 7 μm, for 0.5% (w/v) values around 6 μm and for 1% (w/v) around 4 μm. With the increase of the initial solution concentration there is a decrease in the particle size. Taking into account that the MMAD of the formulation for 0.25% and 0.5% (w/v) casting solutions is above the uplimit of the desired value (between 1 and 5μm) for inhalation, it was already expected that the FPF would be

small, and this also explains the high quantity of powder deposited in the IP. Formulations with 1% (w/v) of the total solids concentration was expected to have higher values of FPF when compared with 0.25% (w/v) and 0.5% (w/v), although with values of MMAD below 5 μm was estimated that the FPF was much higher than around 30%. As for the ED, only in 1% (w/v) CLT-PEtOx-OH the powder exited from the capsule completely.

Table II. 6 - Representation of the aerodynamic properties determined by ACI and DUSA for the CLT microparticles.

	Assay	MMAD (μm)	FPF (%)	GSD	ED (%)
0.25% (w/v)	CLT-IBP ($Q_{\text{CO}_2}/Q_{\text{sol}}=5$)	6.95	25.5	1.9	97.0
	CLT-IBP ($Q_{\text{CO}_2}/Q_{\text{sol}}=8.3$)	6.93	15.7	2.0	98.3
0.5% (w/v)	CLT-IBP ($Q_{\text{CO}_2}/Q_{\text{sol}}=5$)	6.03	23.3	2.8	98.0
	CLT-IBP ($Q_{\text{CO}_2}/Q_{\text{sol}}=8.3$)	6.60	21.4	2.3	98.8
	CLT-PLGA (40:60)	5.37	23.2	2.28	98.0
	CLT-PLGA (50:50)	6.55	21.2	2.13	95.1
1% (w/v)	CLT	3.74 \pm 0.28	34.66 \pm 5.44	2.14 \pm 0.09	99.02 \pm 0.00
	CLT-PEtOx-OH	3.80 \pm 0.03	35.60 \pm 3.17	2.14 \pm 0.04	1 \pm 0.00
	CLT-PEtOx-IBP	3.68 \pm 0.40	39.34 \pm 10.07	2.06 \pm 0.11	97.05 \pm 0.01

MMAD – Mass Median Aerodynamic Diameter; FPF- Fine particle fraction; GSD – Geometric Standard Deviation; ED – Emitted Dose.

3.1.3 Physical-Chemical Properties

FTIR spectra of 1% (w/v) CLT microparticles were obtained to check if all the compounds were present in the formulation. The FTIR analysis (Figure II. 23) confirms the presence of CLT, by the presence of its characteristic absorption bands: 3402 cm^{-1} (OH stretching), 2937 and 2929 cm^{-1} (C-H stretching of CH_3 groups), 1457 cm^{-1} (CH_3 stretching). Figure II. 23 (b) shows the presence of PEtOx-OH, determined by the presence of a new characteristic absorption band at 1635 cm^{-1} (Et(C=O)N- stretching) and Figure II. 23 (c) also present the same absorption band at 1638 cm^{-1} , confirming the presence of PEtOx-IBP.

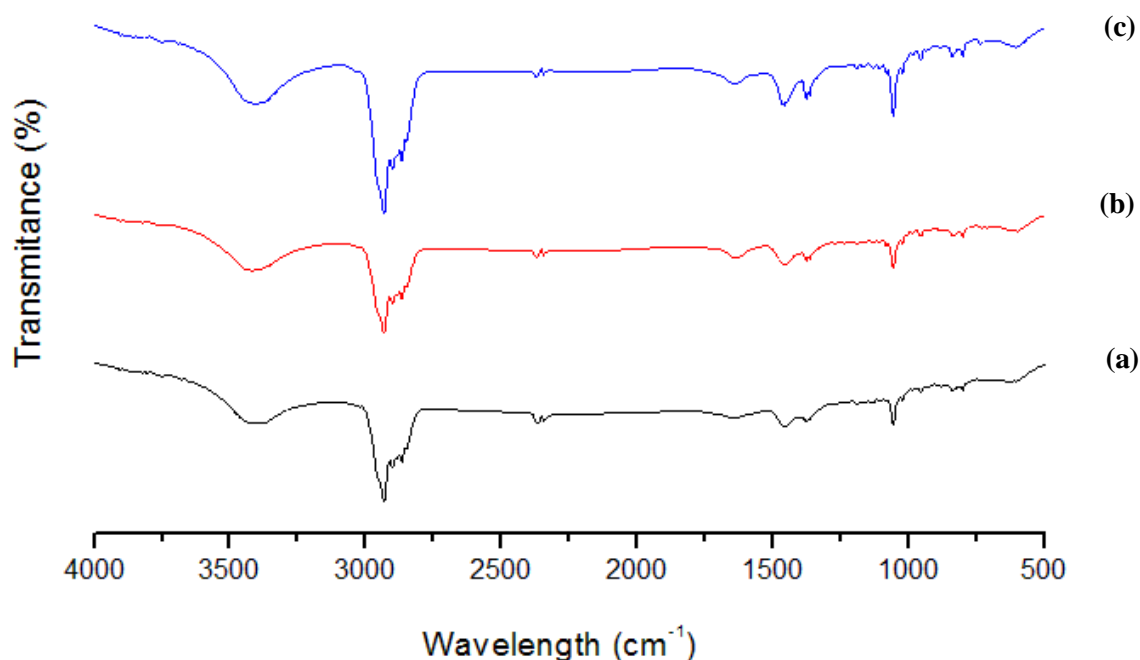


Figure II. 23 - FTIR. (a) CLT microparticles, (b) CLT-PEtOx-OH microparticles and (c) CLT-PEtOx-IBP microparticles.

As for the particles' water content, the percentages of all the formulations are represented in Table II. 7 and in all of them it is safe to say that the amount of water in the particles is very low, which reveals the drying efficacy of the SASD. The formulations 1% (w/v) CLT and CLT-PEtOx-OH shows the same water content value because while PEtOx-OH is hydrophilic, CLT is a hydrophobic lipid, although, taking into account the mass ratio CLT:PEtOx-OH, CLT mass is

twenty two times higher than PEtOx-OH conferring a hydrophobic character to the 1% (w/v) CLT-PEtOx-OH microparticles. 1% (w/v) CLT-PEtOx-IBP shows the lowest water content since both CLT and PEtOx-IBP present a hydrophobic character.

Table II. 7 - Water content values for 1% (w/v) CLT, 1% (w/v) CLT-PEtOx-OH and 1% (w/v) CLT-PEtOx-IBP microparticles.

Assay	Water content (%)
CLT	0.11±0.05
1% (w/v) CLT-PEtOx-OH	0.11±0.01
CLT-PEtOx-IBP	0.09±0.01

3.1.4 Pharmacokinetic Studies

By performing the pharmacokinetic studies it is possible to study not only the behavior of the PEtOx-IBP compound, as a model drug in CLT microparticles, but also the mechanism of its controlled release. The release curve was fitted using the equation represented in Figure II. 24 (b) and Table II. 8. The Korsmeyer and Peppas equation (2) is only suitable for 60% of the release and by the analysis of the n it can be concluded that when PEtOx-IBP is present the release is controlled by anomalous (with n values greater than 0.43) predicting the superposition of diffusion, swelling, dissolution and/or erosion phenomena. Furthermore, in Figure II. 24 (A) the first three hours are represented and in Figure II. 24 (B) it is possible to see that 60% of release is achieved at about 0.25 hours, presenting a fast release. Figure II. 25 shows the fitting to the experimental drug release data.

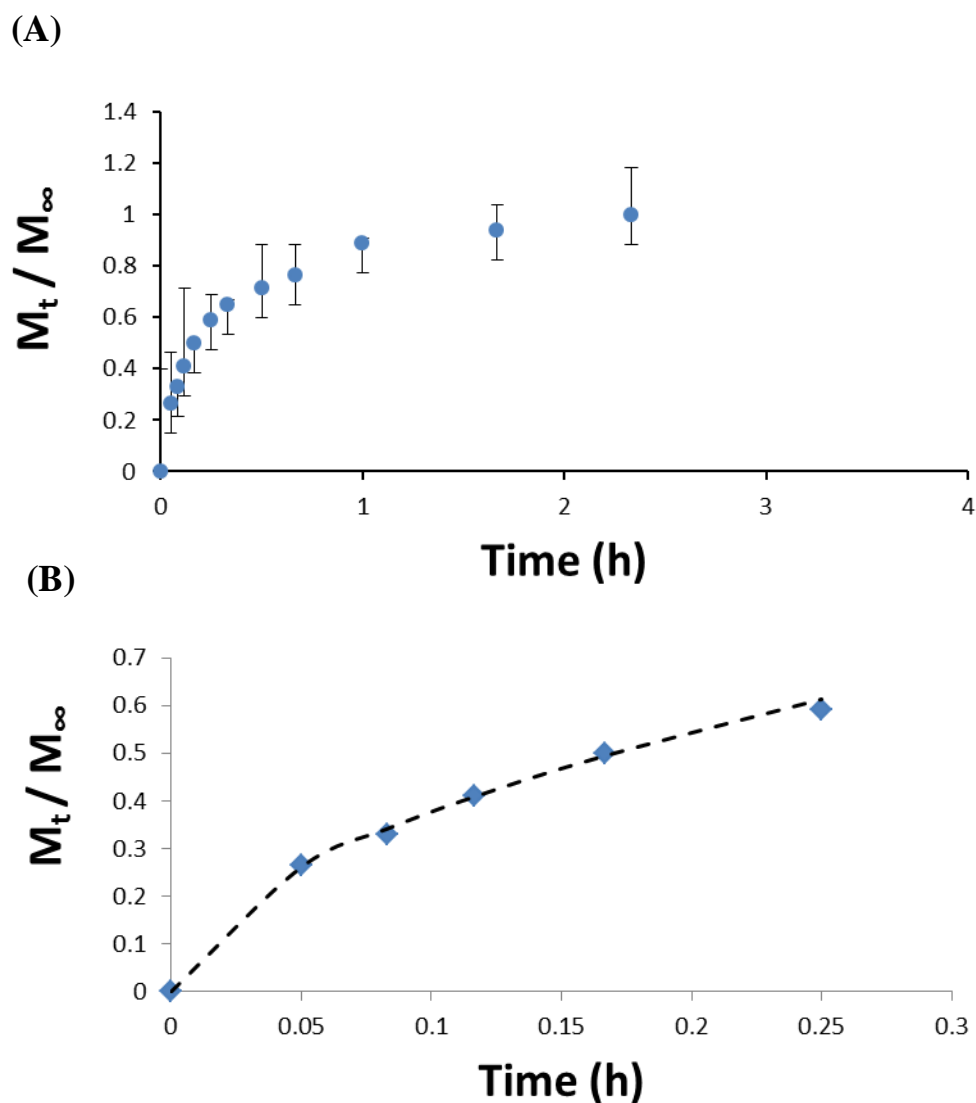


Figure II. 24 - (A) In vitro drug release studies of PEtOx-IBP loaded in CLT microparticles at pH 7.4 and 35 °C and (B) release profile fitted through Korsmeier-Peppas mathematical model for the first 60% of release.

Table II. 8 - Kinetic values obtained from the Korsmeier equation for the 1% (w/v) CLT-PEtOx-IBP microparticles.

Microparticle	Korsmeier Peppas		
	R ²	n	k
1% (w/v) CLT-PEtOx-IBP	0.9922	0.5318	1.2817

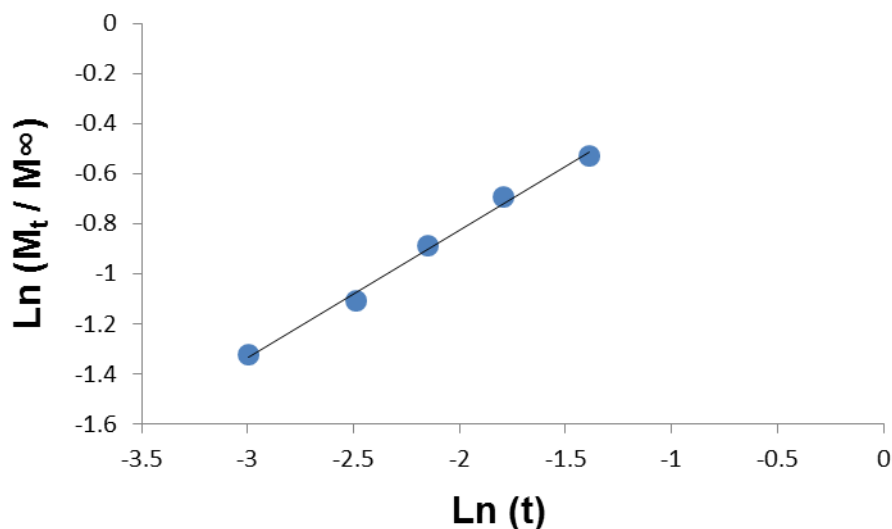


Figure II. 25 - Korsmeyer-Peppas Model for mechanism of PEtOx-IBP release from the CLT microparticles at pH 7.4 and 35° C.

3.2 CHT Microparticles

The CHT formulations were performed only with three different types of components: a *living polymer*, PEtOx end-capped with water, (S)-(+)-ibuprofen salt and a bioactive compound PTM-029, F4, F39 produced in Part I. The chosen solvents were 1% (v/v) acidic water and ethanol in a proportion ratio 4:1 for all the formulations. The static mixer operated at 70°C, while the CO₂ was heated at 60 °C, to guarantee that the mixing occurs at supercritical conditions, the compress air temperature, which is essential for drying the particles in the precipitator due to the presence of acidic water and ethanol's boiling temperature (100 °C and 78.3 °C respectively). The best temperature to be used in the precipitator was around 70 °C with compressed air entering at nearly 100 °C. The used pressure was 10 MPa and the feed gas to liquid ratio ($R=Q_{CO_2}/Q_{sol}$) was 12.5.

All the performed assays are summarized in Table II. 9 as well as the operating pressure and temperature values used for each assay. In general, all CHT microparticles presented lower yields probably because they show a small size or a low density, allowing them to be vented. The addition of the *living polymer* with end-capped compounds to the CHT microparticles increased slightly the yields.

Table II. 9 - Operating parameters of the CHT assays and the respective yields.

Assay	Yield (%)	Tsm (°C)	TCO ₂ (°C)	Tair (°C)	Pressure (MPa)	Q _{CO2} /Q _{sol}
CHT	15.2	70	65	100	10	12.5
1% (w/v) CHT-PEtOx-OH	21.9	70	65	100	10	12.5
CHT-PEtOx-IBP	16.9	70	65	100	10	12.5
CHT-PEtOx-PTM-029, F4, F39	17.1	70	65	100	10	12.5

Tsm – Temperature of the static mixer; TCO₂ – Temperature of the carbon dioxide; Tair – Temperature of the compressed air. ^bQ_{CO2}/Q_{sol} ratio takes into account volumetric flows.

3.2.1 Morphology

By analyzing the diameters obtained in Table II. 10, it is possible to see that they are all between 2 and 4 μm, being the smallest one with only 1% (w/v) CHT. When the polymer-drug conjugates are added to the formulation, the diameter slightly increases. All CHT microparticles have low numeric and volumetric diameters, confirming the presence of mostly small particles with only a few aggregates.

Table II. 10 - Properties of CHT microparticles.

	Assay	D_{v,50} (μm)	D_{n,50} (μm)	Span
1% (w/v)	CHT	7.10	2.43	1.35
	CHT-PEtOx-OH	7.35	3.34	1.13
	CHT-PEtOx-IBP	7.83	2.91	0.96
	CHT-PEtOx-PTM-029, F4, F39	8.62	3.43	1.05

D_{v,50}= Particle volumetric diameter of 50% cumulative distribution; D_{n,50} – Particle number diameter of 50% cumulative distribution.

SEM was performed and the results are shown in Figure II. 26 to 29 (**A** (a), (b) and (c)). The CHT microparticles show a spherical form and there are some particles with diameters smaller than 1μm. The analysis of the images obtained by Morphologi G3 (Figure II. 26 to 29 (**B** (a), (b) and (c))), it is possible to recognize the low numeric and volumetric diameters, confirming the presence of mostly small single particles with a spherical form and with only a few aggregates.

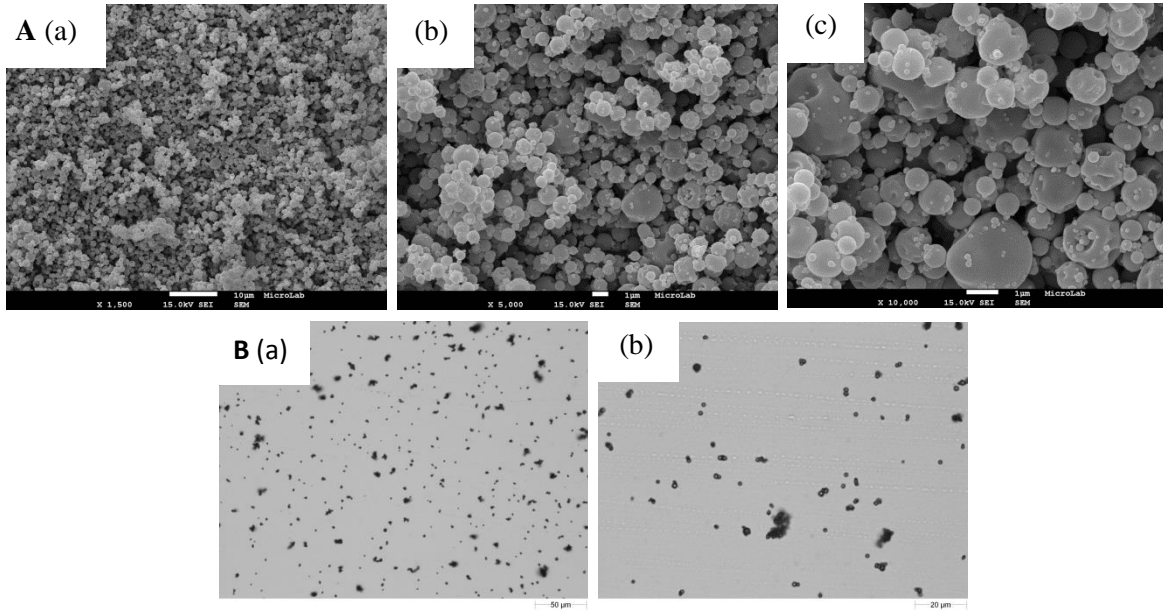


Figure II. 26 - 1% (w/v) CHT microparticles. (A) SEM images of with a magnification of (a) 1,500x, (b) 5,000x and (c) 10,000x and (B) Morphologi G3 images with magnification of (a) 20,000 and (b) 50,000 respectively.

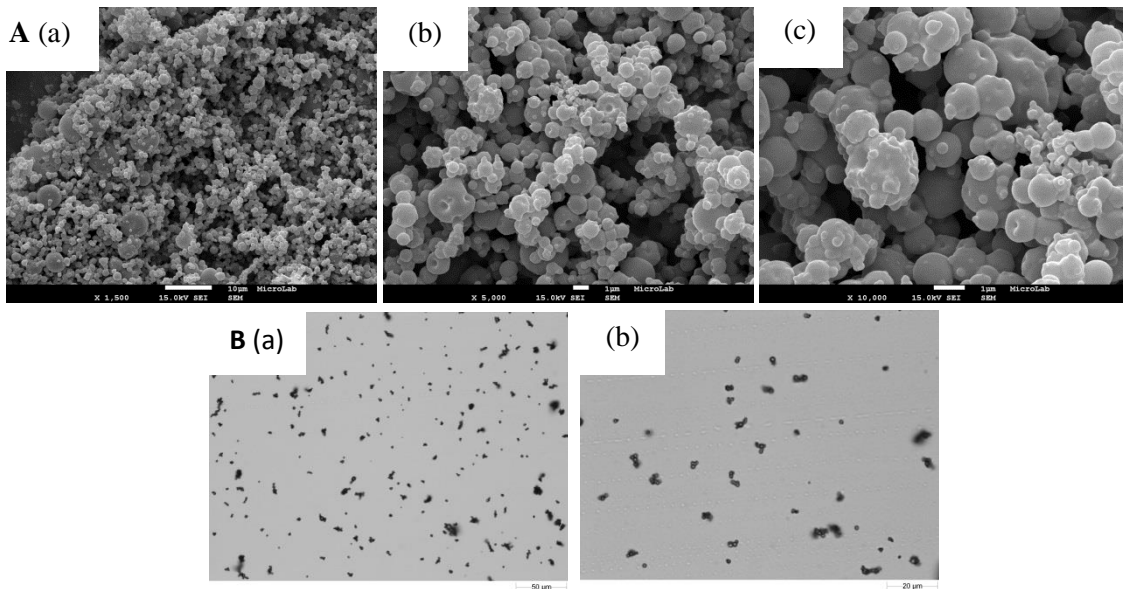


Figure II. 27 - 1% (w/v) CHT-PEtOx-OH microparticles. (A) SEM images of with a magnification of (a) 1,500x, (b) 5,000x and (c) 10,000x and (B) Morphologi G3 images with magnification of (a) 20,000 and (b) 50,000 respectively.

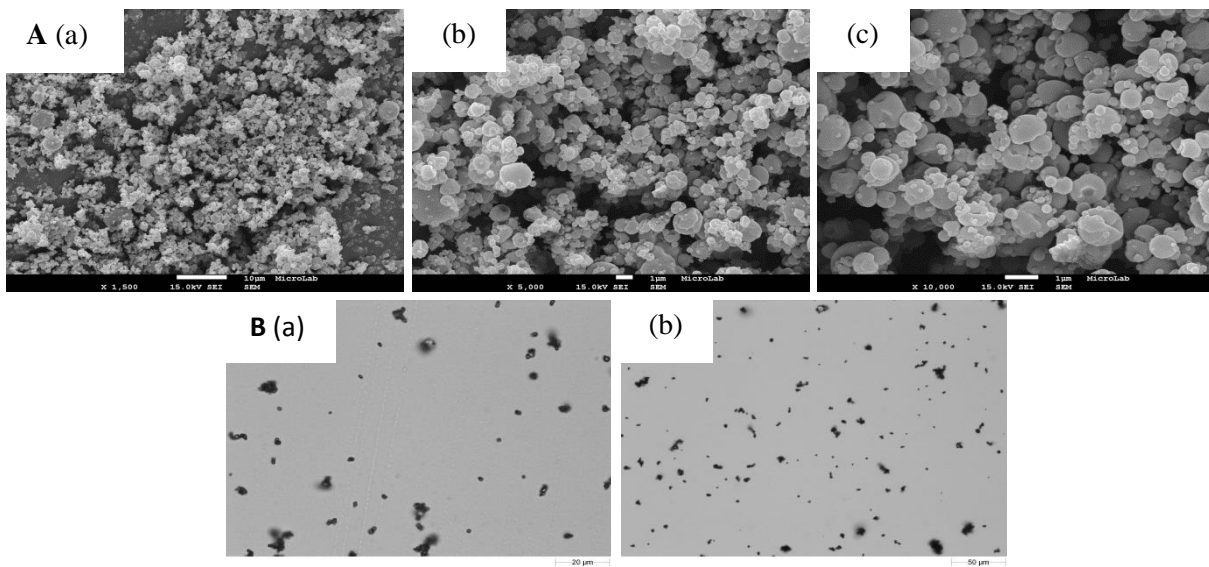


Figure II. 28 - 1% (w/v) CHT-PEtOx-IBP microparticles. (A) SEM images of with a magnification of (a) 1,500x, (b) 5,000x and (c) 10,000x and (B) Morphologi G3 images with magnification of (a) 20,000 and (b) 50,000 respectively.

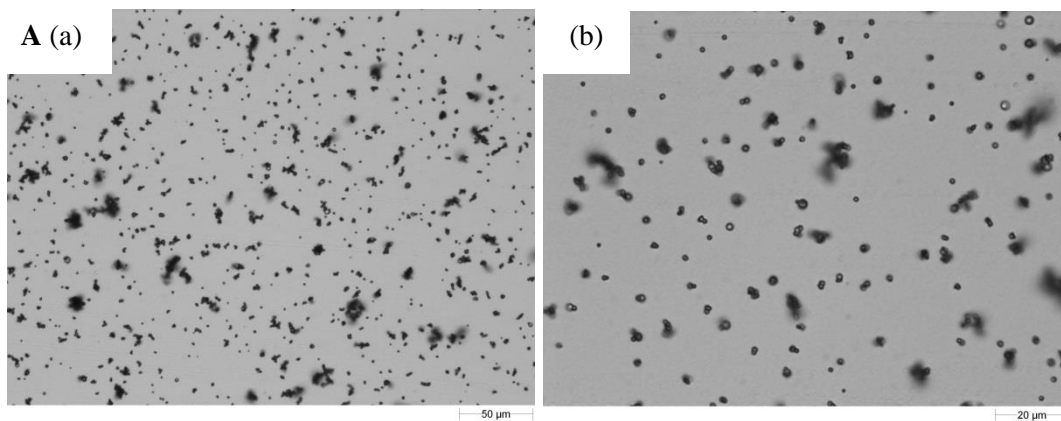


Figure II. 29 - 1% (w/v) CHT-PEtOx-PTM-029, F4, F39 microparticles. (A) Morphologi G3 images with magnification of (a) 20,000 and (b) 50,000 respectively.

3.2.2 Aerodynamic Performance

The particles were then analyzed by ACI measurements, and the results of CHT microparticles are presented in Figure II. 30. They all present similar distributions with exception of 1% (w/v) CHT-PEtOx-PTM.029, F4, F39 that shows the best distributions among all the CHT microparticles. The main problem is the high particle deposition in the induction port.

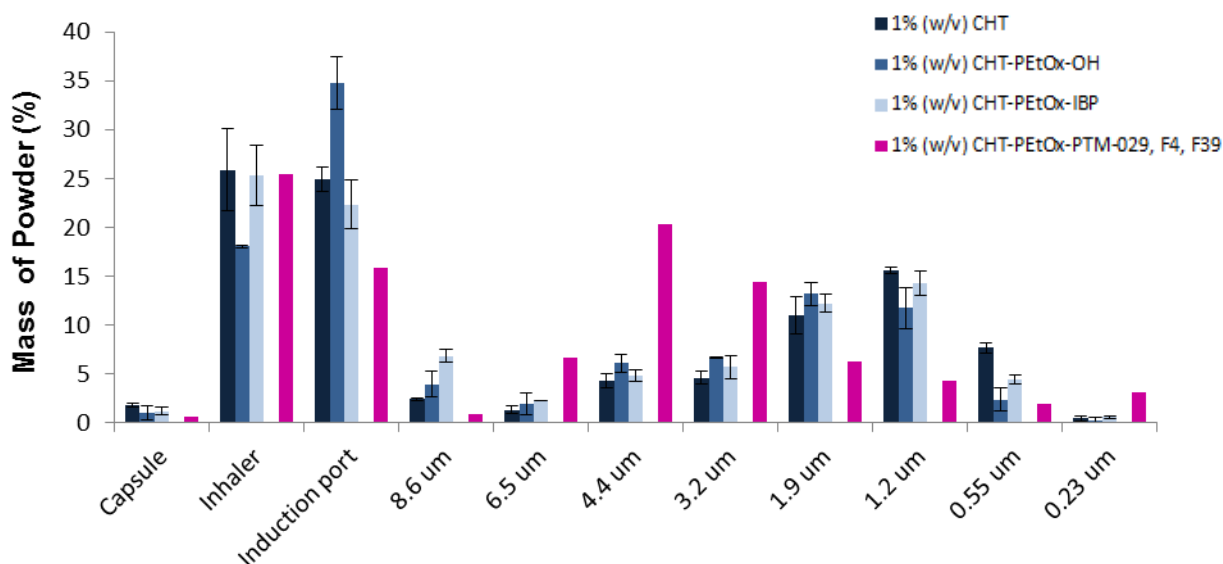


Figure II. 30 - Graphical representation of the powder distribution in the ACI apparatus for the CHT microparticles.

MMAD of the CHT microparticles shows low values, between 1.50 μm and 3.10 μm (Table II. 11). Taking into account that the desired values of MMAD for inhalation should be between 1 and 5 μm, all the CHT microparticles fulfill the requirement. Besides, CHT microparticles present higher FPF values as expected. Although, 1 % (w/v) CHT-PEtOx-PTM-029, F4, F39 microparticles showed the better FPF value of around 70 %, this was not expected since it has the higher MMAD.

Table II. 11 - Representation of the aerodynamic properties determined by ACI and DUSA for the CHT microparticles.

Assay		MMAD (μm)	FPF (%)	GSD	ED (%)
	CHT	1.90 \pm 0.10	60.90 \pm 0.54	2.52 \pm 0.23	98.3 \pm 0.74
1% (w/v)	CHT-PEtOx-OH	1.45 \pm 0.27	50.41 \pm 1.09	2.05 \pm 0.29	99.2 \pm 0.35
	CHT-PEtOx-IBP	1.56 \pm 0.02	58.11 \pm 2.77	2.75 \pm 0.17	98.8 \pm 0.35
	CHT-PEtOx-PTM-029, F4, F39	3.10	70.85	1.91	99.5

MMAD – Mass Median Aerodynamic Diameter; FPF- Fine particle fraction; GSD – Geometric Standard Deviation; ED – Emitted Dose.

3.2.3 Physical-Chemical Properties

The FTIR analysis of 1% (w/v) CHT microparticles (Figure II. 31) confirms the presence of CHT, showing their characteristics absorption bands: 3402 cm^{-1} (OH stretching), 2933 and 2892 cm^{-1} (C-H stretching of CH_3 groups) and 1637 cm^{-1} ($\text{CH}_3(\text{C}=\text{O})\text{N}$ - stretching). In Figure II. 31 (b) and (c), it is not perceptible the presence of PEtOx-OH and PEtOx-IBP since CHT disguised the absorption band at 1637 cm^{-1} ($\text{CH}_3(\text{C}=\text{O})\text{N}$ - stretching).

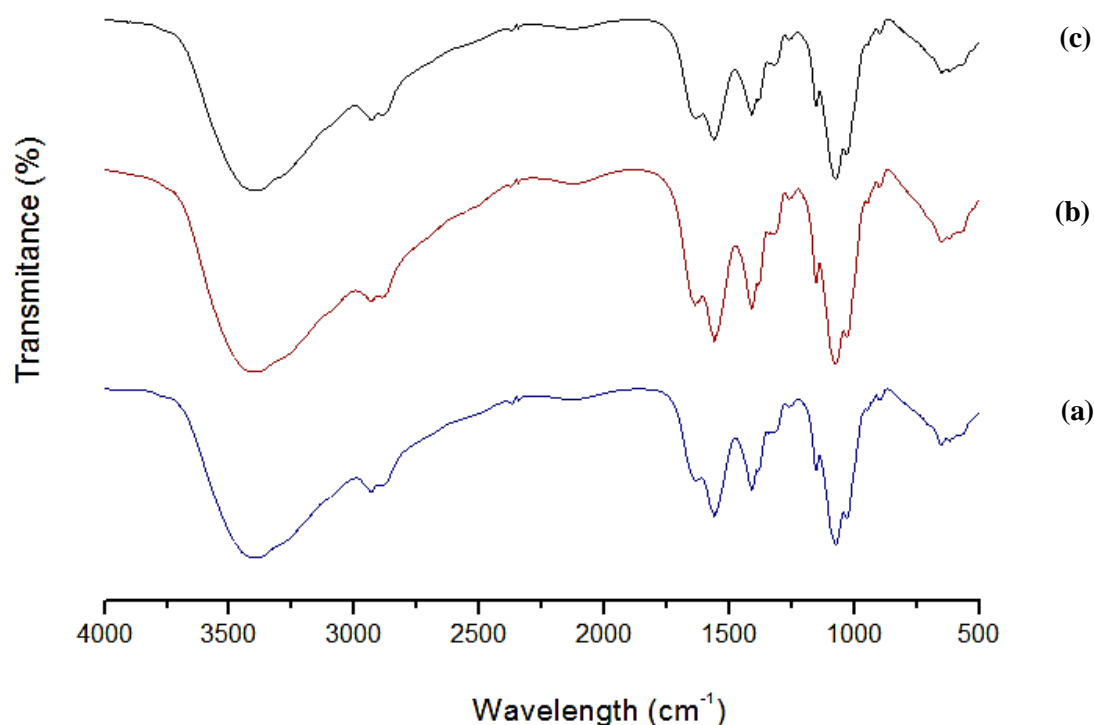


Figure II. 31 - FTIR. (a) CHT microparticles, (b) CHT-PEtOx-OH microparticles and (c) CHT-PEtOx-IBP microparticles.

As for the particles' water content, the percentages of all the formulations are represented in Table II. 12. In CHT microparticles, the amount of water in the particles is very low, which reveals the drying efficacy of the SASD, with exception of 1% (w/v) CHT that shows an inefficient drying.

Table II. 22 - Water content values for the CHT, CHT-PEtOx-OH and CHT-PEtOx-IBP microparticles.

Assay	Water content (%)
CHT	4.18±0.90
1% (w/v) CHT-PEtOx-OH	0.33±0.09
CHT-PEtOx-IBP	0.43±0.07

3.2.4 Pharmacokinetic Studies

In Figure II. 33, it is possible to observe the release of 60% of IBP into the medium being well correlated by Korsmeyer and Peppas equation. The kinetic parameters obtained from the correlation are included in Table II. 13. Looking at Figure II. 33 it is possible to conclude that the release of PEtOx-IBP has an anomalous transport, since diffusional exponent is 0.5734 implying that the release is more controlled by the swelling mechanism than the diffusion mechanism. Also, these particles have a slight amount of agglomerates, meaning that the particles are looser and facilitate the PEtOx-IBP diffusion. Furthermore, in Figure II. 32 (B) the first 0.35 hours are represented, it is possible to see that the release is faster, releasing about 50%, the 100% is achieved in nearly 3.5hours.

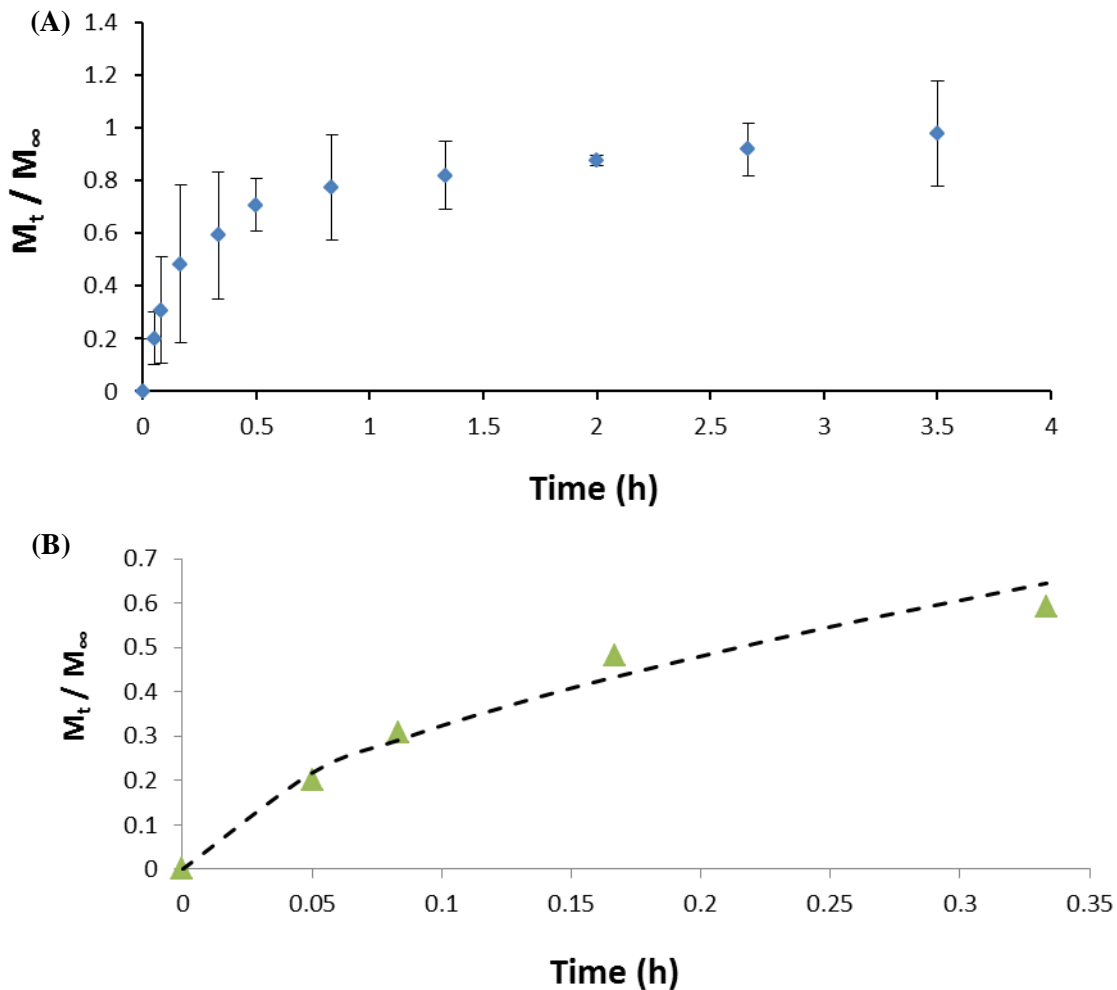


Figure II. 32 - (A) In vitro drug release studies of PEtOx-IBP loaded in CLT microparticles at pH 7.4 and 35 °C and (B) release profile fitted through Korsmeyer Peppas mathematical model for the first 60% of release.

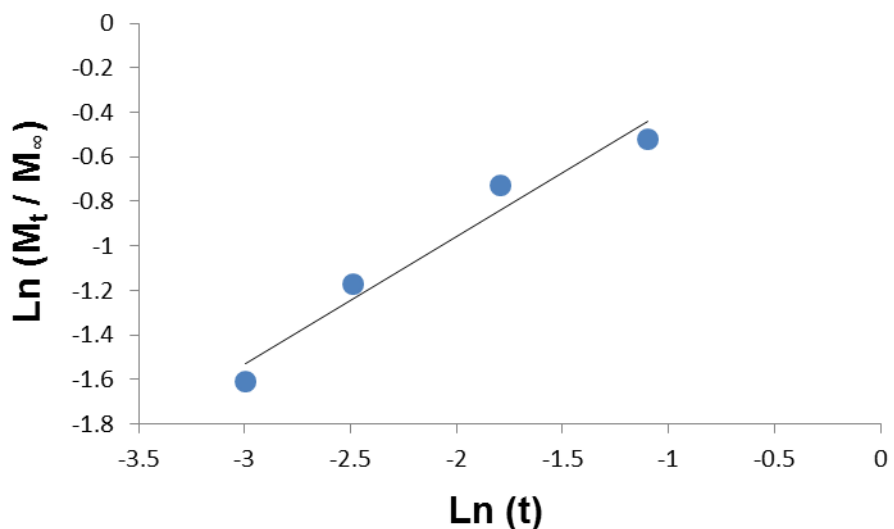


Figure II. 33 - Korsmeyer-Peppas Model for mechanism of PEtOx-IBP release from the CLT microparticles at pH 8 and 35° C.

Table II. 3 - Kinetic values obtained from the Korsmeyer equation for the 1% (w/v) CLT-PEtOx-IBP microparticles.

Microparticle	Korsmeyer Peppas		
	R ²	n	k
1% (w/v) CHT-PEtOx-IBP	0.9587	0.5734	1.2106

3.2.5 Biological Activity

In order to evaluate the antibacterial activity of PEtOx-PTM-029, F4, F39 and microparticles 1% (w/v) CHT-PEtOx-PTM-029, F4, F39, the minimum inhibitory concentrations (MIC) against two pathogenic bacteria, MRSA and VRE EF82 were determined following the procedures described in Part I, section 2.5. The biological tests showed that the conjugated drug, as well as the dry powder formulation, did not present the expected antibacterial activity.

4. Discussion

The 1D NMR spectroscopy (Annex 1) was performed, in order to confirm the success of the synthesis of the *living polymer* end-capped with different compounds namely, water, (*S*)-(+)-ibuprofen salt and with a bioactive compound PTM-029, F4, F39, produced in Part I.

The compound (*S*)-(+)-ibuprofen salt was used as a model drug, since the bioactive compound PTM-029, F4, F39 was available in very few quantities. Once ibuprofen is an optically active compound with (*S*) and (*R*)-isomers, the (*S*) isomer was the chosen one to produce the salt, since it is the more biologically active.

The ^{13}C NMR spectrum for PEtOx-IBP showed a new signal at 176.29 ppm corresponding to the new ester carbonyl group formed in the reaction and a slightly chemical shift of IBP characteristic signals confirming the successful conjugation of the drug by end-capping the *living polymer*. Relatively to the end-capping to PTM-029, F4, F39, the signal disappearance at H-15 (δ 12.28ppm) and also, through the proton ratio H-10 (δ 4.57ppm) and H-29 (δ 1.09 – 0.86ppm) demonstrated the success of this conjugation also.

In general, the particles exhibited mean volumetric diameters around 7 μm for CHT microparticles and 11 μm for CLT microparticles, with correspondent number distribution diameters of 2 and 6 μm , respectively, which revealed the existence of some aggregates in the powder. Morphologi and SEM analysis also confirmed the existence of agglomerated particles. Even though, there is some variance, all the formulations contained agglomerates being more evident in CLT microparticles, indicating that the manufacturing technique must be improved.

The microparticles showed a good aerodynamic properties, which is a major advantage, and it was caused by the CO_2 expansion and consequent droplet burst, affecting directly the obtained aerodynamic diameters (6 μm for CLT microparticles and 3 μm for CHT microparticles). As aforementioned particles should have a high diameter associated with a low density, in a way that the macrophages would avoid them and still they would have the necessary flowability to reach the deep lung.

Considering the results obtained with the ACI measurements, MMAD between 2 and 7 μm were obtained for the produced dry powder formulations. Although some of these values exceed the ideal particle diameter, most CLT containing powders fit in the proper MMAD range and are suitable for inhalation. There is a very accentuated difference between the MMAD and FPF values obtained for the CLT microparticles (7 μm and 20% for 0.25% (w/v), 6 μm and 22% for 0.5% (w/v) and 4 μm and 36% for 1% (w/v), respectively) and for CHT microparticles (2 μm and 56% for 1%

(w/v) and 3 μ m and 71% for 1% (w/v) encapsulated with PTM-029, F4, F39) showing that the addition of the *living polymer* end-capped with compounds, in the microparticles was in fact crucial. A major concern that is visible when performing the aerodynamic tests is the amount of powder that deposits in the induction port. Even though this is usual, as already mentioned, the percentage range is under the one observed with already obtained inhalation CLT and CHT particles.

It is also known that this deposition is highly related mainly to the presence of the aggregates and as a consequence the values of FPF obtained were low, with a maximum of 36% for CLT microparticles. Although, CHT particles showed higher FPF values, with a maximum of 71% due to the presence of only a few aggregates when compared with CLT microparticles. The efficiency of the microparticles entrainment resides on the ability of the DPI to generate forces sufficient to deagglomerate the powder and create a high flow, and that becomes hampered when there is such a large amount of aggregates.

The obtained yields can also be considered small (CLT microparticles: 0.25% (w/v) - 51%, 0.5% (w/v) - 31% and 1% (w/v) - 10%; CHT microparticles: 1% (w/v) CHT - 15%, 1% (w/v) CHT-PEtOx-OH - 22%, 1% (w/v) CHT-PEtOx-IBP - 17% and 1% (w/v) CHT-PEtOx-PTM-029, F4 F39 - 17%), but this can be justified by the inefficient recovery of smaller and lighter particles that were exhausted by the gas flow.

As for the physical-chemical properties of the microparticles, the FTIR analysis confirmed the presence of the compounds by the appearance of characteristic peaks of their functional groups.

From all the pharmacokinetic studies performed there is a biphasic curve for drug release mainly caused by anomalous transport. Drug in contact with the medium, is released as a function of the superposition of diffusion, swelling, dissolution and/or erosion phenomena. The CLT- and CHT-based microparticles showed a similar release behavior, although CLT microparticles presented a slightly faster release than CHT microparticles. This probably occurs because CLT microparticles were produced only in EtOH, which has higher affinity to scCO₂. This allowed the excipients and the encapsulated compounds to be more homogeneously mixed in the matrix when atomized, unlike the CHT microparticles which were performed with a volume proportion of acidic water and EtOH 4:1, having lower affinity to scCO₂.

Relatively to the biological activity, the compound PEtOx-PTM-029, F4, F39 and the microparticles 1% (w/v) CHT-PEtOx-PTM-029, F4, F39 did not present antibacterial activity against the pathogenic bacteria Methicillin-resistant *Staphylococcus Aureus* and Vancomycin-resistant *Enterococcus*. The *living polymer* when end-capped with bioactive compounds, act as polymer-drug conjugates. The poxylated drug remains inactive during its delivery to the site of action, where the hydrolytic or enzymatic cleavage may liberate the drug for action at the target

site.⁸³ The absence of the antimicrobial activity suggests that the OH-15 phenolic hydroxyl group (Annex 1, Figure 5), through which is established the conjugation to the polymer, appears to be important in the antibacterial activity of the compound PTM-029, F4, F39.

5. Conclusion

As presented in the introduction, the development of dry powders for inhalation stands as an outbreak solution to overcome drawbacks associated with drug delivery, while the use of sustainable techniques represents a production substitute to surpass the environment issues that affect the industry nowadays. Also, in order to improve the dry powder formulations it was encapsulated a lead-like drug produced in Part I. For that, this work represents a research field that has been increasingly growing and taken into consideration worldwide.

Herein, it was proven that the SASD apparatus is capable of producing CLT and CHT dry powder microparticles suitable for inhalation. Throughout the analysis of the results, it is possible to conclude that the particles manufacturing process has associated problems, since it is hard to establish a meeting point between ideal powder properties and SASD parameters. However, with the addition of an active pharmaceutical ingredient those problems can be mildly surpassed.

Overall, by adding a living polymer end-capped with different compounds to the CLT and CHT microparticles, these tended to present suitable aerodynamic properties and showed a controlled release profile confirming that CLT and CHT –based dry powders are good carriers that may efficiently perform drug delivery to the lungs. Besides, it also increases the suitability of the particles, by helping out reducing the amount of aggregates present in the powder, which was the biggest issue.

Furthermore, it is possible to conclude that the best formulation for pulmonary delivery was the CHT microparticles encapsulated with a *living polymer* end-capped with a bioactive marine compound 1% (w/v) CHT-PEtOx-PTM-029, F4, F39, with a MMAD of 3.10 μm , a FPF of 70.85% and a yield of 17.1%, which present fully adequate characteristics for inhalation.

Despite that, it would be preferable to proceed with a further particles optimization in order to overcome the problems associated with the aggregation and also the yield, such as the development of a better recovery process, in order to avoid such powder loss and the improvement of the formulation with more concentrated initial solutions. It would also be interesting to study macrophage uptake in order to understand if the particles would be able to remain in the lung tissue during the entire drug's release. It would also be interesting to study the release of the bioactive drug, PTM-029, F4, F39 novel napyradiomycin derivative, from the polymer-drug conjugate by enzymatic cleavage, using lysozyme, an enzyme that is present in the lung epithelium.

6. References

1. Draft, C. *et al.* *Global , regional and national levels of age-specific mortality and 240 causes of death , 1990-2013 : A systematic analysis for the Global Burden of Disease Study 2013. The Lancet* **385**, (Elsevier Ltd, 2015).
2. Cheng, Y.-B., Jensen, P. R. & Fenical, W. Cytotoxic and Antimicrobial Napyradiomycins from Two Marine-Derived Streptomyces Strains. *European J. Org. Chem.* **2013**, 3751–3757 (2013).
3. Ungaro, F. & Vanbever, R. Improving the efficacy of inhaled drugs for severe lung diseases: Emerging pulmonary delivery strategies. *Adv. Drug Deliv. Rev.* **75**, 1–2 (2014).
4. Dasaraju PV, L. C. in *Medical Microbiology* (ed. S, B.) 93 (1996).
5. Haste, N., Farnaes, L., Perera, V. & Fenical, W. Bactericidal kinetics of marine-derived napyradiomycins against contemporary methicillin-resistant Staphylococcus aureus. *Mar. Drugs* **9**, 680–689 (2011).
6. Bérdy, J. Bioactive microbial metabolites. *J. Antibiot. (Tokyo)*. **58**, 1–26 (2005).
7. Fenical, W. & Jensen, P. R. Developing a new resource for drug discovery: marine actinomycete bacteria. *Nat. Chem. Biol.* **2**, 666–673 (2006).
8. Gallagher, K. a, Rauscher, K., Pavan Ioca, L. & Jensen, P. R. Phylogenetic and chemical diversity of a hybrid-isoprenoid-producing streptomyces lineage. *Appl. Environ. Microbiol.* **79**, 6894–902 (2013).
9. Subramani, R. & Aalbersberg, W. Marine actinomycetes: An ongoing source of novel bioactive metabolites. *Microbiol. Res.* **167**, 571–580 (2012).
10. Kuzuyama, T. & Seto, H. Diversity of the biosynthesis of the isoprene units. *Nat. Prod. Rep.* **20**, 171–183 (2003).
11. Gallagher, K. a, Fenical, W. & Jensen, P. R. Hybrid isoprenoid secondary metabolite production in terrestrial and marine actinomycetes. *Curr. Opin. Biotechnol.* **21**, 794–800 (2010).
12. Kawasaki, T. & Hayashi, Y. Biosynthesis of a natural polyketide-isoprenoid hybrid compound, furaquinocin A: identification and heterologous expression of the gene cluster. *J. Bacteriol.* **188**, 1236–1244 (2006).
13. Pawlik, J. R. Marine chemical ecology. *Mar. Ecol. Prog. Ser.* **207**, 225–226 (2000).
14. Xiao, Y., Machacek, M., Lee, K., Kuzuyama, T. & Liu, P. Prenyltransferase substrate binding pocket flexibility and its application in isoprenoid profiling. *Mol. Biosyst.* **5**, 913 (2009).

15. Wu, Zhengchao; Li, Sumei, et al. Antibacterial and Cytotoxic New Napyradiomycins from the *Mar. Drugs* **11**, 2113–2125 (2013).
16. Winter, Jaclyn M., Moffitt, Michelle C., et al. Molecular Basis for Chloronium-mediated Meroterpene Cyclization CLONING, SEQUENCING, AND HETEROLOGOUS EXPRESSION OF THE NAPYRADIOMYCIN BIOSYNTHETIC GENE CLUSTER. *J. Biol. Chem.* **282**, 16362–16368 (2007).
17. Gill SR, Fouts DE, Archer GL, Mongodin EF, Deboy RT, Ravel J, Paulsen IT, Kolonay JF, Brinkac L, Beanan M, Dodson RJ, Daugherty SC, Madupu R, Angiuoli SV, Durkin AS, Haft DH, Vamathevan J, Khouri H, Utterback T, Lee C, Dimitrov G, Jiang L, Qin H, Weidman, F. C. Insights on evolution of virulence and resistance from the complete genome analysis of an early methicillin-resistant *Staphylococcus aureus* strain and a biofilm-producing methicillin-resistant *Staphylococcus epidermidis* strain. *J. Bacteriol.* **187**, 2426–2438 (2005).
18. Soria-Mercado, I. Antibiotic terpenoid chloro-dihydroquinones from a new marine actinomycete. *J. Nat. Prod.* **68**, 904–910 (2005).
19. Soria-Mercado, I. E., Jensen, P. R., Fenical, W., Kassel, S. & Golen, J. 3,4a-Dichloro-10a-(3-chloro-6-hydroxy-2,2,6-trimethylcyclohexylmethyl)-6,8-dihydroxy-2,2,7-trimethyl-3,4,4a,10a-tetrahydro-2 H -benzo[g]chromene-5,10-dione. *Acta Crystallogr. Sect. E Struct. Reports Online* **60**, o1627–o1629 (2004).
20. Shiomi, K. *et al.* STRUCTURES OF NEW ANTIBIOTICS NAPYRADIOMYCINS. *J. Antibiot. (Tokyo)*. **XXXIX**, 494–501 (1986).
21. Shiomi, K., Nakamura, H. & Iinuma, H. NEW ANTIBIOTIC NAPYRADIOMYCINS A2 AND B4 AND STEREOCHEMISTRY OF NAPYRADIOMYCINS. *J. Antibiot. (Tokyo)*. **XL**, (1987).
22. Shiomi, K. I. H. Biosynthesis of Napyradiomycins. *J. Antibiot. (Tokyo)*. **XL**, 1740–1745 (1987).
23. Mynderse, J. S. Antibiotic A80915 and process for its production. (1990). at <<http://scholar.google.com/scholar?hl=en&btnG=Search&q=intitle:No+Title#0>>
24. Hori, Yasuhiro, Abe, Yukiko, et al. NAPYRADIOMYCINS A AND B1: NON-STEROIDAL ESTROGEN-RECEPTOR ANTAGONISTS PRODUCED BY A *Streptomyces*. *J. Antibiot. (Tokyo)*. **46**, 1890–1893 (1993).
25. Motohashi, K., Sue, M. & Furihata, K. Terpenoids produced by actinomycetes: Napyradiomycins from *Streptomyces antimycoticus* NT17. *J. Nat. Prod.* **71**, 595–601 (2008).
26. Farnaes, L. & Coufal, N. Napyradiomycin Derivatives, Produced by a Marine-Derived Actinomycete, Illustrate Cytotoxicity by Induction of Apoptosis. *J. Nat. Prod.* **77**, 15–21 (2013).

27. Farnaes, L., La Clair, J. J. & Fenical, W. Napyradiomycins CNQ525.510B and A80915C target the Hsp90 paralogue Grp94. *Org. Biomol. Chem.* **12**, 418 (2014).
28. Takemura, S., Hirayama, A. & Tokunaga, J. A concise total synthesis of (±)-A80915G, a member of the napyradiomycin family of antibiotics. *Tetrahedron Lett.* **40**, 7501–7505 (1999).
29. Shirai, M. *et al.* Terpenoids produced by actinomycetes: isolation, structural elucidation and biosynthesis of new diterpenes, gifhornenolones A and B from *Verrucospora gifhornensis* YM28-088. *J. Antibiot. (Tokyo)*. **63**, 245–250 (2010).
30. Griffith, L. G. Polymeric biomaterials. *Acta Mater.* **48**, 263–277 (2000).
31. Buttini, F., Colombo, P., Rossi, A., Sonvico, F. & Colombo, G. Particles and powders: Tools of innovation for non-invasive drug administration. *J. Control. Release* **161**, 693–702 (2012).
32. Takami, T. & Murakami, Y. Development of PEG-PLA/PLGA microparticles for pulmonary drug delivery prepared by a novel emulsification technique assisted with amphiphilic block copolymers. *Colloids Surfaces B Biointerfaces* **87**, 433–438 (2011).
33. Sung, J. C., Pulliam, B. L. & Edwards, D. a. Nanoparticles for drug delivery to the lungs. *Trends Biotechnol.* **25**, 563–570 (2007).
34. Pilcer, G. & Amighi, K. Formulation strategy and use of excipients in pulmonary drug delivery. *Int. J. Pharm.* **392**, 1–19 (2010).
35. Beck-Broichsitter, M. *et al.* Characterization of novel spray-dried polymeric particles for controlled pulmonary drug delivery. *J. Control. Release* **158**, 329–335 (2012).
36. Chow, a. H. L., Tong, H. H. Y., Chattopadhyay, P. & Shekunov, B. Y. Particle engineering for pulmonary drug delivery. *Pharm. Res.* **24**, 411–437 (2007).
37. Geiser, M. *et al.* Cellular uptake and localization of inhaled gold nanoparticles in lungs of mice with chronic obstructive pulmonary disease. *Part. Fibre Toxicol.* **10**, 19 (2013).
38. Newman, S. P. & Busse, W. W. Evolution of dry powder inhaler design, formulation, and performance. *Respir. Med.* **96**, 293–304 (2002).
39. Shoyele, S. a. & Slowey, A. Prospects of formulating proteins/peptides as aerosols for pulmonary drug delivery. *Int. J. Pharm.* **314**, 1–8 (2006).
40. Healy, A. M., Amaro, M. I., Paluch, K. J. & Tajber, L. Dry powders for oral inhalation free of lactose carrier particles. *Adv. Drug Deliv. Rev.* **75C**, 32–52 (2014).
41. Malcolmson, R. J. & Embleton, J. K. Dry powder formulations for pulmonary delivery. *Pharm. Sci. Technol. Today* **1**, 394–398 (1998).

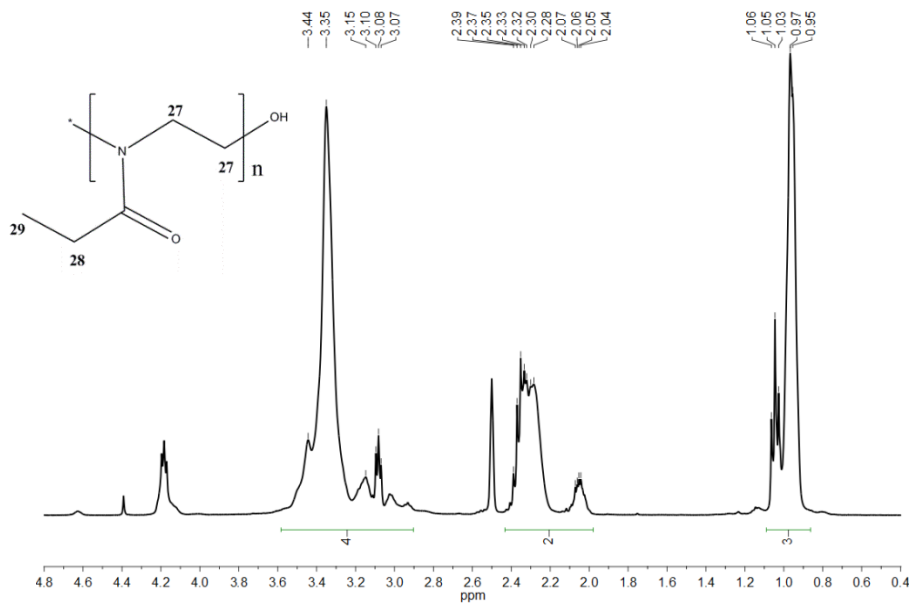
42. Zhou, Q. T., Tang, P., Leung, S. S. Y., Chan, J. G. Y. & Chan, H.-K. Emerging inhalation aerosol devices and strategies: Where are we headed? *Adv. Drug Deliv. Rev.* **75C**, 3–17 (2014).
43. Choi, H. S. *et al.* Rapid translocation of nanoparticles from the lung airspaces to the body. *Nat. Biotechnol.* **28**, 1300–1303 (2010).
44. Wanakule, P., Liu, G. W., Fleury, A. T. & Roy, K. Nano-inside-micro: Disease-responsive microgels with encapsulated nanoparticles for intracellular drug delivery to the deep lung. *J. Control. Release* **162**, 429–437 (2012).
45. Li, Y. Z. *et al.* Inhalable microparticles as carriers for pulmonary delivery of thymopentin-loaded solid lipid nanoparticles. *Pharm. Res.* **27**, 1977–1986 (2010).
46. Yang, Y. *et al.* Development of highly porous large PLGA microparticles for pulmonary drug delivery. *Biomaterials* **30**, 1947–1953 (2009).
47. Bosquillon, C., Lombry, C., Pr eat, V. & Vanbever, R. Influence of formulation excipients and physical characteristics of inhalation dry powders on their aerosolization performance. *J. Control. Release* **70**, 329–339 (2001).
48. Arifin, D. Y., Lee, L. Y. & Wang, C.-H. Mathematical modeling and simulation of drug release from microspheres: Implications to drug delivery systems. *Adv. Drug Deliv. Rev.* **58**, 1274–1325 (2006).
49. Ritger, P. L. & Peppas, N. a. A simple equation for description of solute release I. Fickian and non-fickian release from non-swellable devices in the form of slabs, spheres, cylinders or discs. *J. Control. Release* **5**, 23–36 (1987).
50. Cipolla, D., Shekunov, B., Blanchard, J. & Hickey, A. Lipid-based carriers for pulmonary products: Preclinical development and case studies in humans. *Adv. Drug Deliv. Rev.* **75**, 53–80 (2014).
51. Loira-Pastoriza, C., Todoroff, J. & Vanbever, R. Delivery strategies for sustained drug release in the lungs. *Adv. Drug Deliv. Rev.* **75C**, 81–91 (2014).
52. Van Der Schueren, L. *et al.* Polycaprolactone and polycaprolactone/chitosan nanofibres functionalised with the pH-sensitive dye Nitrazine Yellow. *Carbohydr. Polym.* **91**, 284–293 (2013).
53. Alvarenga, E. S. De. Characterization and Properties of Chitosan. *Biotechnol. Biopolym.* 91–108 (2011). at <<http://www.intechopen.com/books/biotechnology-of-biopolymers/characterization-and-properties-of-chitosan>>
54. Dash, M., Chiellini, F., Ottenbrite, R. M. & Chiellini, E. Chitosan - A versatile semi-synthetic polymer in biomedical applications. *Prog. Polym. Sci.* **36**, 981–1014 (2011).
55. Temtem, M., Barroso, T., Casimiro, T., Mano, J. F. & Aguiar-Ricardo, A. Dual stimuli responsive poly(N-isopropylacrylamide) coated chitosan scaffolds for controlled release prepared from a non residue technology. *J. Supercrit. Fluids* **66**, 398–404 (2012).

56. Jae, H. P. *et al.* Self-assembled nanoparticles based on glycol chitosan bearing hydrophobic moieties as carriers for doxorubicin: In vivo biodistribution and anti-tumor activity. *Biomaterials* **27**, 119–126 (2006).
57. Trapani, A. *et al.* Characterization and evaluation of chitosan nanoparticles for dopamine brain delivery. *Int. J. Pharm.* **419**, 296–307 (2011).
58. Kumirska, J. *et al.* Application of spectroscopic methods for structural analysis of chitin and chitosan. *Mar. Drugs* **8**, 1567–1636 (2010).
59. Kean, T. & Thanou, M. Biodegradation, biodistribution and toxicity of chitosan. *Adv. Drug Deliv. Rev.* **62**, 3–11 (2010).
60. Cruz, L. J. *et al.* Targeted PLGA nano- but not microparticles specifically deliver antigen to human dendritic cells via DC-SIGN in vitro. *J. Control. Release* **144**, 118–126 (2010).
61. Ding, A. G. & Schwendeman, S. P. Determination of Water-Soluble Acid Distribution in Poly(lactide-co-glycolide). *J. Pharm. Sci.* **93**, 322–331 (2004).
62. Casettari, L. *et al.* Surface characterisation of bioadhesive PLGA/chitosan microparticles produced by supercritical fluid technology. *Pharm. Res.* **28**, 1668–1682 (2011).
63. Steve, Makadia Hirenkumar and Siegel Steve, P., Drug, C. & Carrier, D. Poly Lactic-co-Glycolic Acid (PLGA) as Biodegradable Controlled Drug Delivery Carrier. *Polymers (Basel)*. **3**, 1–19 (2012).
64. Woodle, M. C., Engbers, C. M. & Zalipsky, S. New amphipatic polymer-lipid conjugates forming long-circulating reticuloendothelial system-evading liposomes. *Bioconjug. Chem.* **5**, 493–496 (1994).
65. Mero, A. *et al.* Synthesis and characterization of poly(2-ethyl 2-oxazoline)-conjugates with proteins and drugs: Suitable alternatives to PEG-conjugates? *J. Control. Release* **125**, 87–95 (2008).
66. Huang, H. W. Action of Antimicrobial Peptides : Two-State Model Current Topics Action of Antimicrobial Peptides : Two-State Model. *Biochemistry* **39**, 25–30 (2000).
67. A. Aguiar-Ricardo, V.D.B. Bonifacio, T. Casimiro, V. G. C. Supercritical carbon dioxide design strategies: from drug carriers to soft killers. *Phil. Trans. R. Soc. A* (2015). doi:10.1084/jem.20072208
68. De Macedo, C. V., da Silva, M. S., Casimiro, T., Cabrita, E. J. & Aguiar-Ricardo, A. Boron trifluoride catalyzed polymerisation of 2-substituted-2-oxazolines in supercritical carbon dioxide. *Green Chem.* **9**, 948 (2007).
69. Mansour, H. M., Rhee, Y. S. & Wu, X. Nanomedicine in pulmonary delivery. *Int. J. Nanomedicine* **4**, 299–319 (2009).

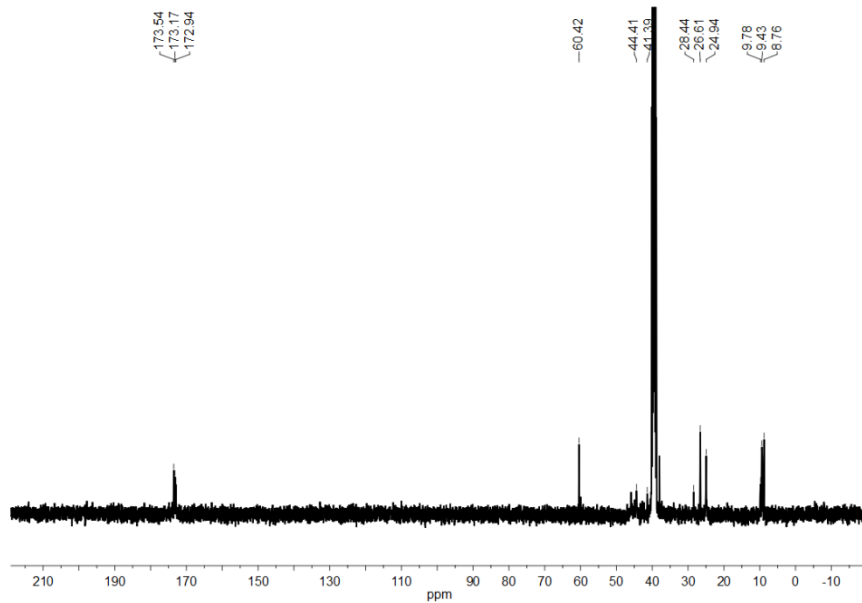
70. Martín, Á., Pham, H. M., Kilzer, A., Kareth, S. & Weidner, E. Micronization of polyethylene glycol by PGSS (Particles from Gas Saturated Solutions)-drying of aqueous solutions. *Chem. Eng. Process. Process Intensif.* **49**, 1259–1266 (2010).
71. Zhang, J., Wu, L., Chan, H. K. & Watanabe, W. Formation, characterization, and fate of inhaled drug nanoparticles. *Adv. Drug Deliv. Rev.* **63**, 441–455 (2011).
72. Marco, G. I. L., Vicente, J. & Gaspar, F. Scale-up methodology for pharmaceutical spray drying. *Chim. Oggi* **28**, 18–22 (2010).
73. Nie, H., Lee, L. Y., Tong, H. & Wang, C. H. PLGA/chitosan composites from a combination of spray drying and supercritical fluid foaming techniques: New carriers for DNA delivery. *J. Control. Release* **129**, 207–214 (2008).
74. Tong, H. H. Y. & Chow, a H. L. Control of Physical Forms of Drug Particles for Pulmonary Delivery by Spray Drying and Supercritical Fluid Processing. **24**, 27–40 (2006).
75. Chattopadhyay, P. & Gupta, R. B. Supercritical CO₂ Based Production of Magnetically Responsive Micro- and Nanoparticles for Drug Targeting. 6049–6058 (2002).
76. Reverchon, E. & Caputo, G. Role of phase behavior and atomization in the supercritical antisolvent precipitation. *Ind. & Eng. Chem.* **42**, 6406–6414 (2003).
77. Reverchon, E., Adami, R. & Caputo, G. Supercritical assisted atomization: Performance comparison between laboratory and pilot scale. *J. Supercrit. Fluids* **37**, 298–306 (2006).
78. Porta, G. Della & Reverchon, E. Engineering Powder Properties By Supercritical Fluid for Optimum Drug Delivery. *Bioprocess Int.* 54–60 (2005).
79. Reighard, T. S., Lee, S. T. & Olesik, S. V. Determination of methanol/CO₂ and acetonitrile/CO₂ vapor-liquid phase equilibria using a variable-volume view cell. *Fluid Phase Equilib.* **123**, 215–230 (1996).
80. Duarte, C., Aguiar-Ricardo, A., Ribeiro, N., Casimiro, T. & Da Ponte, M. N. Correlation of Vapor-Liquid Equilibrium for Carbon Dioxide + Ethanol + Water at Temperatures from 35 to 70°C. *Sep. Sci. Technol.* **35**, 2187–2201 (2000).
81. Adami, R., Liparoti, S. & Reverchon, E. A new supercritical assisted atomization configuration, for the micronization of thermolabile compounds. *Chem. Eng. J.* **173**, 55–61 (2011).
82. Wang, Q., Guan, Y. X., Yao, S. J. & Zhu, Z. Q. The liquid volume expansion effect as a simple thermodynamic criterion in cholesterol micronization by supercritical assisted atomization. *Chem. Eng. Sci.* **75**, 38–48 (2012).
83. Agrawal, N. Polymeric Prodrugs: Recent Achievements and General Strategies. *J. Antivir. Antiretrovir.* **01**, (2015).
84. W, L. & PG, J. *Handb. Green Chem. Weinheim: Wiley-VCH* **1–30**, (2010).

7. Annex 1

NMR data of the *living polymer end-capping with water*

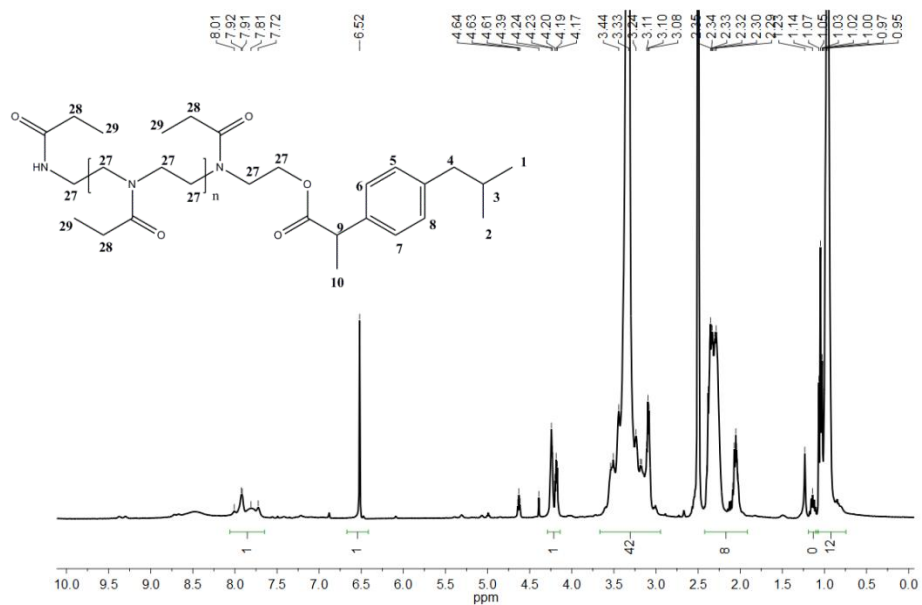


Annex 1. Figure 1 - $^1\text{H-NMR}$ spectrum of PEtOx-OH in $\text{DMSO-}d_6$.

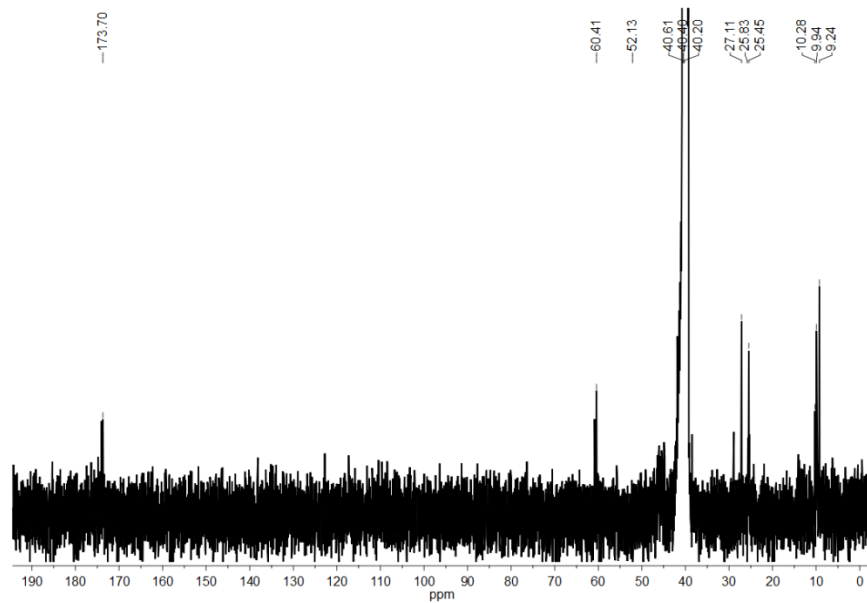


Annex 1. Figure 2 - $^{13}\text{C-NMR}$ spectrum of PEtOx-OH in $\text{DMSO-}d_6$.

NMR data of the *living polymer end-capping with (S)-(+)-Ibuprofen Salt*

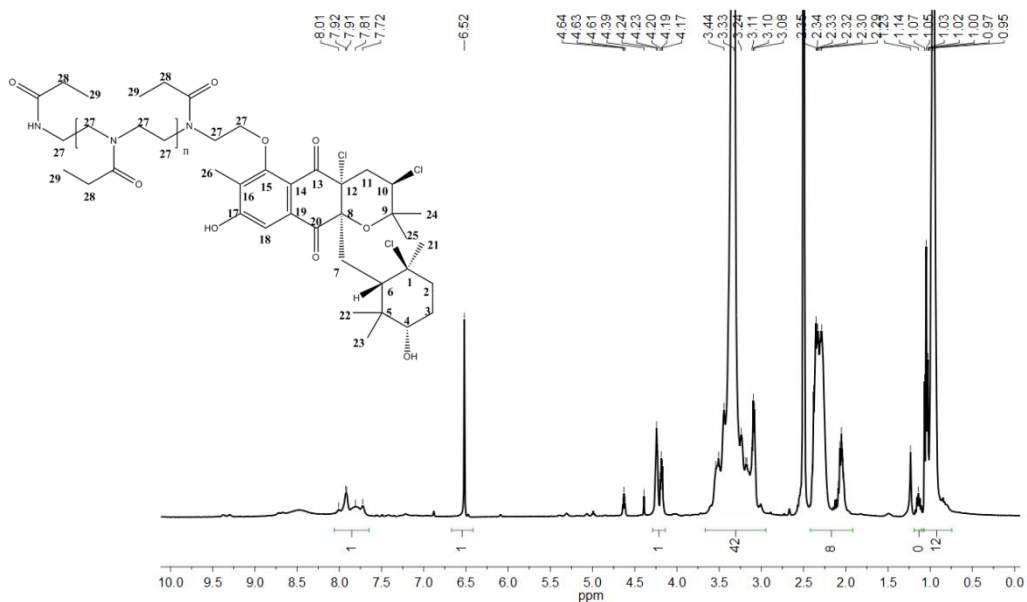


Annex 1. Figure 3 - ¹H-NMR spectrum of PEtOx-IBP in DMSO-*d*₆.

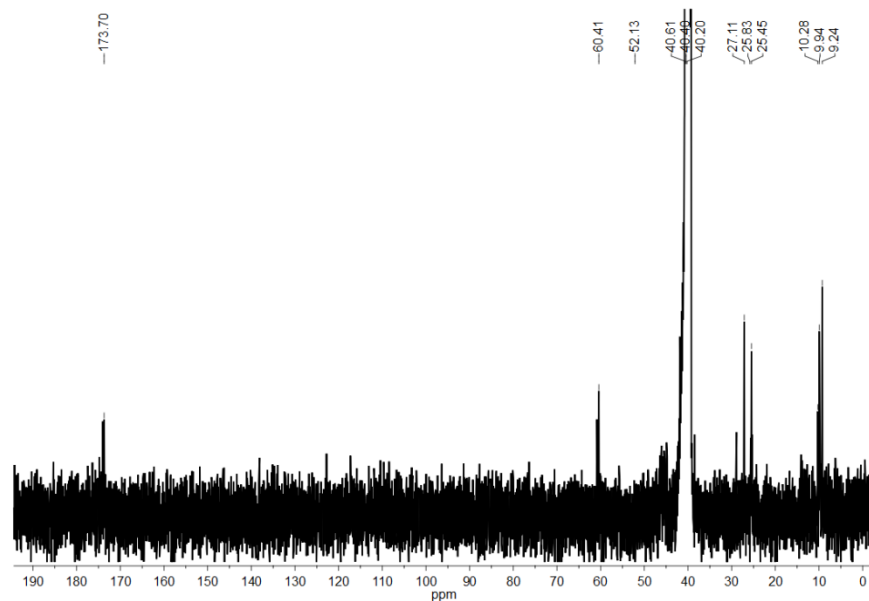


Annex 1. Figure 4 - ¹³C-NMR spectrum of PEtOx-IBP in DMSO-*d*₆.

NMR data of *living polymer end-capping with bioactive compound PTM-029, F4, F39*



Annex 1. Figure 5 - ¹H-NMR spectrum of PEtOx-PTM-029, F4, F39 in DMSO-*d*₆.



Annex 1. Figure 6 - ¹³C-NMR spectrum of PEtOx-PTM-029, F4, F39 in DMSO-*d*₆.

